LIGHTNING PROTECTION OF WIND TURBINES

A thesis submitted to the

University of Manchester for the degree of

Doctor of Philosophy

in the

Faculty of Engineering and Physical Sciences

2010

Vidyadhar Peesapati

School of Electrical and Electronic Engineering

List of Figures

List of Tables

List of Equations

Glossary

1. **Downward initiated lightning**

   A lightning strike that is initiated by a downward leader propagating from the cloud to earth.

2. **Upward initiated lightning**

   A lightning strike that is initiated by an upward leader propagating from the earthed structure to cloud.

3. **Lightning stroke**

   A single discharge in a lightning flash [1].

4. **Short stroke**

   The part of the lightning flash that corresponds to an impulse current.

5. **Long stroke**

   The part of the lightning flash that corresponds to a continuing current.

6. **Peak lightning current**

   The maximum value of current flowing at the point of attachment.

7. **Specific energy**

   The energy dissipated by the lightning current in a unit resistance.

8. **Lightning protection zone**

   Zone where the lightning electromagnetic environment is defined [1].

9. **Lightning protection level**

   The set of lightning current parameter values, maximum and minimum, on which the design of the lightning protection systems are based. The maximum and minimum values are defined is such a way that these values are not exceeded in natural lightning.

10. **Lightning protection systems**

    A system which is built to reduce the physical damage caused by a lightning strike. This includes both the external and internal lightning protection system.

11. External lightning protection system

Part of the lightning protection system which includes the air terminations system, down conductor and an earth termination system [1].

12. Internal lightning protection system

Part of the lightning protection system that provides equipotential bonding and/or insulation to the external lightning protection system [1].

13. Air termination

The part of the lightning protection system which is used to intercept the lightning strike, ideally the first point of attachment.

14. Down conductor

The part of the lightning protection system that is intended to carry the lightning current safely.

15. Peak Current Sensor

A sensor used to indentify the value of the maximum peak current of a lightning flash.

16. **Equipontential bonding**

The bonding/connection of different parts of the lightning protection system, to reduce the potential differences caused by the lightning current.

17. Finite Element Analysis (FEA)

The analysis of a computer model using numerical techniques, by dividing it into finite sized elements.

Abstract

Wind turbines are the largest contributor to renewable energy both in Britain and the rest of Europe. With a rise in the installed capacity and an increase in offshore wind energy due to governments green targets by 2020, there has been a large development in new wind turbines for optimized performance. The present thesis deals with the uncertainties in regards to the lightning phenomenon on wind turbines with emphasis on the rotor blades. Rotor blades are the most expensive part to replace in the event of lightning related damage. The research presents results based on lightning data analysis on wind turbines, backed up by finite element analysis testing of wind turbine systems. The final chapters include the testing and improving of lightning protection systems installed on modern day rotor blades.

The first part of the thesis deals with the theoretical understanding of the lightning phenomenon and its effect on wind turbine systems. The core work of the research begins with the analysis of lightning data collected over Nysted wind farm and different wind turbines installed over the world. The data analysis helps in identifying the parts of the wind turbine that are at high risk to lightning attachment and related damage. The peak current levels of the lightning strikes seen on the wind turbine are compared with those in modern day lightning standards, and show that historic data in the standards are not an exact match to the real case scenarios. The lightning data analysis also sheds light into the importance of upward initiated lightning, which will become important for large wind turbines, especially in their new offshore environment. A full scale 3D FEA model of a wind turbine, with lightning protection systems installed in its rotor blades, is subjected to electrical stresses to find likely attachment points in regards to upward initiated lightning, and these results are later compared to those found in the data analysis.

The second half of the thesis deals with the testing of new materials and prototype blades, to be introduced to reduce their radar cross section. The new materials include a large amount of carbon content which affects the efficiency of the lightning protection system. High voltage and high current tests backed up with finite element analysis have been performed to find how these new materials affect the performance of the lightning protection system. The results indicate that further work needs to be done before these new materials can be integrated into the blade, as they increase the risk of lightning related damage to the blade.

Declaration

No portion of the work referred to in this thesis has been submitted in support of an application for another degree or qualification of this or any other university or other institute of learning.

Copyright

Acknowledgment

I would like to thank my parents Venkateswarlu and Lakshmi for all their support and encouragement, without which I would not have been able reach to this stage in my career. I would also like to thank my brother Sreedhar and sister-in-law Caroline for their constant help and guidance at all times.

I would not have been able to carry out this PhD without the help of my supervisor Prof Ian Cotton, I thank him for all the advice and support he has patiently provided throughout the period of this research.

A special thanks to Prof Simon Rowland who has been a source of help during this PhD.

Finally, I would like to thank my friends Dr Sanjay Bahadoorsingh, Dr Sinisa Djurovic, Dr Antonios Tzimas, Dr Rebecca Firth, Dr Stelios Lelis, Dimitris, Rob, Sahar, Laith, Gary, Pete, Bugz and others for helping me through the difficult times of this PhD.

1 Introduction

Since their first introduction for generating electricity in the early 20th century, wind power has increased and become one of the major options for renewable energy. According to the Global Wind Energy Council, the total installed capacity of wind power around the world reached a massive 60GW, a 10 fold increase, in comparison to 1996 [2]. Figure 1-1 shows the increase in the installed wind turbine capacity worldwide, including both offshore and onshore wind farms.

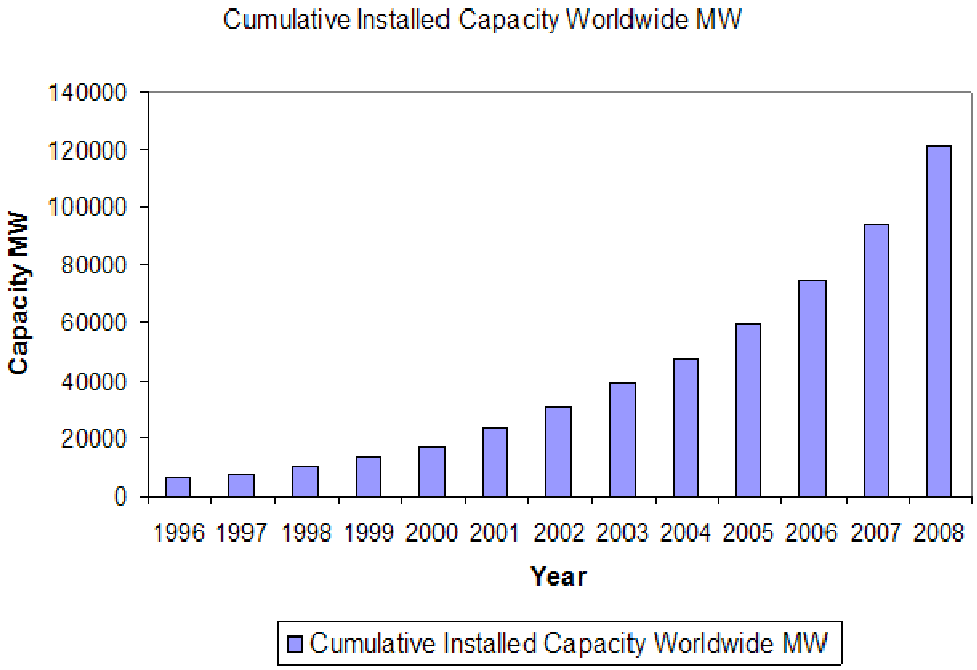

Figure 1-1Cumulative installed capacity worldwide [3]

In the last two years major wind projects have been planned and installed offshore, this has opened new avenues for wind power. This is important for countries mainly in northern Europe, where the availability of shallow coasts has combined with the need for land area for much larger projects. Denmark presently leads in this area with two major offshore projects namely Horns Rev in the North Sea and Nysted in the Baltic. Britain has also taken initiative to increase its role in wind energy by starting to build large individual projects offshore. One of the latest projects that have been recently given the go ahead is the London Array, which is to be built more than 20 km off the Kent and Essex coasts. When completed it should be able to generate up to 1000MW, which would add to other offshore wind projects installed and being developed off the coast of Britain. The recent increase in the field comes in accordance with the governments plans to try and supply 10% of Britain power needs through Wind Energy by 2010. Other Projects include the Atlantic Array (1.5GW) and Burbo Bank (90MW).

Between 1991 and 2007, alongside an increase in installed capacity, wind turbine technology has advanced. Early turbines were of the order of 300 kilowatts (kW), compared with todays modern turbines which have reached 5 MW of capacity and above – a 16-fold increase in power rating. With the opening of offshore sites for prospective wind farms, turbine manufacturers have taken a positive approach on increasing the size of these already tall structures. Figure 1-2 shows the scale of a multi megawatt wind turbine with respect to other tall objects.

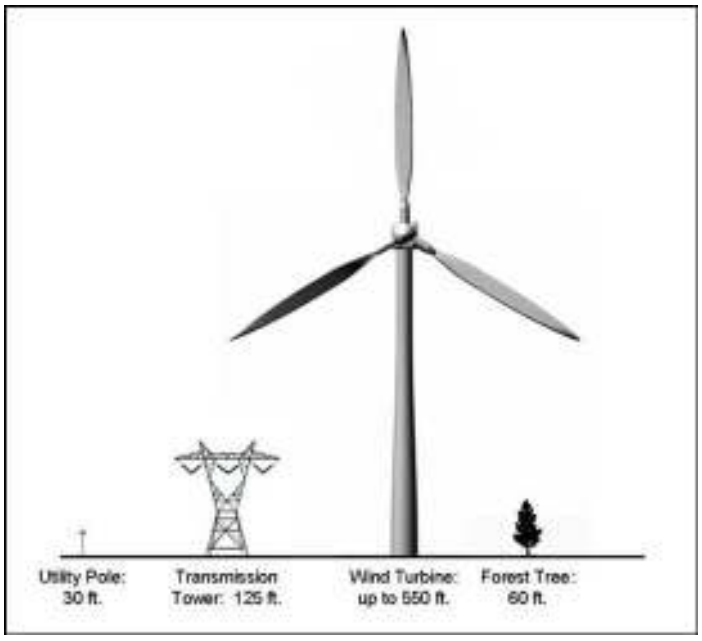

Figure 1-2 Comparison of heights [4]

Most of the new MW wind turbines are more than 100m tall. The largest wind turbine presently in operation is the Enercon 126, rated at 7MW; it stands at a total height of 198m and has a blade diameter of 126mts.

1.1 Modern Wind Turbine Design

The wind turbine can be broadly classified into 3 parts

1. The Tower
2. The Nacelle
3. The Blades

Figure 1-3 shows the main components of a modern day wind turbine.

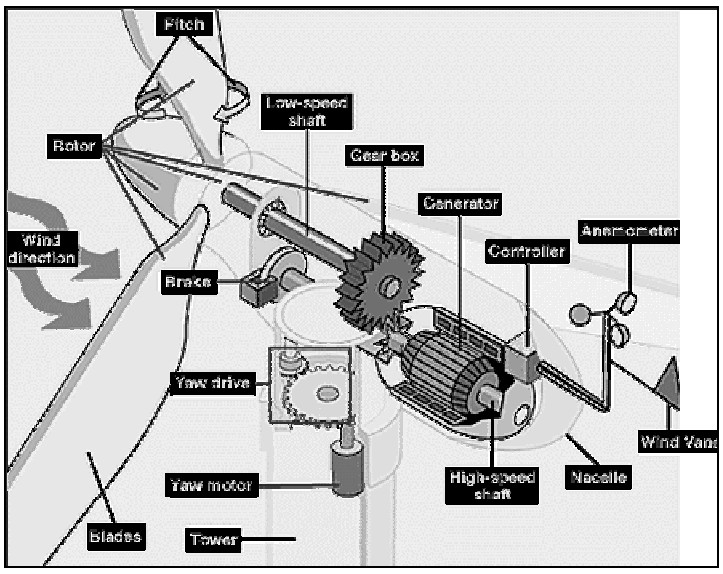

Figure 1-3 Basic wind turbine components [5]

The nacelle is the heart of large MW wind turbines. Most of the electrical equipment is housed in the nacelle, sometimes the transformer might be located separately, but this depends on the manufacturer. The nacelle is mounted on a bearing, commonly known as the yaw bearing, it is in turn connected to the tower. The yaw bearing allows the nacelle to turn in the direction of the wind.

The nacelle houses the generator, the gear box and the controller. The gear box is connected to a low speed shaft, which in turn is connected to the hub and the rotor blades. Most widely used wind turbines of today have 3 blades, usually made of glass fibre reinforced plastic (GFRP). It is not unusual to find wind turbines that have blades made of wood epoxy as well. More detailed information about the history and the designs of wind turbines can be found in different books [6]. The use of GFRP is because of both its high mechanical strength and light weight properties.

The power generated by a wind turbine is directly proportional to the area covered by the blades, thus the size of the blades in new wind turbines is increasing. The power from the blades is transmitted to the gear box through the low speed shaft where it is transferred to a high speed shaft. The mechanical power transferred to the high speed shaft rotates the rotor of the generator, this generating power. All wind turbines must have some form of power regulation to limit the maximum mechanical power that the driveshaft and all components connected to it are subjected to [7]. A wind turbine is designed to generate maximum power at wind speeds between 13-15ms^{-1}. If the wind speed increases above the mentioned value, the rotor needs to be less efficient so as to counter balance this increase in speed. This means of controlling the blades, and is called regulation, which can be classified into two types, pitch and stall. Pitch regulation

is performed by mounting the blades onto pitch bearings when they are mounted on to the hub; this allows them to freely rotate radially along their axis. Thus when required the angle of incidence (Figure 1-4) of the blade can be varied so as to minimise the power transferred from the blades to the driveshaft. The change of the angle of incidence is done by the use of actuator systems.

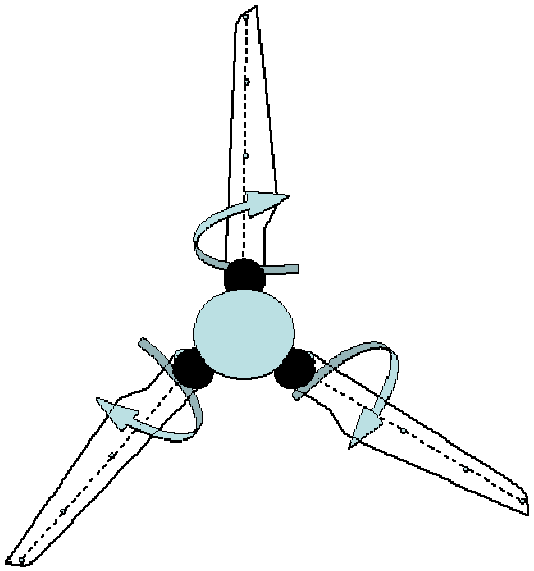

Figure 1-4 Change of angle of incidence of blades (Pitch Regulation)

Stall regulation is a passive method which relies on the blades inherent characteristics, where the aerodynamic properties of the blades limit the torque produced at high wind speeds. The control of the rotor power is achieved by exploiting the stall characteristics of the rotor blade. A blade is said to stall when the laminar flow over the airfoil breaks down and the blade loses lift. This is similar to an aircraft wing “stalling” which happens when sufficient lift to counteract gravity is not available. The blade is designed in such a way that the higher the wind speed, the greater the section of blade in stall. The appeal of this form of regulation is the lack of moving parts (or an active control system) and the speed of response of the system. These blades are sometimes equipped with aerodynamic tip brakes as well. Other components that are installed on the wind turbine are the aviation warning lights, the anemometer and the wind vane.

1.2 SUPERGEN V Wind Energy Technologies– Phase 1

The past decade has seen the increase in the use of wind power as a major source of green energy. The increase in their installation has been followed by research in trying to understand the physics and engineering of the wind turbines in detail, in an effort to try and develop new and better wind turbines. The present work titled ‘Lightning Protection of Wind Turbines’, was part of the Environmental issues theme of the

SUPERGEN Wind Consortium Project which is sponsored by the EPSRC. The SUPERGEN Wind Consortium was broadly classified into 4 themes, followed by further sub-themes within.

- **Theme W - Baseline Wind Turbine Performance.**
  - Reliability and availability analysis.
  - Turbine instrumentation, measurement and data processing.
  - Turbine configuration.
  - Wake development and interactions
  - Forest canopies effect.
- **Theme X - Drive-train Loads and Monitoring the outputs**.
  - Turbine blade, electrical and mechanical characteristics.
  - Condition monitoring systems.
- **Theme Y - Structural Loads and Materials.**
  - Wake effects on blade loading.
  - Novel materials.
  - Structural blade model
  - Tower & blade load reduction.
- **Theme Z - Environment Issues.**
  - Foundation scour.
  - Turbine Radar Cross Section (RCS).
  - Lighting protection and wind farm radar model
  - Interaction of structural, lightning protection and RCS issues.

The present research highlights the risk of lightning to large wind turbines, especially in their new offshore environment. A wide range of issues investigating the effectives of existing lightning protection methods on existing wind turbines are tackled. The effect of the possible new stealth blade concept, for low radar interference, on the lightning protection system of wind turbines are investigated .The work partners include the Communications Department and the Northwest Composite Centre at the University of Manchester.

The present research has dealt with five specific areas. These areas are briefly explained below. In addition to the main sections this thesis will discuss, the lightning phenomena and the different lightning protection methods on existing wind.

➢ **Lightning Data Analysis**: With the help of the lightning strike data acquired from the wind turbine industry, a detailed analysis of the lightning strike pattern on wind

turbine components has been completed. The data analysis identifies the vulnerable parts of the wind turbine in the event of a lightning strike. The data has also been analysed to find a seasonal strike pattern to highlight the risk of increased lightning attachment during winter. The method of recording the lightning strike currents itself has been tested with the help of high current tests to answer discrepancies found in the data sets. The analysis raises questions regarding the new IEC 61400-24 and its relevancy to actual lightning strike phenomena on wind turbines observed worldwide.

- **Modelling of Upward Lightning Initiation and Subsequent Attachment to Wind Turbines:** For use in various studies including those relating to attachment processes, prediction of lightning strike attachment points and the analysis of various lightning protection system designs, it is required to produce an accurate model of a wind turbine within electrostatic finite element software. The model must accurately model the areas around the likely attachment points such as the blade tips and the lightning rods protecting the rear of the nacelle / the aircraft warning lights. The initial use of this model is intended to examine the differences in the electric fields responsible for producing upward propagating leaders from the wind turbine under a near-uniform field as produced by a cloud, a near-uniform field as produced by a low cloud (representing winter lightning). The finite element analysis based in this thesis is mostly based on static models. Whilst the propagation of the upward and downward leader is mostly a dynamic situation, the limitation in the software have only allowed in modelling a static based scenario.

- **Interaction of Lightning Protection with Radar Cross Section Minimization and Carbon Fibre Strengthening:** Collaborative work with the radar and materials side of the project was done to look into novel materials capable of acting as a reflective layer for the a low radar cross section solution and flexible enough to be added into existing blade for strengthening purposes. Though these novel materials are claimed to be highly conductive, their capability of carrying lightning currents has still not been verified. High current tests were performed on sample sheets of the composite novel material to verify if they were capable of carrying actual lightning currents. Also using 3D FEA techniques a blade tip model was developed with the new conductive material integrated into the blade laminate. This model was tested within the electrostatic finite element software, for lightning attachment and to locate possible risk areas due to the addition of the new layer.

- **High Voltage Testing of Blade Lightning Protection System:** High voltage tests on blade tip models were performed and the results have been analysed. The

tests have been performed in accordance to the new IEC 61400-24 standard [1]. Using a UV sensitive camera the streamer activity on the surface of the blade was captured for both positive and negative impulses. AC corona tests have been devised from a research oriented perspective, and these results are later compared to those obtained through 3D FEA techniques. The blade samples tested, also included a prototype sample which includes a carbon layer as part of its bulk laminate.

- **Material Enhancement for Improved Lightning Protection:** The addition of fillers and additives is not a new concept in increasing the electrical breakdown strength in dielectric materials. New ideas and concepts have been discussed to use these principles on wind turbines so as to improve material strength, especially at areas around the lightning receptors, where blades suffer from physical damage.

2 Lightning

Thunderstorm clouds or ‘cumulonimbus clouds’ [8] are often used terms for lightning producing clouds. These clouds are usually represented as a vertical tripole structure from a modeling perspective. The vertically stacked charges are said to be located at different altitudes of the cloud. The heights at which these charges are situated vary from model to model. A basic model is shown below in Figure 2-1.

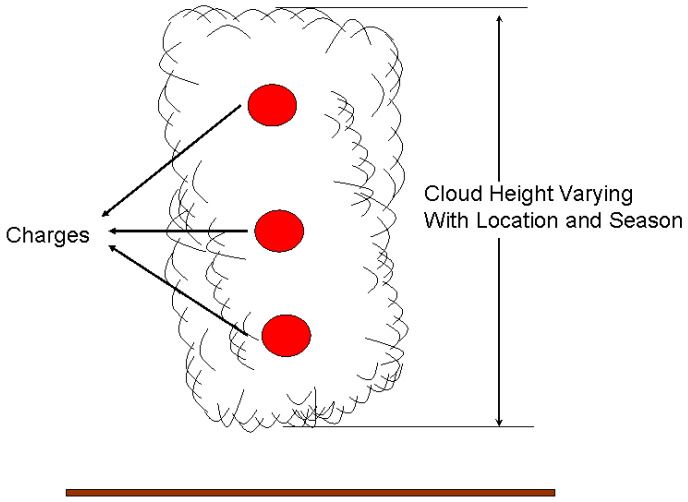

Figure 2-1 Charges in a cloud

The top two charges are said to be the main charges. The charge values vary from model to model. A summary of various models of the electrical structure of the lightning producing clouds is found in [8, 9]. A thunder cloud is formed when parcels of warm, moist air becomes buoyant relative to their surroundings and starts to rise. The heating of the air is usually caused by sunlight. According to [10], the initial cloud models are derived from measurements involving the static charges in the cloud and also how these charges are neutralized due to the lightning phenomena.

Lightning is an atmospheric discharge of current. The highest recorded value of lightning current is around 250kA [11, 12]. However, this value is very rarely seen, the median (for a downward negative stroke) being about 30kA with the median values of charge transfer and specific energy being 5.2C and 55kJ/Ω respectively [11, 12]. The visible part of the lightning strike process, whether lightning strikes the ground or not, is termed as a “lightning flash”. The individual components of this lightning flash are defined as strokes and are shown in Figure 2-2.

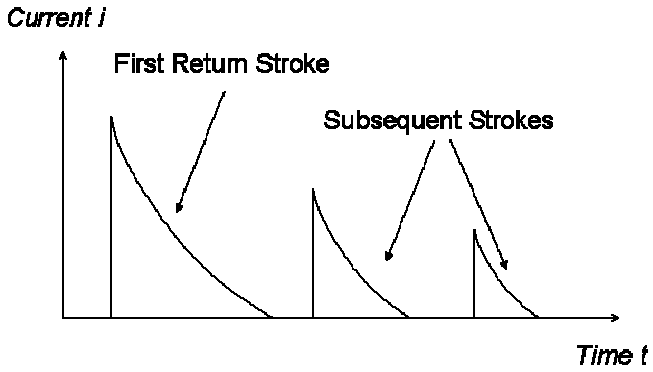

Figure 2-2 Lightning flash and strokes

The numbers of subsequent strokes depend on the geographical location and the type of lightning. This will be discussed in later sections.

Lightning can be classified into two main types, upward and downward initiated. These are also known by the names, cloud-to-ground and ground-to-cloud lightning. These two forms of lightning can be further subdivided into positive and negative polarity respectively, the polarity being that of the charge transferred from the cloud to the ground.

2.1 Downward Initiated Lightning

Downward initiated lightning starts from the cloud with a stepped leader moving towards the earth. The leader tip, is in excess of 10MV with respect to the earth [1]. As the tip gets near to the earth, it raises the electric field strength at the surface of the earth. Where this field is elevated significantly, typically around sharp and/or tall objects, answering leaders are emitted and travel towards the downward propagating leader. When an answering leader and stepped leader meet, this completes the channel or path from the cloud to earth, thus allowing the charge in the cloud to travel through the ionised channel. This is the first return stroke, and has a peak value of upto a few hundred kilo amps and a typical duration of a few hundred microseconds. After a certain time interval, further strokes may follow the already ionised path and are known as subsequent return strokes Figure 2-3. Usually a negative downward lighting flash may contain 2 to 3 subsequent return strokes. Positive downward flashes (only 10% of those observed worldwide) are higher in current magnitude but typically contain no subsequent strokes [1].

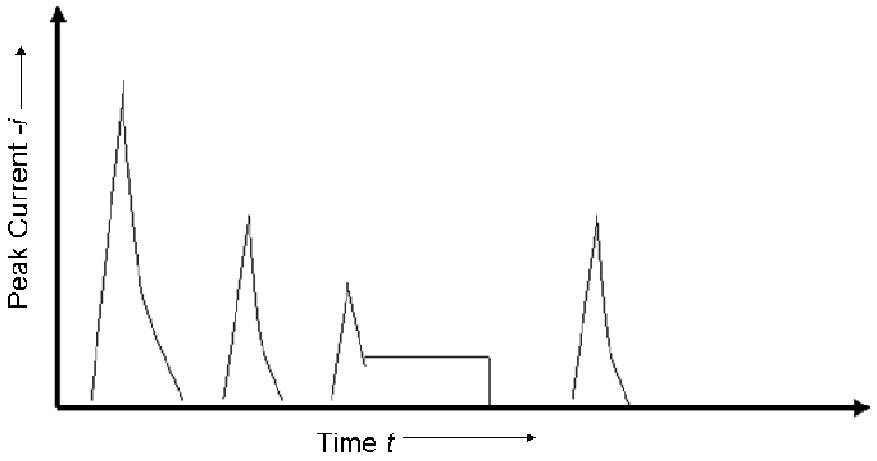

Figure 2-3 Typical profile downward negative initiated lightning

2.2 Upward Initiated Lightning

The presence of tall structures and objects brings rise to another form of lightning, which is upward initiated. Tall structures enhance the electric field produced by a thundercloud and this can give rise to upward propagating leaders that move towards the cloud and which can then develop into a lightning flash. This phenomenon is particularly common where the cloud height is low (often during winter months in coastal areas or in mountainous regions). The profile of an upward discharge is different as compared to that of a downward initiated discharge Figure 2-4. An upward initiated discharge typically starts with a continuing current phase on which may be superimposed short duration high magnitude current pulses. Though the peak current values are quite low at around 10kA [1] as compared to downward lightning, the charge transfer associated with the continuing current phase can be quite high. The initial continuing current in upward initiated lightning may be followed by a number of return strokes that are similar to those observed in a negative downward lightning flash.

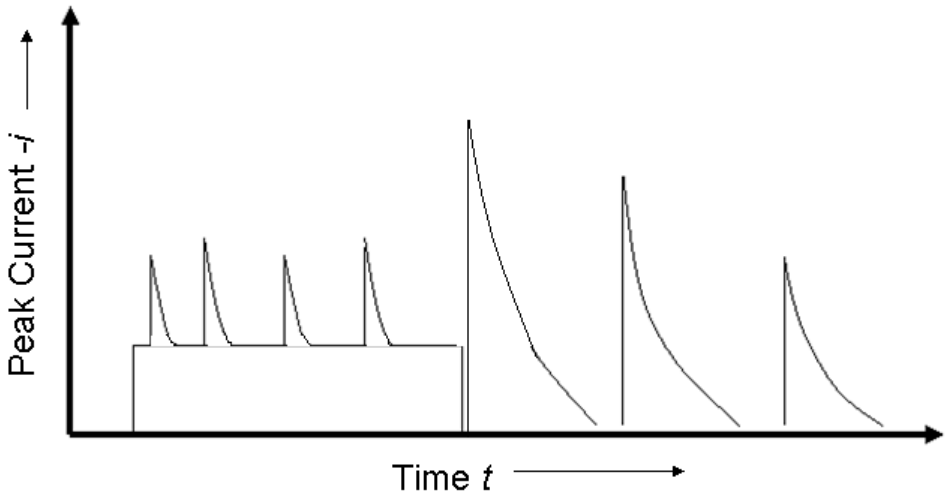

Figure 2-4 Typical profile upward negative initiated lightning

2.3 Lightning Current and Magnitudes

Lightning strikes to small towers and buildings are mostly downward initiated while those from larger structures tend to be upward initiated. According to [9] there have been a large number of instrumented towers on which lightning studies have been conducted. One particular research that stands out is the one performed by Berger at Mont San Salvatore [11] on which most of the lightning standard parameters are based. Most of the observations made on top of Mont San Salvatore are of downward initiated lightning. From Berger's observations, the median value of the negative polarity strikes was found to be 30kA. 5% of these strikes were above 80kA. The positive strikes had a median value of 35kA and 5% of these strikes were above 250kA. Similarly, results found from Italian research stations [13, 14] gave a median of 28.4kA from 27 first strokes. Berger's observations from Mont San Salvatore also included 135 subsequent strokes which had a median of 12kA. In the above analysis, all the strikes were downward initiated. With increase in structure heights, the risk of upward initiated lightning increases. The effect of the structure height was investigated in [15] where 624 flashes on chimneys in Czechoslovakia, Poland, Sweden, Norway, Great Britain and Australia where evaluated. The chimneys were divided into different groups of height. A cumulative distribution showed that 50% of the values exceeded 28kA, 10% 70kA and 4% exceeded 100kA [15].

The earliest investigation of upward initiated lightning was performed on the Empire State Building in New York. Out of the 135 strikes recorded on this 431m tower (which include both downward and upward leaders), the median current exceeded 10kA. Similar recordings were made on the Gaisberg Tower in Austria and Peissenberg Tower in Germany. These two towers are 100m and 160m tall respectively [10, 16, 17] thus falling in the range of modern day wind farms. For the Peissenberg Tower a total of 80 lightning strikes were evaluated [16]. All of the lightning strikes were found to start with a continuing current and thus take to be upward initiated. On the continuing current were superimposed impulse currents. The maximum measured value for the impulse currents was 20.9kA and median current of all the impulse strikes was 4.8kA [16]. In the case of Gaisberg Tower 164 flashes out of 170 measured during a three year period were upward initiated and a maximum peak current of 38 kA was recorded [17].

Lightning parameters are now covered in the new IEC 61400 – 24 standard. The parameters for the downward and upward initiated lightning as adapted from [1] are shown in Table 2-1 and Table 2-2. The table includes the specific energy and the

maximum rate of change of current. The specific energy is the “energy dissipated by the lightning current in a unit resistance” [1]. The term ‘short’ is the part of the lightning flash that corresponds to an impulse current (this current has a rise to half time value of less than 2 ms) [1].

Parameter	Values			Type of stroke
	95 %	50 %	5 %	
I (kA)	4(98 %)	20(80 %)	90	*First negative short
	4,9	11,8	28,6	*Subsequent negative short
	4,6	35	250	First positive short (single)
W/R (kJ/Ω)	6	55	550	First negative short
	0,55	6	52	Subsequent negative short
di/dt_{max} (kA/μs)	25	650	15 000	First positive short
	9,1	24,3	65	*First negative short
	9,9	39,9	161,5	*Subsequent negative short

Table 2-1 Downward initiated lightning parameters [1]

Parameter		Maximum value
Total charge transfer	C	300
Total duration	s	0,5 - 1,0
Peak current	kA	20
Average rate of rise superimposed impulse currents ...		20
Number of superimposed impulse currents		50

Table 2-2 Upward Initiated Lightning Parameters [1]

2.4 Geographical dependence of Lightning

The number of lightning flashes/strikes a location will experience depends on its geographical location. One of the fundamental parameters used in calculating the lightning incidence to an object is known as the ground flash density. The ground flash density is defined as the number of lightning flashes experienced by a square kilometre of area. The ground flash density, during the seventies, was determined by using lightning flash counters [18]. These are now calculated by lightning registration systems which use the principles of magnetic direction finding and time of arrival techniques[19]. Also lightning maps are easily available, an example of such a map is shown in Figure 2-5. Most wind farm operators now have access to such equipment and data thus allowing them to evaluate the threat due to lightning strikes on wind farms.

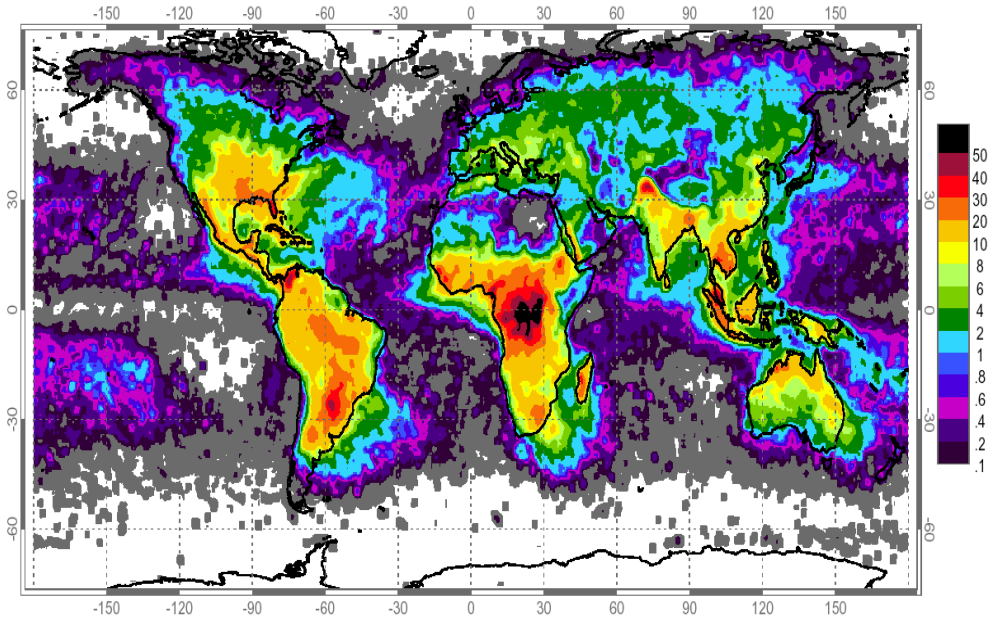

Figure 2-5 Worldwide lightning Strike frequency (flashes/sqkm/yr)

In some research cases there have been platforms which have been installed prior to the installation of wind farms for gathering such data. One such project is the FINO research platforms set in the North Sea which gathers data constantly, lightning parameters being one of them [20].

Using the ground flash density for a particular location the lightning strike frequency at that location can be calculated. A widely used Equation 2-1 for calculating the lightning incidence N (per year) to ground based objects was derived by Eriksson [21], where H_s is the height of the structure in question. The result includes both the upward and downward initiated flashes that attach to the object.

$$N = 24 \times 10^{-6} H_s^{2.05} N_g \text{ flashes/sqkm/yr} \quad \textbf{(2-1)}$$

Where, N_g is the ground flash density and varies depending on the geographical location.

3 Literature Review

3.1 Lightning protection of wind turbines

The increase in the height of the turbines increases the risk of lightning attachment and corresponding damage, the most vulnerable part of the wind turbine being the blades . The main mechanism of damage is when the lightning current penetrates the blade and forms an arc inside [22-24]. The pressure/shock wave could damage the blade, or cause cracks on the surface[24]. Sometimes this shockwave causes damage to the neighbouring blades, even though they have not been struck by lightning directly. The amount of damage that a blade can withstand needs to be in the permissible limits, which are pre-defined. Other damage mechanisms such as punctures, tracking, holes and stitching (where the lightning punctures the blade at several points which making a pattern) also increase the risk of serious damage due to lightning [25]. Due to the risk of damage and possible downtime due to the same, most of the new wind turbines are equipped with different lightning protection systems.

Wind turbine components are divided into Lightning Protection Levels (LPL). Lightning Protection Levels depending on the location of that component with respect to the lightning attachment process. According to [1], “LPL number related to a set of lightning current parameters values relevant to the probability that the associated maximum and minimum design values will not be exceeded in naturally occurring lightning”. The minimum value of this level is used to define out the radius of the sphere in the rolling sphere method (explained later in this chapter), and the maximum value, is the level of peak current that the component will have to withstand during standardisation.

According to [1] “The lighting protection shall be sufficient to enable the blade to accept LPL I lightning strikes (unless otherwise shown by risk assessments) without structural damage that would impair the functioning of the blade“. Lightning protection systems include down conductors and air termination points for conducting the lightning current safely without creating damage to the blade itself.

The Lightning effects on wind turbines can be classified into two types

1. Direct Effects and
2. Indirect effects.

Direct effects are seen as burns, erosion and damage to the structure due to arc attachment. Indirect effects are those which are due to the electromagnetic field that

accompany lightning strikes. The lightning parameters that cause direct and indirect effects are peak currents, specific energy, rate of current rise and charge transfer. Table 3-1 shows the how each of these parameters effects different parts of the wind turbine [26].

Lightning Parameter	Effect	Endangered Components
Peak Current (kA)	Direct	Blades, lightning protection system, and equipment in nacelle
Specific Energy (J/Ω)	Direct	Blades, lightning protection system, and equipment in nacelle
Rate of Current Rise (A/s)	Indirect	Control and electrical system of wind turbine
Charge Transfer (C)	Direct	Bearings and blades

Table 3-1 Lightning Parameters and Endangered Components of wind turbines

From the above table it can be seen that lightning strikes are capable of causing damage to all the main components of a wind turbine. To minimise and limit the damage caused to due to lightning attachment, most wind turbines consist of lightning protection systems to components that are at risk.

Lightning protection of wind turbines is done by divided them into lightning protection zones. Division of the wind turbine into different zones ensures that components such as machinery and control systems are shielded from the effects of a strike that may be prevalent in which the components are placed. The principle of lightning protection in general are [26, 27],

1. Successful interception of downward propagating lightning leaders to preferred attachment point.
2. In case of upward initiated lightning, to make sure the preferred attachment point is the location of the upward leader initiation.
3. Minimizing the heat generated in vicinity of the arc.
4. Conducting the current safely towards the ground, potentially through metallic structures capable of carrying this current.
5. Minimisation of induced voltages and potential gradients.

Lightning protection zones (LPZ) are defined depending on whether or not direct lightning attachment is possible and the magnitude of the lightning current and

associated magnetic and electrical field expected in that zone [1]. The definition of these zones is given below in Table 3-2.

Zones	Direct Lightning Attachment	Full Lightning Current	Electromagnetic field
$LPZ0_A$	Yes	Yes	Un-attenuated
$LPZ0_B$	No	Yes	Un-attenuated
LPZ1	No	Reduced	Attenuated
LPZ2…n	No	Further Reduced	Further Attenuated

Table 3-2 Definition Of Lightning Protection Zones [28]

The differentiation of different components into their lightning protection zones is done using the Rolling Sphere Method [1, 28]. The credibility of this method has been questioned for complex structures [29]. The rolling sphere method is based on the following assumptions stated in [29], and are quoted below.

- "The point of strike of lightning is determined when the downward leader approaches the earth or a structure with the striking distance, and
- The lightning strikes the nearest earth object from the orientation point and so its worst position is the center of a sphere which attaches several earth objects."

In this method the likely locations on the wind turbine that are likely to attach to lightning flashes are identified by rolling an imaginary sphere around the turbine. The radius of the sphere R, is determined by the protection level of the turbine [1]. This imaginary sphere is rolled over the turbine and all the points the sphere contacts is a possible attachment point. For example the Figure 3-1 below shows how to identify the vulnerable points on the wind turbine.

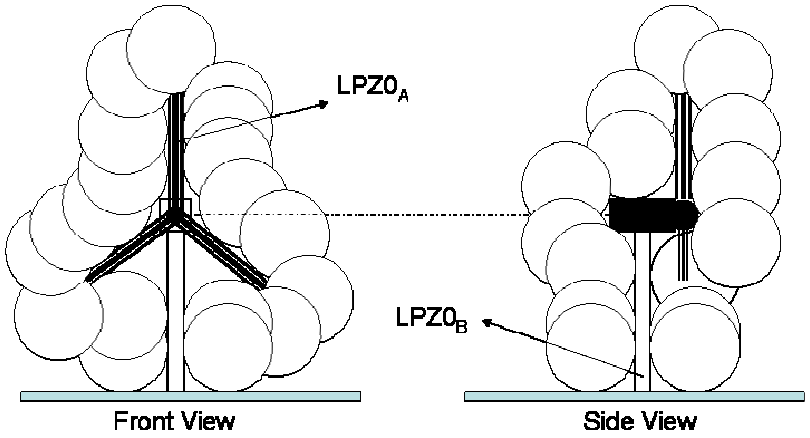

Figure 3-1 Identification of LPZ through rolling sphere method on a wind turbine

From Figure 3-1, the sphere is in contact with the turbine, in all but certain regions, such as under the blades in the front view and under the nacelle in the side view. All

areas that the sphere is in contact are at risk to lightning attachment both direct and indirect effects. The nacelle and the blades fall under the $LPZ0_A$, where they have to withstand both full lightning current and direct attachment.

The nacelle is at risk of being struck by lightning on the top and the sides as well. The lightning protection of the nacelle must ensure that all the components housed in the nacelle itself are not damaged by the lightning strike. Over-voltages and lightning currents conducted or induced should be tolerated. A nacelle made of metal is good for withstanding the direct effects due to lightning attachment, but it is a prerequisite that electrical connection between the metallic cover and the bed plate of the nacelle are sufficient enough to conduct the lightning current[30].To minimise electromagnetic fields from the lightning current equipotential bonding connections are recommended to encircle the interior of the nacelle like a Faraday cage. This is shown in Figure 3-2.

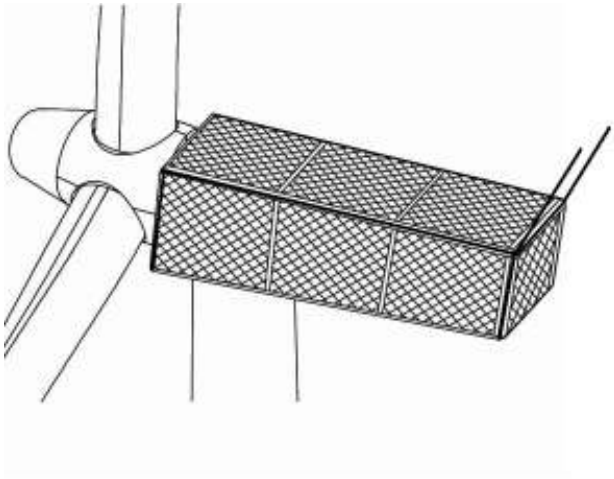

Figure 3-2 Faraday Cage around the Nacelle [1]

Not all manufacturers have a metal nacelle as part of their wind turbine designs. Some of the existing turbines are made partly or completely of non-conducting materials e.g. GRP. In such cases an air termination system is used to protect the nacelle from direct strikes. This can be seen from Figure 3-3.

The air-termination system consists of lighting rods, mesh network and down conductors, thus reproducing a Faraday cage around the nacelle. The positioning of the air termination is decided again by the rolling sphere method.

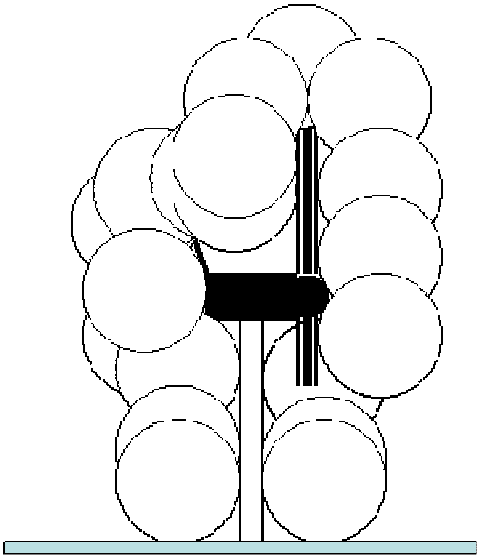

Figure 3-3 Lightning rod protected nacelle

Most of the tower can be struck by lightning; this can be seen from the rolling sphere methodology (Figure 3-1 and Figure 3-3). The lightning flashes usually do not cause considerable damage to steel towers, but still a good connection between different tower sections must be provided. In a concrete tower, it must be ensured that a continuous electrical connection is available via the steel reinforcement inside.

The next component that falls under lightning protection zone $LPZ0_A$ is the blades. This present research will mainly focus on the lightning protection of wind turbine blades, though there are areas where other parts of the actual wind turbine have been discussed.

The blades are the most expensive parts to replace in a wind turbine [23]. With wind turbines moving offshore and the need to mobilise large cranes the financial aspect of replacing these will definitely increase. Thus avoiding any kind of damage due to lightning has become an important issue for both wind turbine manufacturers and operators.

The basic principles of any lightning protection system have been mentioned at the beginning of this section. These principles are achieved on blades by different methods, which have changed and improved with the development of newer and bigger wind turbines. As they are particularly prone to lightning attachment, owing to being the highest part of the turbine, the blades are usually considered an especially important part of the wind turbine in terms of lightning protection. According to [22], rotor blades with built in lightning protection are far less likely to experience extensive

damage as compared to those without. Examples of lightning damage seen on blades without any lightning protection system are shown in Figure 3-4.

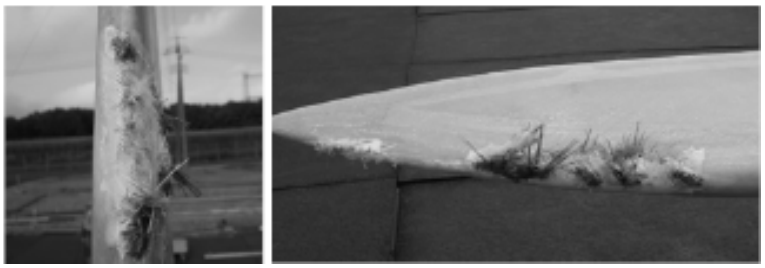

Figure 3-4 Damage caused to an unprotected blade [31]

The different types of lightning protection installed in wind turbines blades are [1]:

i. Air termination systems on the blade surfaces
ii. High resistive tapes and diverters
iii. Down conductors placed inside the blade
iv. Conducting materials for the blade surface

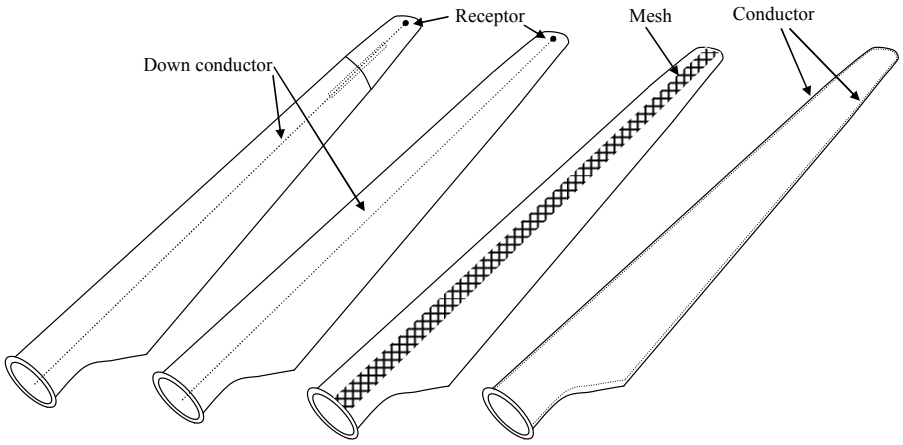

Figure 3-5 Lightning protection systems on blades

Figure 3-5 shows the different kinds of lightning protection systems on blades. In all types of LPS, the metallic air terminations, strips and diverters and down conductors should be of sufficient cross sections that they safely conduct the lightning current without any physical damage.

A system that is widely used is the internal lightning protection system consisting of a internal lightning down conductor capable of carrying the lightning current. This could be due to ease of manufacturing, replacing in case of damage, reliability and costing factors. Metal receptors which act as air terminations penetrate the blade surface and are then connected to the down conductor as show in Figure 3-6.

Figure 3-6 Receptor/Down Conductor based lightning protection system [32]

This system of external receptors connected to an internal down conductor is being widely used for blades upto 60m [1] and the system is not likely to change for blades of larger lengths. The number of receptors on each blade depends on the design of the manufacturer. Even in blades where multiple receptors are fitted, the blade tip receptor is said to be the one which is hit by most lightning strikes [33]. Attachment tests have proven that the blade tips are the most exposed part of the turbine [34]. The maximum electric field seen on the blade depends on its position and in most cases is on the tip of the blade [35].

Statistics of lightning damage to wind turbines has been covered in different parts of literature. Some of the most widely referred to are given in [1, 23, 26]. Some of this data is old and dates back to 2002.
The IEC TR 61400-24 'Lightning Protection of Wind Turbines' is one of the most comprehensive studies regarding lightning protection of wind turbines. Initially developed as a technical report, it is now been reviewed as a full standard. Some of the main summarized points of surveys on lightning damage, for both offshore and onshore wind farms is given below [1, 23],

- 914 lightning damages have been reported over 11364 operational years.
- 4 to 8 lightning faults have been experienced per 100 turbine years for northern European countries.
- 25% of incidents are direct lightning strikes.
- 914 lightning damages represent approximately only 4% of the total number of reported damage.
- As compared to the smaller wind turbines the larger and newer wind turbines show fewer failures in the control system. A sign that the new wind turbines have a much more effective lightning protection system.

According to [1], Denmark and Sweden experienced 3.9 and 5.8 faults per 100 turbines due to lightning. In study performed by the National Renewable Energy Association in 2002 it is said that upto 8 out of 10 wind turbines could be expected to receive one

direct lightning strike a year [36]. Another report from Germany stated that between 1992 and 1995, almost 124 direct lightning strikes were reported on wind turbines [36]. The pie chart in Figure 3-7, which is an extraction from [1], shows that the control system is the part mostly affected by lightning strikes.

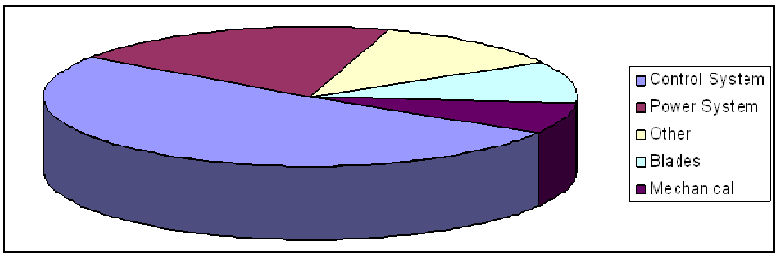

Figure 3-7 Lightning damage to different wind turbine components [1]

It must be noted that from the above that the control system is the most damaged part of the wind turbine. But while assessing the damage done to the wind turbine, the financial losses incurred while replacing a damaged part and also the related downtime must be taken into account. According to [1], the blade damage is the most expensive type of damage to repair. The rotor blades incur the highest losses due to downtime as well. A breakdown of the cost analysis in repairing individual components is given in [23]. This expense increases with the increase in the size of the wind turbine and also to where they have been installed. Offshore repairs are obviously higher compared to those onshore.

3.2 Lightning damage to blades and failure mechanism

New wind turbine blades are made out of composite materials. On of the most commonly used material is Glass Fibre Reinforced Plastic (GFRP). GFRP is known both for its flexibility and mechanical strength over long life cycles. Blade manufacturers are keen in developing new innovative blades, but composite materials still seems to be the choice for manufacturing these blades. Determining the resistance of a blade towards a lighting strike is quite complicated. The addition of the lightning protection system to the composite blade makes it neither completely conductive nor completely insulated. Though there are several kinds of lighting protection systems on blades the basic two principles to avoid damage are still the same.
Successful lightning attachment to preferred locations on the blade and safe conduction of the lightning current away from non conductive parts of the blade.

Each of these tasks is done by different parts of the lightning protection system of the blade. The air terminations, mostly metal receptors, penetrate the blade surface and

are connected to the down conductor. The effects of lightning damage on wind turbine blades have been replicated in labs. One such attempt was performed in [31]. In the tests the blade was tested to lightning attachment in different orientations. Mechanisms of damage included tracking, erosion (Figure 3-8) and in some cases punctures through the blade laminate. Similar damage mechanisms where observed during high voltage testing of blades in [26].

Figure 3-8 Tip receptor and erosion towards the edge of the blade

Inspite of the lightning protection system, there are still cases of lightning damaging wind turbine blades. This will become more obvious with the increase in blade sizes. Lightning can damage the blades in many ways. Some of these are highlighted below,

- There is a possibility of the lightning penetrating the blade surface on polluted blades due to water ingress, moisture etc. Water ingress is the process in which water can enter into the blade laminate, either through cracks or joints in the blade, this could happen over the life time of the blade.
- Surface discharges could damage the blade surface, and over time cause weak points for possible electrical breakdown of the blade laminate.
- Internal discharges inside the blade due to the field enhancement on the down conductor could cause damage over prolonged periods.

While considering the performance of the lightning protection system on a wind turbine blade environmental factors play a vital role. Over its life time a wind turbine blade is exposed to natural forces, which vary depending on the site of installation. For example, wind turbines installed on offshore and coastal sites will experience a lot of salt deposition on the blades. The accumulation of pollutants and other conductive deposits on the blade decrease the efficiency of the lightning protection system and compromise material integrity. According to [37] surface pollutants on the blade increase the risk of lightning leader developing from unprotected areas of the blade. It also states that if the polluted area is not in contact with the air termination, there is a large risk of lightning puncturing through the laminate if it attaches to these polluted areas. Similar results were observed in [31].

Testing of full size blades is very difficult due to the lack of facilities that would allow testing of such huge structures. The above tests are still a good example of the physical damage that is possible due to environmental factors. The surface characteristics are another thing that are affected by the aging of the blade, and in turn affects the performance of the lightning protection. It has been found that wind turbines hit by lightning during operation develop eroded tracks on the surface. The tracks sometimes begin from the receptor and then lead towards the edge of the blade (Figure 3-9). This is a phenomenon which is commonly seen on high voltage insulators. Surface contamination gives rise to localised field enhancement and also forms dry bands. This deteriorates material quality and thus its electrical characteristics.

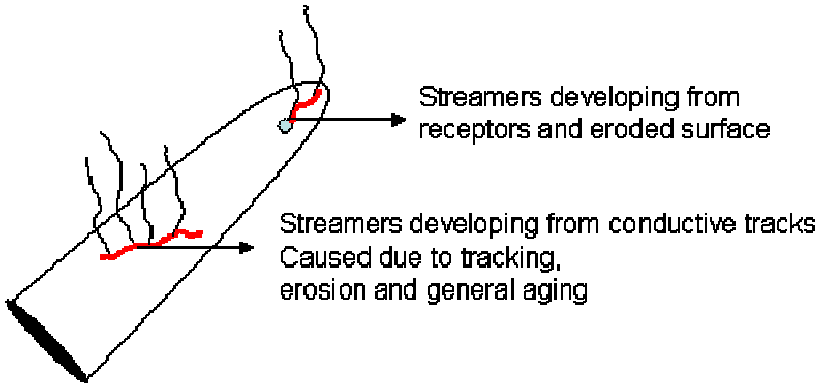

Figure 3-9 Streamers developing from unwanted location of blade

One of the important properties of GRFP is its ability to withstand degradation from water ingress. When composites begin to absorb moisture, the absorbed water will affect the fibre bond in the laminate, leading to a gradual and steady loss in mechanical properties. It was seen in [38] that breakdown strength of the blade laminate play a vital role in determining the efficiency of the lightning protection system.

There are other factors that could be influential in determining the lightning damage to wind turbines. These factors involve things that are not necessarily linked to the electrical or mechanical characteristics of the blade, but are more in relation to the lightning phenomena and the operation of the wind turbine. During lightning attachment to wind turbines, the lightning discharge is not the only process that is moving, the wind turbines blades are moving as well. The attachment process in this case might be different as to normal circumstances. The constant movement (apart from when they are shut down due to maintenance or severe weather conditions) of wind turbines, make it hard to predict the attachment point. An average wind turbine rotates at approximately 15 revolutions per minute. This translates into a 90 degrees change in position within the time span of a long duration lightning strike [24]. This means that the

lightning strike attached to one blade might shift to another blade. With most of the specific energy released in the first return stroke, most of the damage may be experienced by the initial attachment zone. The subsequent strokes might attach to the next blades or different locations, which might explain for the burn and tracking marks.

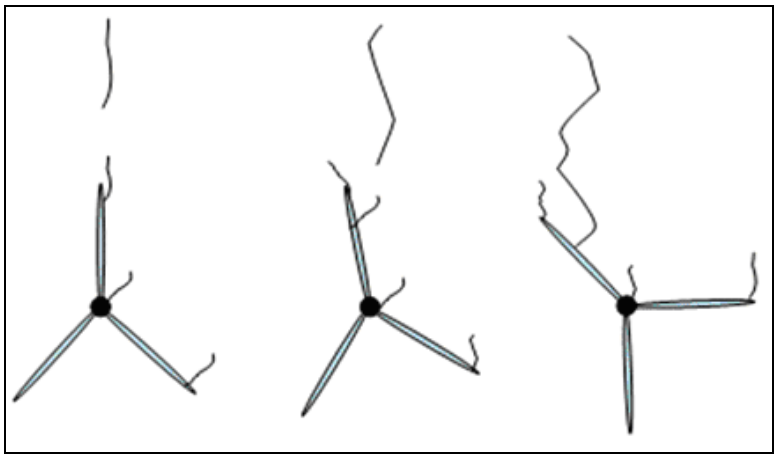

Figure 3-10 Shifting of lightning attachment point

According to [24] the increase in the length of the blades would minimise this problem as the number of the revolutions decrease with the size. But with the increase in the size of the blades, the risk of attachment increases with respect to upward lightning as well. The development of leaders from different parts of the blade might make the attachment point less predictable (Figure 3-10). The extended time of the upward strike might cause the discharge to sweep along the blade length, a phenomena commonly referred as swept stroke and quite common in aircraft lightning research. This phenomenon is shown in Figure 3-11.

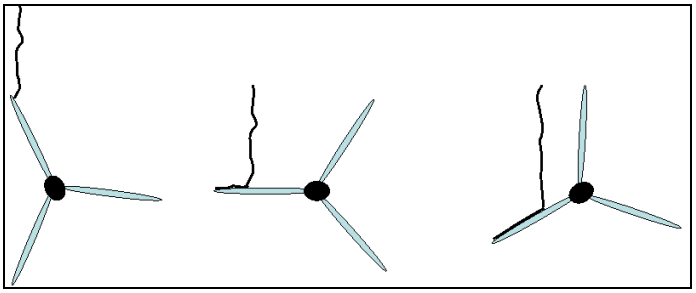

Figure 3-11 Swept stroke in wind turbine blades

Once again, this could be one of the reasons for erosion and tracking on the blade surface. The swept stroke phenomenon depends on the surface properties of the blade and this influences how the channel sweeps along it and determines the different attachment points. This could possibly explain to why the protection is not successful in intercepting the lightning discharge every time. With the help of [39, 40], which explains the phenomenon of swept stroke in relation to aircrafts, resemblance of the phenomenon on wind turbines is discussed below. When the wind turbine blades are in motion, the attachment point may dwell at the same point and thus follow the blade as

it moves through the air (Figure 3-12) or the attachment point may continuously sweep along the surface of the blade (Figure 3-13).

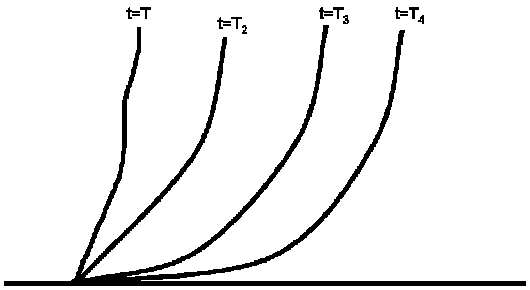

Figure 3-12 Swept Stroke - Attachment point dwelling

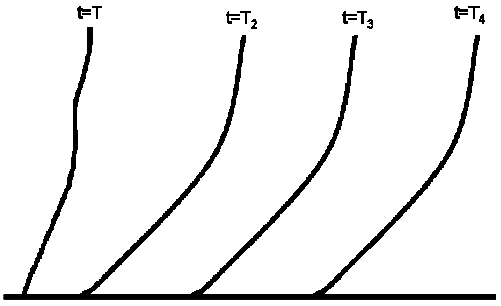

Figure 3-13 Swept Stroke - Sweeping of attachment point.

There is a possibility of reattachment (or reconnection) between a part of the channel and surface. Reattachment occurs when the potential drop along the channel together with the channel displacement and deformation creates a condition where an electrical breakdown between a segment of the channel and the surface is possible (Figure 3-14).

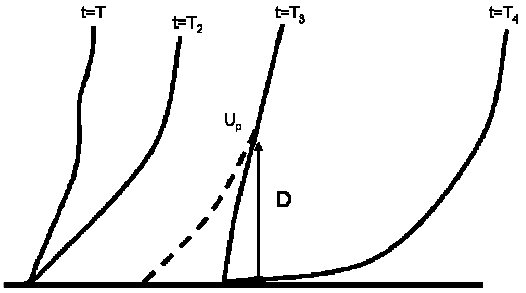

Figure 3-14 Swept Stroke - Reattachment between channel and surface

According to [41], on a base metal surface the lightning channel sweeps continuously or dwells (shortly) at each attachment point, and for a painted metal surface it can be compared to a metallic electrode covered with a dielectric layer. Thus, for an attachment on a paint surface, the painted surface must be punctured. If all these are related to wind turbines, then the lightning channel continuously sweeping across the surface would cause tracking on the wind turbine blade surface thus damaging the laminate. In the case of reattachment the lightning channel can attach to a point where there is no air termination, damaging the laminate. All the above are theories and

assumptions based on available knowledge of the lighting channel moving across an aircraft. This has not been tested practically before on wind turbines. But the burn marks, tracking and general punctures on the blade could possible linked to this phenomenon.

All the above discussed phenomenon, by themselves or together make the lightning attachment process on the blades less predictable. Thus, the challenge arises to how to protect the blades whilst keeping damage at a minimum.

The present thesis deals with the uncertainties in the lightning phenomenon on wind turbines, by analysing lightning data and detailed lightning attachment process on a full scale wind turbines. The present research has also looked into new blade technologies and their impact on the lightning protection system and full scale high voltage testing of prototype new blade technologies. Areas such as new test methods for blades and new material for enhanced blade performance during lightning attachment have been looked into as well.

4 Lightning Data Analysis

Latest wind turbine lightning protection systems are constantly refined to make lightning related damage as low as possible. This is increasingly important as wind turbines move offshore where access for maintenance is more difficult than for most land based wind farms. Manufacturers have been trying to make sure that the lightning protection systems they install comply with the highest protection levels stipulated in the relevant IEC standards. In this chapter, data from the Nysted Offshore Wind farm in Denmark and that from a large number of other wind turbines worldwide is reviewed to show the range of lightning currents that have been measured on wind turbines currently in operation. These current values are compared with the required protection levels within the standards.

The data reviewed in this chapter comes from two specific sources. The first is the Nysted Offshore Wind farm. The wind farm consists of 72 wind turbines placed in eight rows of nine wind turbines each (Figure 4-1). Each wind turbine is 110m high from the mean sea level to the tip of the blade (when one blade is in its vertical position). The distance between wind turbines in the rows is 500 m and the distances between the rows is 850m.

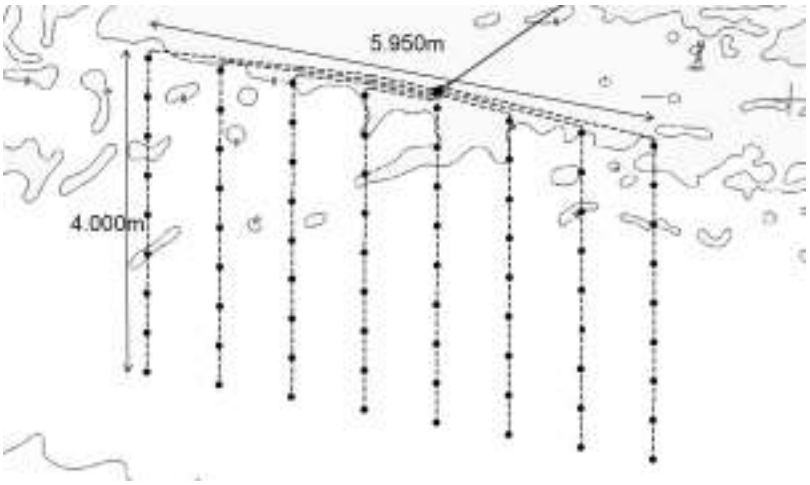

Figure 4-1 Nysted Wind farm

The data has been collected over a period of over three years, the oldest lightning strike record being in June 2003 with the last reading analysed being from in October 2006. This is an equivalent of 216 turbine years. It must be noted that the equivalent turbine years calculated for the turbines present in the Nysted wind farm should not be compared to data collected from an equal number of wind turbines present in different locations of the world. The data thus collected at the offshore wind farm will shed light on the local lightning phenomenon only.

Data at this wind farm is collected in two ways. The first measurement system is the active Jomitek system. This consists of two antennas which are placed on opposite sides of the tower [42, 43]. In the event of a lightning strike to the wind turbine, the lightning current flow induces a voltage into the antennae system as a result of the rate of change of magnetic field around the tower. Lightning strikes away from the wind turbine are discriminated against by adding the outputs of the antennae together. The Jomitek system has a simple analog trigger level which at Nysted Offshore Wind Farm is set to 1 kA peak. The output of this measurement system is connected to the turbine SCADA system. In the event of the system being triggered, an alarm is raised but no data regarding the possible magnitude of the lightning current is obtained. For this reason, peak current sensor (PCS) cards manufactured by OBO Bettermann are placed on the down-conductor of each of the blades and of the air terminals protecting the aviation lights and the wind-vane. These cards have a magnetic strip imprinted with a pre-defined signal. When placed near a down conductor, the magnetic field resulting from the flow of lightning current erases a portion of this magnetic strip and by the use of a card reader, the current that the card has observed can be found.

The erased pattern depends on the value of the peak current, and this pattern is then read by the card reader which initially moves from left to right of the magnetic strip and then right to left of the magnetic strip. This is shown in Figure 4-2

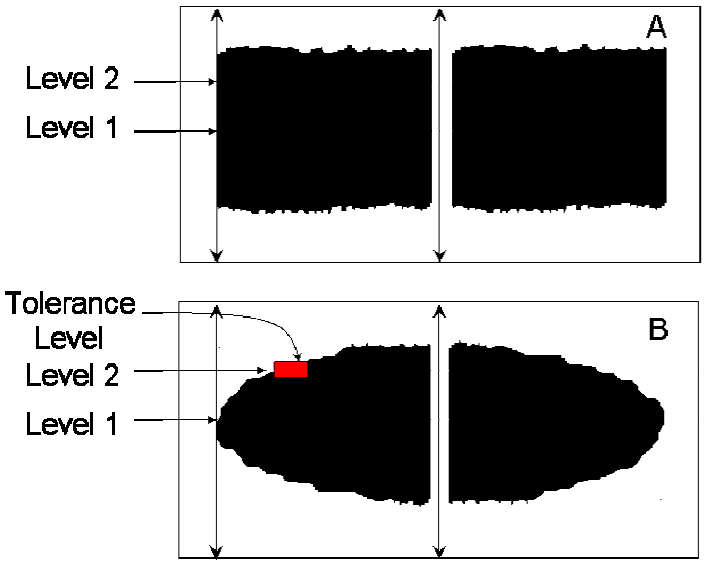

Figure 4-2 Working of PCS card A) Unexposed Card B) Exposed Card

Card A in Figure 4-2, indicates the magnetic strip on a card that has not been exposed to any current. Card B in Figure 4-2 indicates a card that has been exposed to a certain level of current and thus has a part of the magnetic strip erased. When this card is placed in the card reader, it compares the pattern, both from left to right and right to left

of the strip. By comparing the level 1 and level 2 values indicated on the magnetic strip and comparing this with the reference magnetic patterns, the card reader will be able indicate the current level. Also it must be noted that there is a tolerance level in which the level to requires to within. Any deviation from this tolerance level is said to cause an error on the reading and will not indicate the current value [44].

Once the Jomitek system has been triggered, it is possible to go to the wind turbine to remove the PCS cards and therefore gain knowledge of the lightning strike magnitude along with the component struck. Such data is probably as best as can be achieved using the lightning monitoring systems available at present but there remain limitations and difficulties in sorting the data:

- The tolerance levels on the PCS cards means that they fail to record small peak currents (lower than around 5kA according to the manufacturers specification) [45]. In 25% of cases when the Jomitek system was triggered, no readings were observed on the cards. This either means the lightning current amplitude has been too small to be detected by the PCS system or the Jomitek system has falsely registered a lightning strike. There is also a possibility that these strikes could have attached to other parts of the wind turbine where no lightning card has been fitted.

- In 50.8% of cases when readings were observed on the PCS cards, the Jomitek system was not triggered. However, all cards are also changed during the summer maintenance cycles when no corresponding Jomitek reading would be available

- The PCS cards are capable of only recording one peak current (the highest observed) and if multiple attachments are experienced by a component, it is not possible to determine the number of strikes or which strike had the higher peak current. In Nysted Offshore Wind Farm the service instruction was to send a service boat to wind turbines to inspect and exchange PCS cards as soon as practically possible after a lighting alarm had been received from the Jomitek system. Usually the PCS cards were exchanged within few days, and hence the likelihood of multiple lightning flashes being recorded on a PCS card is small.

- The system cannot determine if one component of the wind turbine was hit before another. For example, did the initial stroke go to a blade tip and then a subsequent stroke to another component?

The second data set that has been analysed comes from wind farms all over the world. The database contains records of over a 450 wind turbines recorded over a span of 7 years. However, no active alarm systems are fitted to these wind turbines, Only PCS cards. In addition to the limitations regarding the PCS cards for the Nysted case, this means that between the installation and replacement date of the cards (typically between 5 to 6 months) they could have been exposed to more than one lightning strike. They would not record all of these due to their inherent character of just being able to record the highest peak current.

4.1 Lightning Data Analysis at Nysted Wind farm

4.1.1 Data Analysis Based on Wind Turbine Component

The data from the Nysted wind farm is firstly examined by showing the components of the wind turbine on which the PCS cards indicated current readings following an alarm. Multiple registrations were present on a number of occasions. The data in Figure 4-3 shows that the wind vane and aviation lights PCS cards detected lightning current flowing through these components regularly.

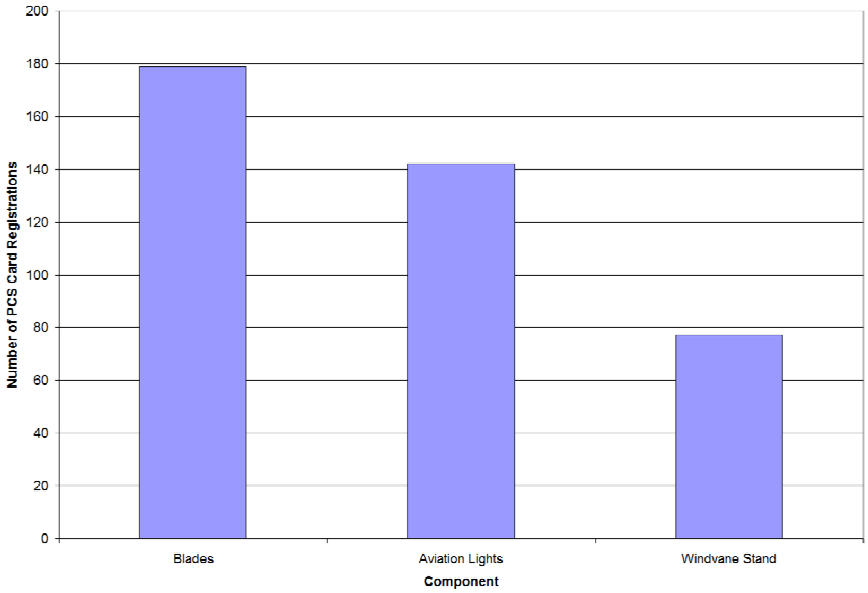

Figure 4-3 Number of PCS cards showing a registration following an alarm

The data from the Nysted wind farm is firstly examined by showing the components of the wind turbine on which the PCS cards indicated current readings following an alarm. Multiple registrations were present on a number of occasions. The data in Figure 4-3 shows that the wind vane and aviation lights (right and left) PCS cards (actually fitted onto the lightning protection rods of these components) detected lightning current

flowing through these components regularly. This result could be perceived as being in contrast to the work by a number of other researchers who suggest that the blades are the parts of a wind turbine that are most likely to be hit by lightning [1, 22, 46, 47]. Results of these papers are mostly derived from data collected from different wind turbines, similar to the data that has been analysed in this chapter. However as most wind turbines are not equipped with PCS cards, and those who are then mainly in the blades, there are for most wind turbines, simply no effective registration of lightning strikes elsewhere but the blades. Thus the information found form the Nysted data in this chapter becomes vital in understanding the lightning attachment phenomenon on different components, due to the installation of the PCs cards is areas other than the blades.

Multiple registrations on different components for a single lightning strike could be accounted for by the following.

Firstly, there is likelihood of increased lightning strikes to the wind vane when the case of upward propagated lightning is considered. The production of upward initiated lightning initially depends on a given level of electric field enhancement existing around a component such as the wind vane / blade and also their position [48]. As a downward leader is not involved, this will purely depend on the overall geometry of the structure.

Secondly, it is possible that upward leaders forming from the wind turbine in the presence of a downward leader result in the passage of currents through the wind turbine down-conductor systems. A typical leader would contain some 45μC of charge per metre [49]. With a typical propagation speed of 1.5cm/μs, this would correlate to an average current requirement of 0.68A for propagation. A sudden collapse in the leader due to a nearby lightning strike / change in electric field could cause higher currents to flow. Assuming a 112 m leader collapsing, at 45μC of charge per metre, the total charge in the leader would be

$$112\times45e^{-6}=5.04e^{-3}C$$

If this leader collapses in 1μs and all the charge in the leader returns to the attachment point, then the current flow through that component would be,

$$5.04e^{-3}\Big/_{1^{e-6}}=5.04kA$$

Thus produce a current of 5kA, a 112m upward leader would need to collapse in around 1μs (equivalent to 1/3rd the speed of light).

4.1.2 Data Analysis Based on Season

The hypothesis of upward lightning being a major contributor to the lightning strike rate is strengthened when the distribution of lightning strikes by month is examined. The data shown in Figure 4-4 gives the peak current readings from each of the PCS cards due to an event detected by the active alarm system by date. In total, 33 out of 58 lightning events occurred during the winter months. This shows that winter lightning is a significant phenomena, even in Denmark which is not in an area particularly prone to winter lightning.

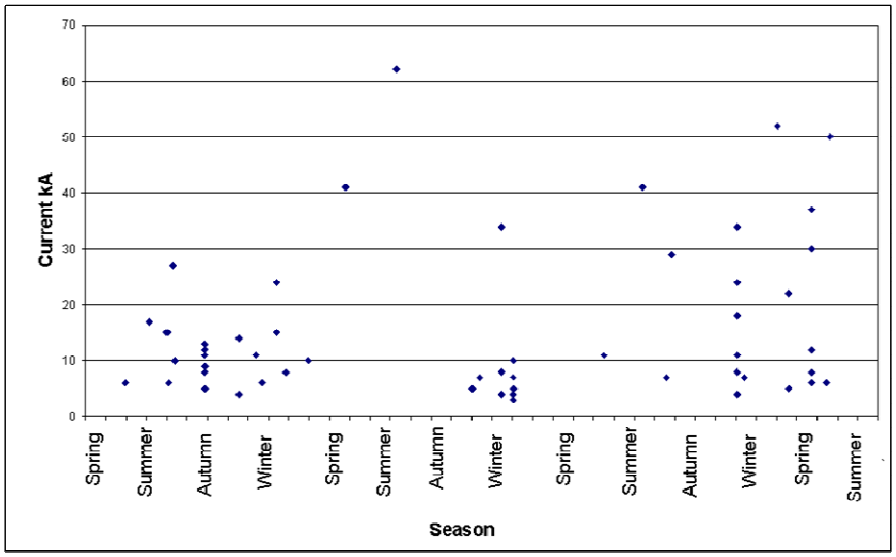

Figure 4-4 PCS Registration and a Corresponding Jomitek alarm notification

Generally, in areas prone to winter lightning, the following has been shown to be observed:

- The incidence of lightning strikes to tall structures during winter is greater relative to that during summer [8].
- A large percentage of these lightning strikes, up to 98% are upward propagating (it is noted that any significantly tall structure in any season is likely to receive mainly upward propagating lightning). Even on flat terrain and for objects of moderate height, there is a large number of upward strikes [8] [50].
- Winter lightning simultaneously strikes more than one tower within a lightning flash. The probability of occurrence of these simultaneous strokes to multiple points was up to 20% in the studies detailed in [50].

4.1.3 Data Analysis Based on Peak Current

The main function of the PCS cards is to record the peak currents of a lightning strike. As mentioned before this does have its limitations. The major damage caused due to lightning is due to the high peak currents of a lightning strike. The peak currents of the

PCS cards installed in the blades and other components in the wind turbine were compared with each other. Examining the data regarding the probabilistic distribution of lightning current values also yields some interesting findings. This data is shown in Figure 4-5.

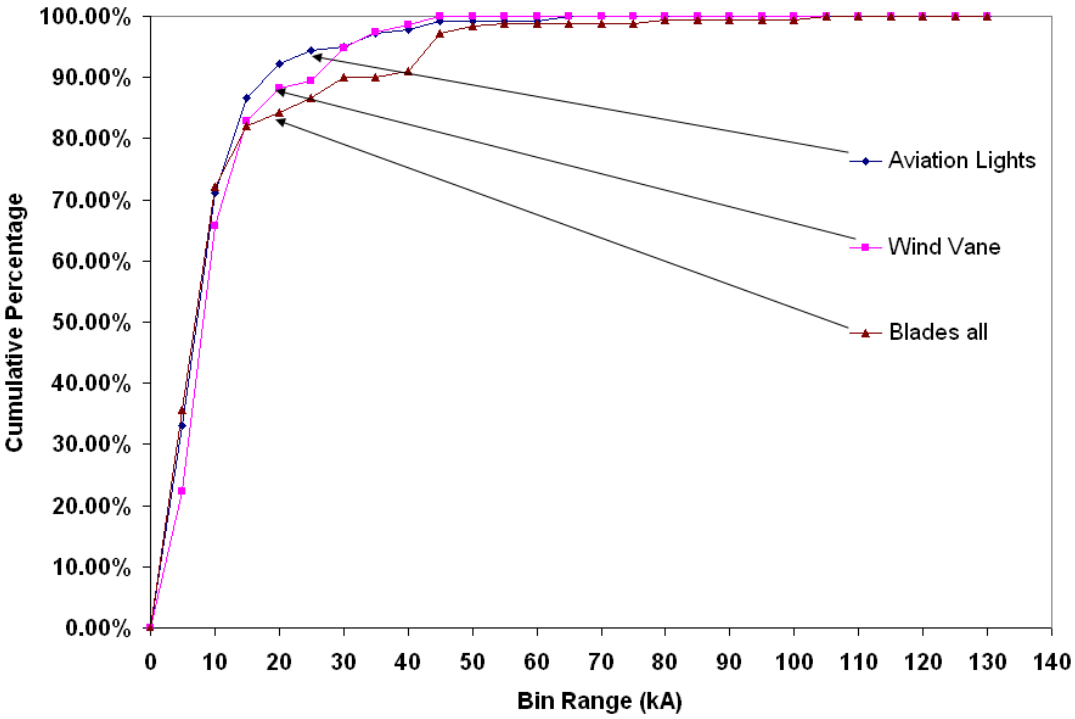

Figure 4-5 Probability distribution of strikes at Nysted.

The blades are shown to capture lightning strokes with the higher peak currents. This is something predicted by the typical downward lightning attachment models such as the electro geometric model [51]. However, in all cases, the mean value of the peak currents lies between 6-8 kA, much less than the mean values of the first return and the subsequent strokes defined in the literature for downward strokes [28].

These small values could be explained by the two options previously stated, i.e. the possible prevalence of upward lightning or the measurement of current produced during leader growth and collapse. A third option is also possible, namely that the standard distribution of lightning strike currents as used by the IEC standards is conservative. The distribution used in the IEC standards is based on measurements carried out by Berger Mont San Salvatore (Switzerland), and further analysed by Kroninger H, Anderson R.B and Eriksson A.J [11, 12, 52] The measurements were done using two towers each 70m high and separated 400m apart. The peak of Mont San Salvatore is 915m above sea level [11]. This site was prone to upward and downward lightning as of recorded over an 8 year period [11], 129 of these have been identified as downward propagating (these being used to formulate the IEC lightning

current distributions). The question that arises here is how relevant it is to base the general lightning parameters used for design of lightning protection systems on (particularly in the case of downward lightning) a small data-set that has been gathered from a mountain which evidently is prone to a large number of strikes the nature of which appear to be strongly influenced by the mountain site itself.

The final analysis of data in relation to the Nysted wind farm relates to the lightning strike frequency and to the distribution of lightning strikes within the wind farm. This is done using Equation (2-1) mentioned in Section 2.4. The result includes both the upward and downward initiated flashes that attach to the object. Using a ground flash density between 0.2 and 0.3km^{-2} yr^{-1} (this has been selected by analyzing the lighting maps of the area supplied by the operator and also through personal communication with the operator of the wind farm), each turbine should have experienced between 0.07 and 0.11 lightning flashes per year. With 72 wind turbines the theoretical value of the number of flashes that the entire farm should experience is between 5.3 and 7.9 yr^{-1}.

Another means of calculating the number of lightning strikes across the entire wind farm would be taking into consideration the equivalent area collection of each wind turbine. The equivalent collection area is defined as the area of ground surface with the same annual frequency of direct lightning flashes as the structure. According to [1], while calculating the equivalent collection area of the wind turbine the wind turbine is assumed as a tall mast whose height is equal to the height of the tower plus one rotor radius. The collection area is equal to the area of a circle whose radius is 3 times the equivalent mast height of the wind turbine (Figure 4-6).

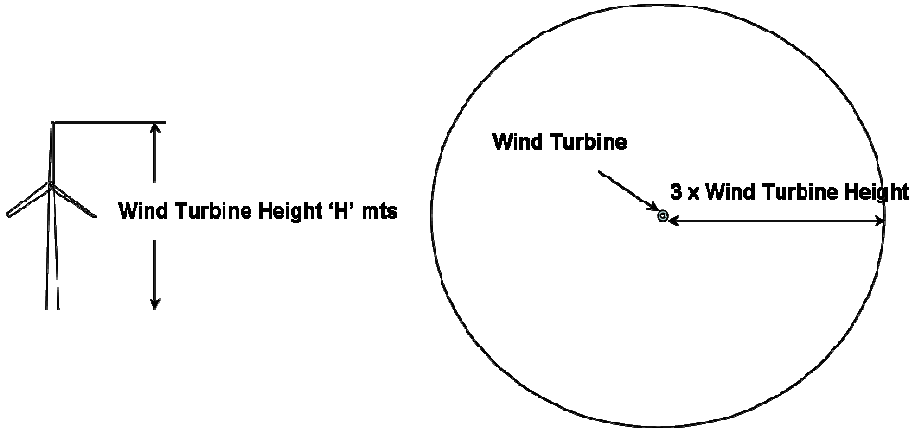

Figure 4-6 Equivalent Collection Area of a Wind Turbine [1]

According to [1], the annual number of lightning flashes to a wind turbine using the equivalent collection area is given by Equation 4-1.

$$N_d = N_g \times 9\pi H^2 \times 10^{-6} \text{ flashes/sqkm/yr} \quad \textbf{(4-1)}$$

Once again using a height of 110 meters and a ground flash density between 0.2 and 0.3km^{-2} yr^{-1}, each turbine should have experienced between 0.08 and 0.13 lightning flashes per year. With 72 wind turbines the theoretical value of the number of flashes between 6.2 and 9.3 yr^{-1}.

The number of flashes that the wind farm actually sees can be estimated in a number of ways using the actual data collected over the wind farm. If the alarm events with a related PCS registration are considered as a flash then there are 127 recordings of current in a three year period, i.e. 42.3 recordings an year, almost six times as much of the highest theoretical value.

If all the PCS registrations were taken into consideration, assuming that each of these registrations relates to a stroke, there were a total of 398 recordings. This equates to a total number of flashes between 398 (i.e. all strokes in a single lightning flash go to one attachment point) and 133 (where with an average of 3 strokes per flash each stroke attaches to a different location – something that is possible but is accepted not to be probable).

This can be compared with 166 alarm events (including those without a corresponding PCS card registration). If each of these alarms is to be considered as a flash, the value is within the region (133-398) of the number of flashes calculated from the total PCS card registrations.

The distribution of these lightning flashes within the wind farm can also be examined. There are a total of 72 wind turbines present in the offshore wind farm, arranged in 8 rows of 9 turbines each. The outside perimeter consists of 30 turbines (42%), leaving 42 turbines inside. The number of recordings on the PCS cards (excluding multiple registrations on different cards on each turbine itself) that the total wind farm has experienced is 127. Out of these 127 strikes, 54 (42%) attached to a wind turbine on the perimeter while the remaining 73 strikes affected a turbine inside the perimeter. The lightning incidence to turbines on the perimeter is therefore similar to that within the perimeter.

If the farm is divided into eastern and western sides, then the eastern side of the array experiences 61 strikes while the western side of the array experiences 66 based on PCS card data. If only those alarm notifications with a corresponding PCS card

registration are taken into consideration, then the western side of the farm experiences 37 strikes while the eastern side experiences only 24 strikes. This data suggests no significant correlation between wind turbine position and lightning risk. If the data relating to blade strikes only is examined, similar figures are found.

In summary, the lightning data from the offshore wind farm has shown:

- All components (i.e. blades, wind vane and aviation lights) are affected by lightning. This would suggest that models predicting lightning strike attachment points need refinement.
- There is a very low average lightning current level detected by the PCS cards. This would again be explained by false readings of the PCS cards, which will be discussed in later sections, or by a high probability of upward lightning strikes or leaders.
- The wind farm is particularly exposed to lightning in the winter months.
- The fact that the wind farm is experiencing lightning strikes six times as high as the theoretical calculations.
- Lightning flashes appear to strike evenly across the wind farm.

4.2 Lightning Data Analysis of Worldwide Data

The second data set that has been analysed comes from wind farms all over the world. The database contains records of over 450 wind turbines, and their lightning registrations over a 6 year period (2000 – 06). However, no alarm systems are fitted to these wind turbines and for this reason, any registration on the PCS cards must be taken as a lightning attachment. As there is no data other than the component on which the PCS cards were fitted, the data analysis is simplistic. The limitations and difficulties in sorting the data were:

- Due to the lack of an alarm system, the PCS cards could have been exposed to more than one lightning strike between the date placed and the date replaced (typically between 5 to 6 months). They will fail to record all these strikes due to their inherent character of only being able to record the highest of these lightning strikes, thus erasing any possible lower peak registrations made before.

- It is not possible to state that a particular component was exposed to the first return stroke while others saw a subsequent stroke

Figure 4-7 shows the peak current readings taken from the blades of all of the wind turbines in the world wide data set. Over 1800 PCS card readings were taken from the blades of the worldwide wind turbines.

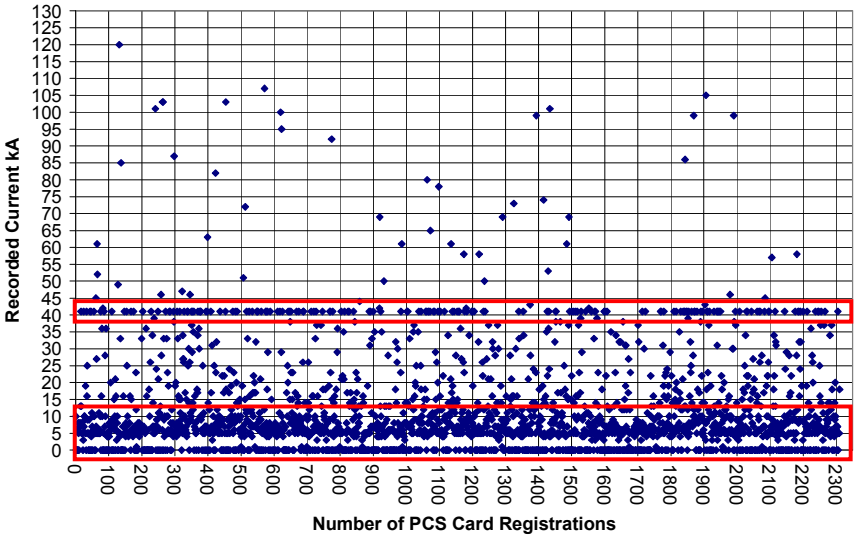

Figure 4-7 Current Distribution of Strikes to Blades from the Worldwide Data

From the readings, it can be observed that peak currents reach a maximum with one reading of 120 kA. As PCS cards are limited to register only peak currents upto 120kA, the actual maximum current could be higher than this, but as there is only one reading at 120 kA this clearly show that very high peak currents are rare . There is a peculiar abundance of readings of 41kA within the data set. This is something that should not be expected from a natural phenomenon and suggests an issue with the measurement system. This will be dealt with in section 4.3.

A probability distribution of the peak currents is seen in Figure 4-8. This is similar to that produced for the data gathered at Nysted, thus allowing a comparison between both sets of data.

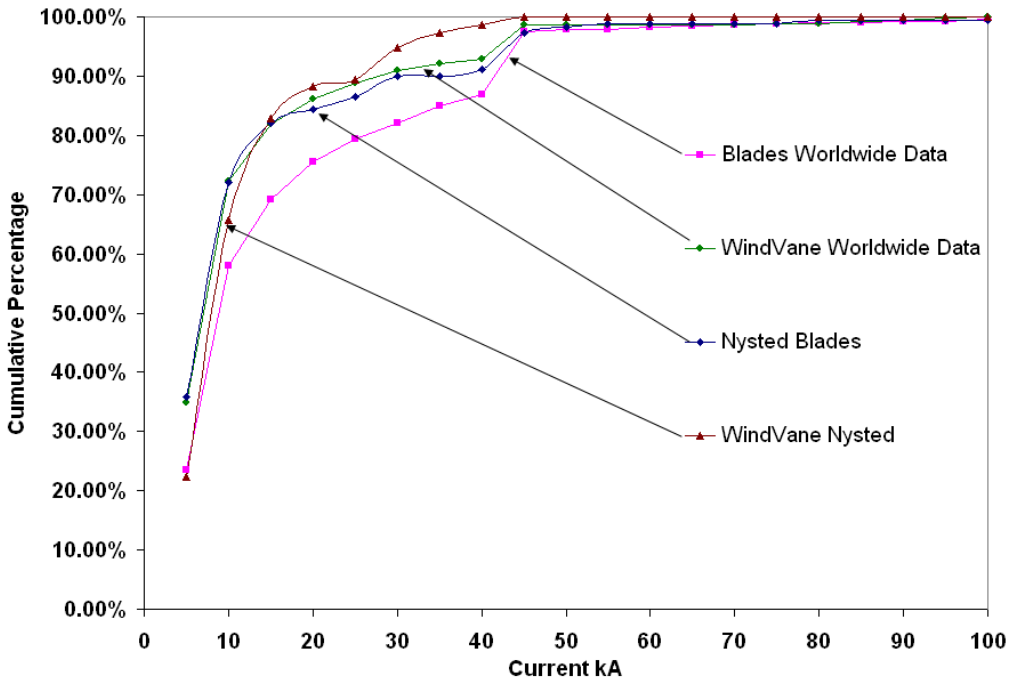

Figure 4-8 Cumulative probability of peak currents on different components.

From Figure 4-8, there is a higher probability of strikes with low peak currents attaching the wind vane as compared to the other components. The aviation lights have not been compared in this graph due to the absence of a significant amount of lightning registration data for that component in the worldwide wind turbine lightning strike data. This is due to the reason that many of these turbines installed worldwide might not have a lightning registration system installed on the aviation lights. Also comparing the lightning strikes of the blades collected worldwide and to that of Nysted, there is a larger possibility of low peak currents attaching themselves to the blades offshore as compared to the rest. This once again brings back the possibility of a large number of these low peak currents being upward initiated lightning. If this is the case, then the move of the wind farms offshore increases the risk of upward lightning as it can be seen from the peak current distribution of the rotor blade strikes compared to those compared to the rest of the world. However, it is difficult to be certain of this conclusion since the cards at Nysted are generally exchanged more frequently than those in other wind turbines. This itself would also lead to a probability distribution of lightning current that has a lower average value or higher as in the case of the worldwide data as the PCS cards are not changed as frequently as compared to Nysted, thus there is a possibility of the cards being overwritten by a strike of a higher peak current.

According to [10], the probability of the stroke current 'P_I' exceeding the stroke current I (kA) is given by:

$$P_I = \frac{1}{1+(\frac{I}{31})^{2.6}} \qquad \textbf{(4-2)}$$

where P_I is the probability of exceeding a certain value of stroke current I kA.

Equation 4-2 can be used to verify the percentage of strikes that theoretically would exceed a certain value of peak current. This can then be compared to the real data to see if the values do coincide. Using (3) the theoretical number of strokes that would exceed a certain peak current value for the 2127 strikes observed at the worldwide wind turbine data and the 397 of strikes across Nysted Wind farm are compared with those actually seen.

Stroke Current I (kA)	Number of strikes exceeding I according to Equation (4-2)	Number of strikes exceeding I according to the real lightning data
120	54	0
100	86	8
80	148	21
60	287	37
40	642	257
20	1430	483
5	1872	1889

Table 4-1 Comparison of Theoretical and Observed Current Magnitudes for the Worldwide Turbine Data

Stroke Current I (kA)	Number of strikes exceeding I according to Equation (4-2)	Number of strikes exceeding I according to the real lightning data
120	11	0
100	18	1
80	31	2
60	60	3
40	135	20
20	300	48
5	393	269

Table 4-2 Comparison of Theoretical and Observed Current Magnitudes for the Nysted Wind farm Data

From Table 4-1 and Table 4-2, a large number of the strikes from the real data set lie between 5 and 20 kA. This coincides with the previous assumptions that a large percentage of the lightning strike data consists of low peak current strikes and that these may be upward initiated lightning.

4.3 Testing Of PCS Cards

To ascertain the detection limits of the PCS card more accurately, a series of high current tests were carried out. According to the manufacturer, the PCS cards are said to be able to record peak currents between 3kA – 120 kA. However, the accuracy of these cards has been questioned before [44]. The OBO PCS cards claim to have a range of 3kA to 120kA with results deviating not more than ±2 kA, but according to the tests performed in the above research the cards failed to detect small (2kA to 5kA) currents, subsequently it was concluded by the authors that the minimum current required to trigger the cards was above 5 kA.

To verify these results and to try and explain the phenomena of the recurring registrations of 41kA, tests were performed on PCS cards in a high current laboratory. The tests would also help explain whether the way in which the cards were mounted would have any significant impact on the readings.

The PCS cards used in the collection of the data are of the size of a credit card, with a magnetic strip. This magnetic stripe has a magnetic pattern impressed on it. The card is held in a card holder which is then clamped to the down conductor. The basic principle of the cards operation is as follows; when current passes through the down conductor, the magnetic field formed around the down conductor erases the already impressed magnetic field pattern on the magnetic strip of the card. The cards are then read by a specific card reader, which senses the magnetic field by swiping the read head across the magnetic strip. A detailed working of the cards is given in [44].

Tests were performed on two sizes of down-conductors, a 6.6mm diameter copper stranded wire and a 10mm diameter steel wire Figure 4-9

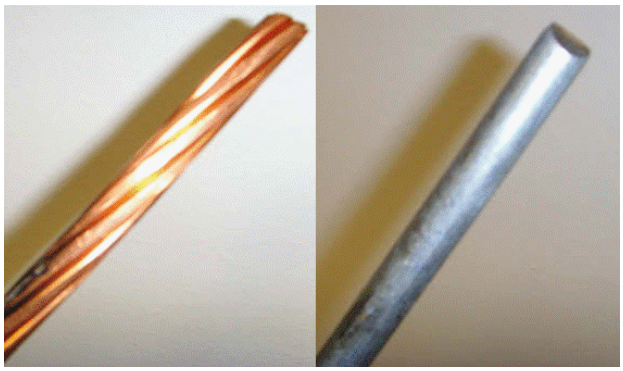

Figure 4-9 Down Conductors for PCS card tests

Five PCS cards were used for each test in order to examine the variation between the readings of individual cards. They were mounted as shown in Figure 4-10.

Figure 4-10: Mounting of PCS cards on down conductor

Peak currents of three waveforms, a 10/350, an 8/20 and a 12/53µs, were used at current levels of 10, 20, 30, 50, 70 and 100 kA. Lightning rise and decay times vary, and no two lightning strikes are the same in terms of waveshape. The testing of the cards on different waveshapes will confirm if the different rise and decay times have any effect on the registration system of the PCI cards. The cards were read and replaced after each level of peak current. Tests confirmed that for the wave shapes tested, the cards showed little variation. The tests also showed that the larger diameter conductor does reduce the level of current read by the cards as would be expected owing to the lower level of magnetic field that the cards will be subject to.

Figure 4-11 gives the average of the 5 PCS card readings for the 10/350 wave shape. Overall, the mean readings of the cards show a reasonable linearity but the error bars indicate that individual measurements can be grossly inaccurate.

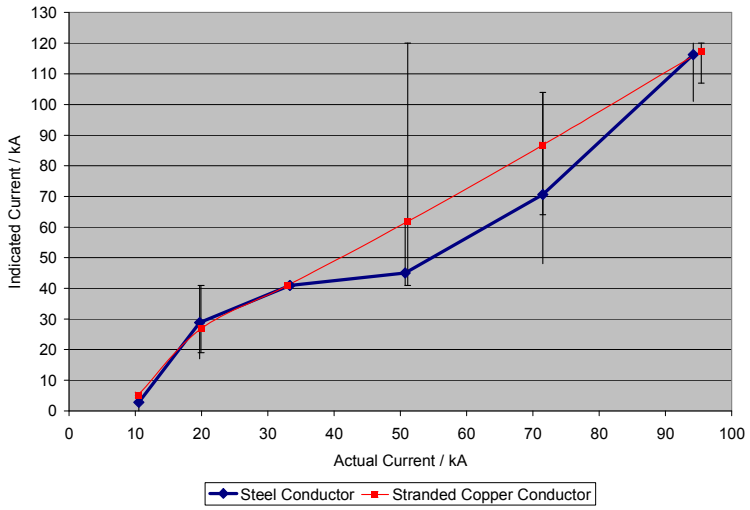

Figure 4-11: Results of PCS Cards Exposed to Peak Currents – Wave shape 10/350µs

Measurements taken at currents of 30kA and 50kA had a tendency to indicate 41kA on all occasions. The 41kA readings observed in the lightning current data are therefore likely to have been caused by lightning currents in this region. On the lower side of the spectrum, the PCS cards fail to register peak currents below 5 kA. The cards were

tested at under 5 kA with an 8/20 wave shape (Figure 4-12), and all cards fail to register any peak current.

Figure 4-12 Testing of PCS cards for peak currents below 5kA

4.3.1 Assessment of Impact of Multiple Lightning Strikes on Card Readings

To examine the effect of PCS cards being exposed to multiple lightning strikes, a set of five cards were subjected to multiple strikes. The set of cards that had already been exposed to an initial strike on the steel conductor were used for this test. After reading the registrations on the cards after the initial strike, they were exposed to a further two strokes each of 20 kA, to see if this changed the initial recorded values. The results of the test are shown below in Table 4-3:

Initial Applied Current kA	Reading After Initial Strike			Reading After Subsequent Strokes		
	94.5	**50.5**	**33**	**94.5**	**50.5**	**33**
OBO card 1	>120	41	41	>120	41	41
OBO card 2	104	50	41	104	50	41
OBO card 3	104	41	41	105	41	41
OBO card 4	108	41	41	108	41	41
OBO card 5	>120	41	41	>120	41	41

Table 4-3: PCS cards exposed to multiple strikes

From Table 4-3, it can be said that there is no impact of subsequent strokes on PCS cards that have already registered a peak current. The cards still read the same results after exposure to two immediate strokes of 20 kA.

The final test performed was the variable distance test, where the cards were bundled together, one on top of each other, but at a constant distance of 2 mm (denoted by ‘d’ in Figure 4-13) from the previous card. The cards are connected on a steel conductor of 10mm diameter. The basic arrangement of the cards attached on the conductor is shown in Figure 4-13.

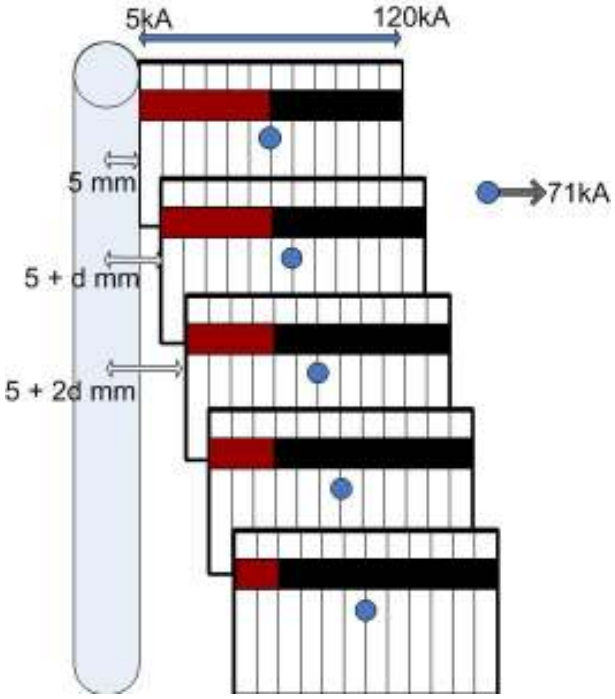

Figure 4-13 Arrangements of Cards for Variable Distance Test

This test was performed inorder to simulate the effect of using the PCS cards on conductors of different diameters. This can be understood by observing Figure 4-14, which shows the relationship between the magnetic field and the radius of the conductor for the same peak current of 71kA, calculated using Equation 4-3 $H_{threshold} = \frac{I_p}{2\pi(x+r)}$ A/m **(4-3)**. From the figure it can be seen that the magnetic field strength for the same peak current decreases with the increase in the radius of the conductor. Thus from the arrangement shown Figure 4-13, this effect can be simulated, and the effect of larger diameter conductors on the PCS registrations can be observed.

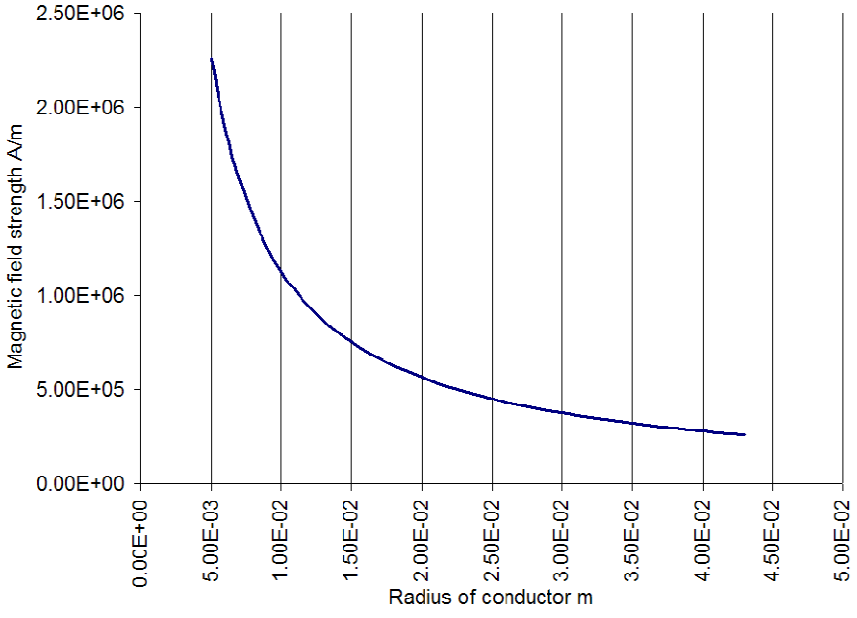

Figure 4-14 Relationship between radius and magnetic field strength

After arranging the cards as shown in Figure 4-13, they were exposed to a peak current of approximately 71kA with a 10/350μs wave shape. As would be expected, the level of current indicated on the cards reduces as the distance from the conductor increases (Figure 4-15).

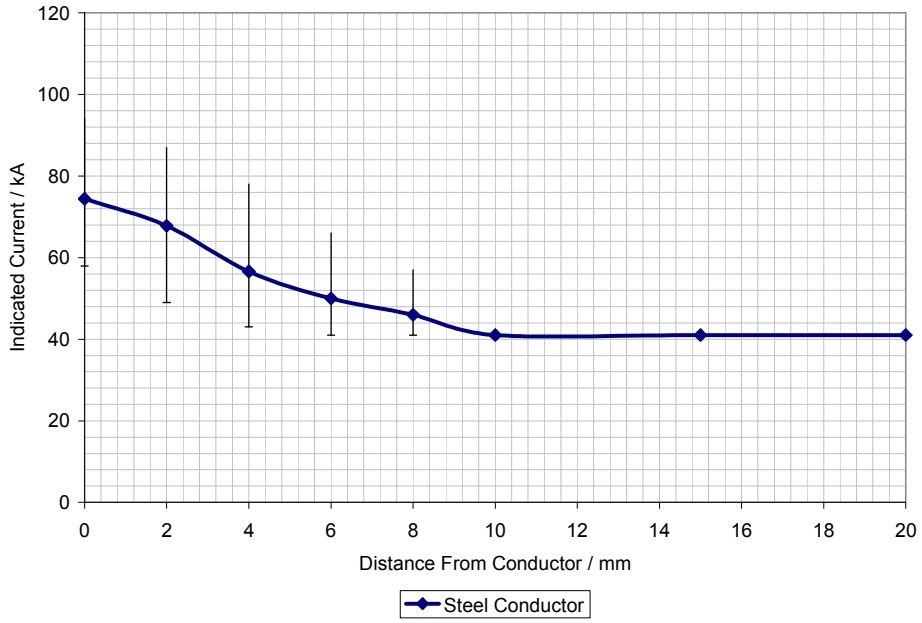

Figure 4-15: Variable Distance Tests

The results can be explained from Figure 4-13. The red shaded area is the required length of the strip that has to be magnetised for a 71kA registration. But as the radius of the conductor increases, the magnetic field strength decreases, only magnetising a part of the required area and thus indicating a lower magnitude of peak current than 71kA. These results are compared with those calculated theoretically. As mentioned before, the card uses the magnetic field created when the lightning current passes through the conductor to magnetise the strip, the length of the strip magnetised depending on the magnitude of the current passing through the conductor. It was seen from the tests cards capture peak currents ranging from 5 – 120kA. Depending on the level of current a certain length of the PCS card is magnetised, the range being from 5kA to 120kA.

A threshold magnetic field is calculated using Equation 4-3, for the maximum of 71kA.

$$H_{threshold} = \frac{I_p}{2\pi(x+r)} \text{ A/m} \qquad \textbf{(4-3)}$$

Where 'I_p' is the peak current, 'r' is the radius of the conductor, and 'x' is the length of the magnetic strip on the PCS card that needs to be magnetised for indicating a peak current 'I_p'.

In Equation 4-4, for a 5kA minimum reading *x*=0m, and *x*=85mm for the maximum120 kA.

From Equation 4-4, and using the magnetic field strength of 5kA and 120kA, the magnetic field strength $H_{threshold}$ for 71kA is found to be 159.1kA/m.

Using the above threshold magnetic field value the required length of magnetic strip that needs to be magnetised for 71kA on the PCS cards tested through variable distance (theoretically performed for cable sizes of radii 5, 7, 9, 11, 13, 15, 20 and 25mm respectively) is calculated.

The magnetic field required for the peak current readings obtained form the variable distance tests is calculated to find the current level that would have been indicated if the same PCS card was placed on a conductor of 0.005m radius.

Table 4-4 shows the results and how they can be interpreted.

PCS card distance from conductor 'd' m	Effective radii of conductor = (r+d)m	Indicated current on cards kA (I_I)	Calculated Current kA (I_c)
0.00E+00	5.00E-03	74.4	7.09E+04
2.00E-03	7.00E-03	67.8	6.80E+04
4.00E-03	9.00E-03	56.6	6.52E+04
6.00E-03	1.10E-02	50	6.24E+04
8.00E-03	1.30E-02	46	5.96E+04
1.00E-02	1.50E-02	41	5.69E+04
1.20E-02	2.00E-02	41	5.02E+04
1.40E-02	2.50E-02	41	4.37E+04

Table 4-4 Effect of conductor diameter on PCS registration

A comparison of the current levels indicated on the PCS cards used on the variable distance test, to that of what would have been indicated on a PCS card that has been attached to 0.005m radius conductor is shown in Figure 4-16.

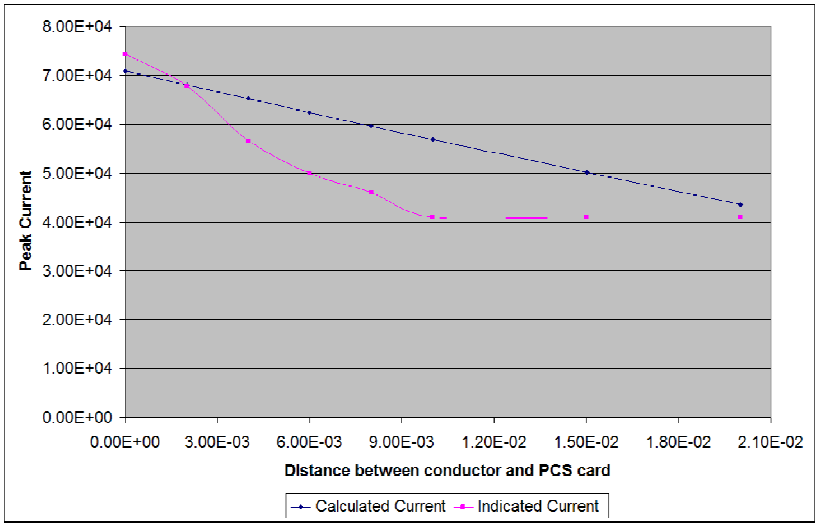

Figure 4-16 Peak current indicated on variable tests Vs calculated for 0.005m conductor

From the results it is seen that there is seen that theoretically for a conductor of smaller radius the values are higher than that compared to one which in larger. An increase in the conductor size decreases accuracy, and therefore indicating a much lower current. These test results have not been applied to the data sets within the data analysis but they do show the importance of considering the radius of the down conductor when trying to analyse lightning current data. The PCS cards analysed in the lightning data have been connected to a down conductor of cross sectional area of 50mm^2 this is in accordance to the IEC 61400-24 'Lightning Protection of Wind Turbine' standard minimum stipulation for the down conductor cross sectional area, corresponding to a radius of 3.99mm. The use of OBO Bettermann PCS cards on a conductor of this size would provide accurate lightning current results. However, for larger diameter conductors, PCS card registrations could experience discrepancies as seen from the varying distance tests.

The conclusions from the tests can be summarised as:

- The PCS cards are generally accurate at measuring lightning current values when large quantities of measurements are taken but cannot be relied on for accurate individual measurements.
- Measurements of 30-50kA tend to always indicate 41kA on the reader.
- Use of the cards on conductors with radii of around 5mm will yield the most accurate results.
- Wave shape has little impact, peak current is important.
- Subsequent lower amplitude strokes do not affect the peak current reading.
- Currents of less than 5kA could not be registered.

4.4 A Comparison of the Lightning Data with Standardized Lightning Parameters

The new IEC 61400 – 24 consists of the main informative section and new testing sections. The informative section includes information relating to the lightning phenomena and the types of lightning. The test regimes described in the standard are divided into high voltage and high current tests. The tests can be used to determine [4]:

- The location of possible leader attachment points and flashover or puncture paths on blades and non-conducting structures.
- The optimal positioning of the location of protection devices (air terminals, receptors etc)
- The likelihood of flashover or puncture paths being formed along or through dielectric surfaces.
- The performance of lightning protection devices.

The new tests in the standard have been formulated with the help of aircraft industry lightning standards [12 - 13]. The standard also introduces measures for earthing of wind turbines, information regarding personal safety and lightning exposure assessment.

The high voltage tests that have been proposed are not discussed in detail in this chapter since they are used to assess the likelihood of successfully capturing the lightning strike to a preferred attachment point. What will be discussed are the current levels stipulated in the high current tests. High current tests are used to determine that a component can withstand the temperature rise, charge transfer and mechanical forces imposed on it in the event of a lightning strike. The exact test and the manner by which current is applied to a component depends on the location of that component within the wind turbine. For example, a tip receptor will be subject to arc attachment damage while the blade down-conductor would not. The current level at which a component needs to be tested is decided according to the protection level of the component. Protection levels of different components of a lightning protection system are selected according to [7]. For wind turbines, category I lightning protection is recommended in [4]. Components categorized in under lightning protection level I are tested at 200kA. This value of lightning current is based on historic data (discussed in more detail later). Too low a value set by the standard will result in an increased level of lightning damage. Too high a level will result in a design of wind turbine that may not be economical. In the next section actual levels of peak currents that do attach to wind

turbine components are analyzed. The relevancy of test current levels in the IEC 61400 – 24, in accordance to actual lightning data that has been gathered over different wind farms, will be discussed in this section.

IEC 61400 – 24 only takes into consideration downward initiated lightning. The lightning parameters that are based in this standard are based on data that has been gathered on instrumented towers, part of various research projects [9]. One such research that stands out from these is the one performed by Berger at Mont San Salvatore [5] on which most of the lightning standard parameters are based. Most of the observations made on top of Mont San Salvatore are of downward initiated lightning. From Berger's observations, the median value of the negative polarity strikes was found to be 30kA. 5% of these strikes were above 80kA. The positive strikes had a median value of 35kA and 5% of these strikes were above 250kA. Similarly, results found from Italian research stations [33] [34] gave a median of 28.4kA from 27 first strokes. Berger's observations from Mont San Salvatore also included 135 subsequent strokes which had a median of 12kA.

The parameters in the IEC 61400 – 24 standard are compared, to those seen in the lightning data collected from the Nysted wind farm and the worldwide data, using the cumulative probabilities of the peak currents on different components (figure 28). As stated before the median value of the peak currents for this data lies between 6-10 kA, much less than the median values of the first return and the subsequent strokes defined in the literature for downward strokes (30kA and 12kA respectively) [9]. Two possible reasons for this have been explained before. The third option which is detailed in this section, namely that the standard distribution of lightning strike currents as used by the IEC standards is conservative.

The relevancy of the real lightning data with that of the current parameters can be done by comparing values present in the standard with those found from the lightning data analysis in this chapter. Table 4-5 is a comparison between the values based in the standard [4], [7] for the first stroke (positive and negative) and the subsequent stroke of a lightning flash with those found from Figure 4-8.

From standards	
First Short Stroke +ve kA (50%)	**35**
First Short Stroke –ve kA (50%)	**20**
Subsequent Negative –ve kA (50%)	**11.8**
From measurements	
Blades kA (50%)	**10**

Windvane kA (50%)	**7**

Table 4-5 Comparison between IEC Lightning Parameters and Real Data

From Table 4-5, the values from the probability distribution of the real data is compared with those in the IEC 61400 – 24 and the 50% value of the strikes on all components is shown to be less than those of the first return stroke (both positive and negative). The peak current seen on all components is closer to the subsequent stroke parameter stated in the standard. This once again shows the presence of a large number of strikes with low peak currents – potentially caused by upward lightning which needs to accounted for in the standard. The errors could also be caused by the data on which the standard is based.

The next analysis examines different scenarios and computes theoretical cumulative probability distributions of lightning current based on the known capabilities of the PCS card readers and combinations of upward / downward lightning. The simulation considered lightning striking 10,000 objects all fitted with a PCS card.

The lightning current parameters in the IEC 62305 'Protection against lightning – Part 1', are based on the results and findings of [12, 52] and are presented in the International Council on Large Electrical Systems. [28] Presents the statistical distribution of these parameters as a logarithmic normal distribution. The mean value μ and the dispersion σ_{log} of the peak current are given in
Table 4-6.

Parameter	Mean μ	Dispersion σ_{log}	Stroke Type
I (kA)	**(61, 1)**	**0.576**	**First negative short (80%)**
	33, 3	**0.263**	**First negative short (80%)**
	11, 8	**0.233**	**Subsequent negative short**
	33, 9	**0.527**	**First positive short (Single)**

Table 4-6 **Logarithmic normal distribution of lightning current parameters – Mean μ and dispersion σ_{log} calculated from 95 % and 5 % values**

In this analysis, these probabilistic distributions are used in combination with knowledge from the PCS card tests. The conditions applied during the statistical analysis in regards to the PCS cards are as follows:

- A strike of less than 5kA will be ignored on the basis it is unlikely to be detected by the PCS card system

- Strikes of over 120kA will be limited to a reading of 120kA owing to the limitation of the PCS card system
- Where multiple strikes are assumed to hit one wind turbine, the highest peak current will be stored on the PCS card.

4.4.1 Downward Initiated Lightning Based Scenarios

The first set of scenarios assumed all the lightning was downward initiated. These assume only one component of the wind turbine is hit, i.e. the first stroke location is the same as the subsequent strokes.

The results are shown in Figure 4-17 and the scenarios are given below the plot.

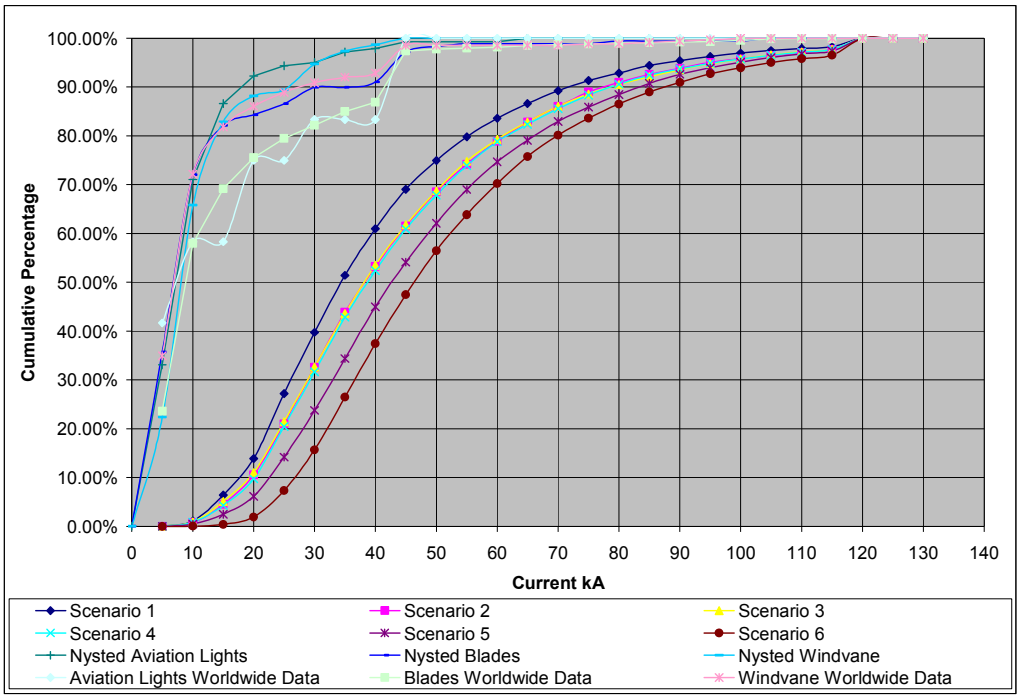

Figure 4-17 First Set of Scenarios Vs Real Data

Scenario 1: One first negative Return Stroke followed by two Subsequent Negative Strokes

Scenario 2: Similar to Scenario 1 but with 30% of the cards struck by an additional first return stroke

Scenario 3: Similar to Scenario 2 but with the 30% of cards being hit by an additional first return stroke also being struck by an additional subsequent

Scenario 4: Similar to Scenario 3 but with the 30% of cards being hit by an additional first return stroke being struck by two additional subsequent stroke

Scenario 5: Similar to Scenario 1 but with 60% of the cards struck by an additional first return stroke and two subsequent strokes

Scenario 6: Similar to Scenario 1 but with all of the cards struck by an additional first return stroke and two subsequent strokes

4.4.2 Downward Initiated Lightning Followed by Subsequent Stroke Based Scenarios

The next set of scenarios take into consideration the possibility of different strokes attaching different components of the wind turbine.

The results are shown in Figure 4-18 the scenarios are given below the plot.

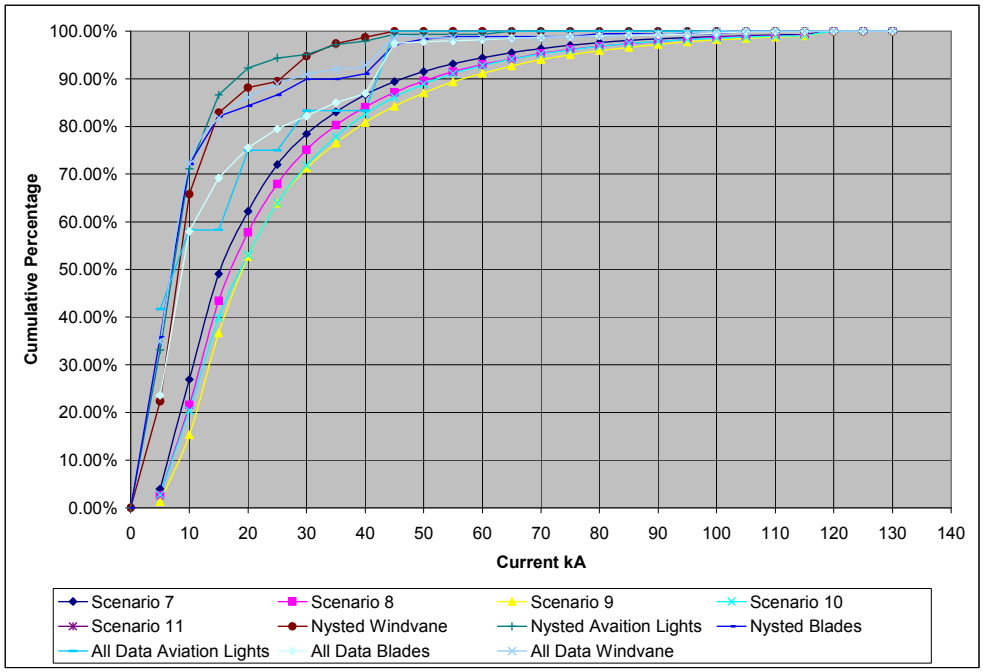

Figure 4-18 Second Set of Scenarios Vs Real Data

Scenario 7: A first negative stroke followed by two subsequent strokes, each attaching to a different location.

Scenario 8: Similar to scenario 7, but 30% of these cards are struck for a second time (first return and subsequent strokes going to the same location as in the previous case)

Scenario 9: Similar to scenario 7, but 60% of these cards are struck for a second time (first return and subsequent strokes going to the same location as in the previous case)

Scenario 10: Similar to scenario 7, but 30% of these cards are struck for a second time (first return and subsequent strokes going to a different location to the previous case)

Scenario 11: Similar to scenario 7, but 60% of these cards are struck for a second time (first return and subsequent strokes going to a different location to the previous case)

4.4.3 Downward Initiated Lightning and Upward Initiated Lightning Based Scenarios

Set 3 starts to look into the effects of including upward initiated lightning strikes into the existing scenarios. For upward lightning, data detailing the cumulative distribution of lightning current observed for upward lightning strikes was considered [16] . In this data, upward lightning is divided into α and β components. These are the impulse currents that are superimposed on the continuing current or that follow the continuing current respectively. In a study performed on the Peissenberg tower, 249 α – components and 74 β – components were measured. The same ratios were taken in order to replicate the upward lightning phenomena.

The results are shown in Figure 4-19 and scenarios are given below the plot.

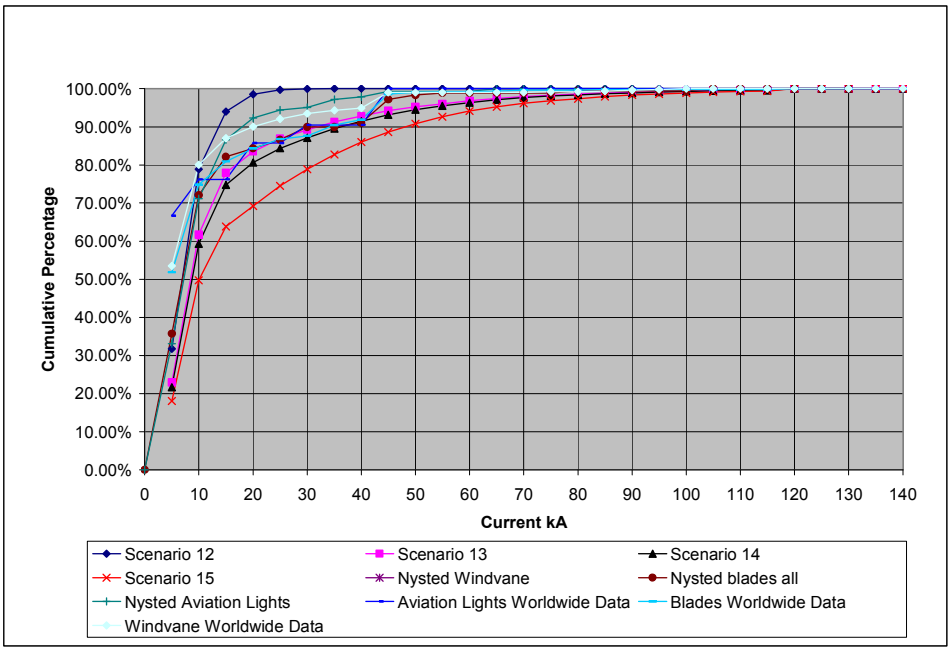

Figure 4-19 Third Set of Scenarios Vs Real Data

Scenario 12: 30,000 upward lightning strikes consisting both α – components and β – components.

Scenario 13: 80 % upward initiated and 20% downward initiated strikes (attaching to multiple components).

Scenario 14: 75 % upward initiated and 25% downward initiated strikes (attaching to multiple components).

Scenario 15: 70% upward initiated and 30% downward initiated strikes (attaching to multiple components).

The Downward strikes only consist of the first negative strike in the above calculations, no subsequent strokes are considered.

As would be expected, set 1 that only includes downward propagating lightning, produces a cumulative probability distribution of current that is considerably different to the measurements observed in the field. Even though there is an inclusion of subsequent strokes in some of the scenarios in set 1, this only moves the probability distribution away from the Nysted and Worldwide data by virtue of lower current values not being able to overwrite the higher values already on the PCS cards. Set 2 moves the probability distribution towards the Nysted and Worldwide as the cards that are affected by the subsequent strokes will register lower average currents than those in the first two scenarios. All of these scenarios are some way from the real data that has actually been observed.

Set 3 provides a close match between the observed data and the predicted cumulative probability distribution of lightning current. It is accepted that an 80% probability of upward strikes is high based on the accepted equations for estimating upward lightning strike frequency probability. However, this high probability of upward lightning would appear to fit with the prevalence of lightning during the winter months and the high percentage of upward lightning strikes found during such periods by other researchers [50].

4.5 Conclusions

1. From the offshore wind farm and worldwide lightning data, the blades are shown to be the most exposed components of the wind turbine. This is in accordance with many other models. However, in the case of the offshore wind farm data and if the external hardware on the nacelle is taken as one entity, the number of strikes to these locations strikes exceed that of the rotor.

2. The results from the PCS cards tests reveal that cards registering peak currents of 41 kA are actually lighting strikes with currents ranging from 30-50 kA, this range could be higher if the conductors used are not of the right diameter The PCS cards are still not sensitive for low peak currents. Strikes below 5 kA are not registered.

3. Testing components for standardisation is a general practice in lightning protection systems. The level of testing is pre-defined in these standards. For example, blades which are characterised as a LPZ 0A and LPZ 0B zones should withstand the effects of direct lightning attachment (or no lighting attachment for LPZ 0B), full lightning current and unattenuated magnetic field. Components in these zones are tested at 200kA. In reality with only a couple of strikes out of thousands reaching this level, the test levels in terms of peak current appear to be very high. However, it must be noted that the data analysed in this chapter only covers 7 years and it is difficult to confirm this conclusion considering the estimated 20 years lifetime of a wind turbine.

4. By simulating different scenarios, it was observed that the lightning parameters found in probability distributions of the new IEC standard are not a perfect fit for large wind turbines. The current distribution of the strikes shows that there are a large number of peak currents below 15kA. The existence of this larger than expected number of low peak current strikes can be reproduced using a probabilistic model that includes 80% of the total strikes being upward initiated.

5 Modelling of Upward Lightning Attachment and Subsequent Attachment to Wind Turbines

Testing of wind turbine blades still remains a challenge, mainly due to their size, which makes it possible to test full scale samples for lightning attachment only in a few places in the world. To overcome this problem, the new IEC 61400-24 standard advices that the first few meters of the full scale blade be tested, and based on the results of these tests, the full scale blade is certified. Certifying a full scale blade based on results obtained from sections of the blade is still questionable, but for the present development of blades, this method has proved successful. There still is still a considerable gap between the actual lightning phenomenon on full scale wind turbines blades in service and the testing them in controlled labs. Using FEA methods, it is possible to now test a full scale wind turbine model. The model can be built to exact specifications to those wind turbines in service and also subjected to electric fields similar to those seen during real thunderstorm. The advantage of being able to model and test a full scale model is that it will help in understanding the interaction of other components (other than the blade) on the actual lightning attachment process. FEA Modelling of lightning attachment to wind turbines has been carried out by other researchers, [34, 35, 48] being examples of some of the work carried out. However, with few exceptions, most of these models were focused on downward propagating lightning and therefore involved the modelling of a stepped leader to examine the resultant electric field environment on/around the wind turbine. One example where upward propagating lightning is considered is where the authors have looked specifically at upward propagating lightning in terms of comparing the likely lightning attachment points when the blades are in motion and when they are stopped [48]. The authors analyze the electric field enhancement for different angular positions of the blades when they are stationary. It was concluded in this paper that the wind turbine was prone to higher field enhancement and that leaders would form in more locations when the blades are in motion. According to [53], this could be due to the rotational effect of the blades, and possibly the reason in self triggering lightning, though there is not much information available in justifying the above find. It was thus advised in [48] that the halting of the blade movement therefore reduces the risk of lightning strike attachment. One other attempt in finding likely attachment points on a wind turbine was performed in [34]. In this paper the authors have built a full scale wind turbine model in FEA and subjected it to electrical fields simulated by charged clouds. The results of this paper showed that the tip of the blade was the most exposed part to direct attachments and with high average peak currents. There are a few drawbacks in the analysis performed in [34]. Firstly the model does not include a detailed lightning protection

system in the blades. Secondly, the material properties of the blade and the other components of the wind turbine have not been included in the analysis. The authors have had to model the entire wind turbine as one material and then set the entire wind turbine to zero potential or ground. This is not the case in reality. The wind turbine blades are mainly made out of GFRP, which is effectively an insulator, and is not grounded. The lightning protection system however is conductive and is grounded. In this chapter however an improved model has been generated so as to try and overcome the above drawbacks.

From the lightning strike data that has been analysed in Chapter 4, it can be seen that upward initiated lightning might contribute to a large portion of the lightning strikes that attach to a wind turbine. Thus while evaluating likely attachment points from a wind turbine in this section, only upward lightning is taken into consideration. In comparison to previous wind turbine models [34, 35, 48] the model used includes the wind vane at the back of the nacelle and the risk of lightning attachment to the same is analysed along with the blades.

In both upward and downward propagating lightning, the formation of upward propagating leaders from the wind turbine is critical in terms of defining the location on the structure that will be struck. For downward propagating lightning, the downward stepped leader provides a non-uniform electric field in the air around the wind turbine. This high electric field, when intensified by elements of the wind turbine lightning protection system, will allow the formation of upward propagating leaders should specific conditions be met. For upward propagating lightning, the mechanism for the formation of upward propagating leaders is nearly identical but in this case the electric field in the air is near uniform being generated by the cloud and not by a stepped leader [34]. This means that the strong influence of the stepped leader position is removed from the consideration of upward leader formation and it is likely that the likelihood of formation will be dominated by the geometry of the wind turbine structure itself.

To consider this issue further, it is therefore important to consider the conditions necessary for the propagation of a leader. These are as follows and have been used in other papers relating to upward / downward lightning (even though these conditions have been derived from laboratory experiments for the streamer inception from Franklin rods) [54]:

Condition (i): The inception of a streamer discharge at the tip of the object by the creation of an electric field in the order of 3MV/m

Condition (ii): The availability of the critical background field necessary for the transition of a streamer into a leader and the continuous propagation of that leader (the magnitude of this critical background field depending on the height of the structure)

There is a constant voltage drop as the leader tip propagates towards the cloud. Thus the background field must be sufficient enough to compensate for the leader voltage drop. It must be noted that though these are the conditions required for the successful attachment, they do not need to be fulfilled in the same order. For example, the background field might be enough for the streamers to develop into leaders, before the inception of streamers itself. Also, if one condition is fulfilled it is not necessarily the case that the other is readily available. For example, a streamer might not develop into a leader if the background field necessary for the propagation is not available. In such a case, according to [54], the streamers will be incepted again and again until there is enough background field for them to develop into leaders.

In this work, finite element models of a cloud and a wind turbine are used to examine the likely locations of upward lightning formation from a wind turbine

5.1 FEA Modelling Of A Cloud And Wind Turbine

In this chapter, the effect of the height of the cloud on the ambient atmospheric electric field is evaluated and the necessary fields for streamer inception and propagation are discussed in view of current wind turbine heights.

5.1.1 The Cloud Model

The basic accepted model of the electrical structure of the cloud as seen in many pieces of the literature is the one consisting of an electric tri-pole (figure 4). A summary of various models that have been modelled based on measurements taken outside clouds can be found in [8]. The cloud model that has been simulated here is taken from this source and consists of three point charges suspended in air at different heights from the ground. In the simulation, the ground has been modelled as a perfect conductor. The three charges of 3C, -40C and +40C are placed at heights of 2, 7 and 12 km from the ground respectively. The charges are modelled as spheres of radii 900m for the 40C charges and 150m for the 3C charge. The size of the spheres is

picked in such a way that the actual meshing of the same would yield the most accurate results. The model is shown in Figure 5-1.

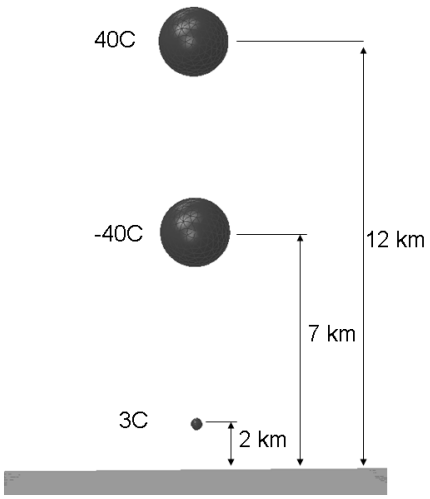

Figure 5-1 Cloud Model (charge sizes not to scale)

Figure 5-2 gives the vertical component of the electric field at the 0m, due to this vertical tri-pole. This plot agrees with that shown in literature [8] and has a maximum ambient field of just over 5kV/m. According to the convention adopted in electrostatic field analysis software, a downward directed field is taken to be positive in polarity [8].

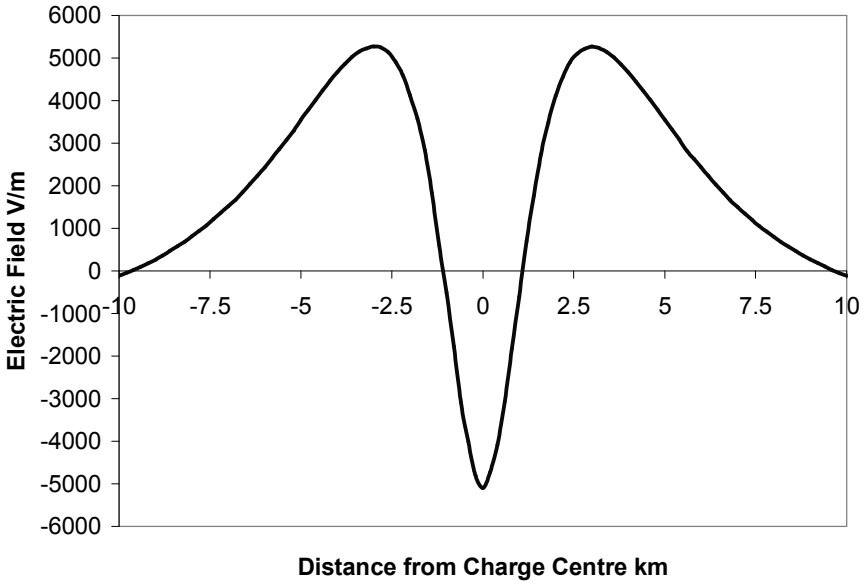

Figure 5-2 Electric Field (Ey) Plot above Ground

There is a perceived risk of wind turbines being more likely to be struck by lightning during winter due to the low cloud height, as mentioned in Chapter 4.

To evaluate the change in the electric field distribution caused by low clouds, Figure 5-3 shows the increase in peak electric field due the lowering of the charges in 100m

steps. The x-axis of this figure refers to the height of the lowest 3C charge. The electric field dramatically increases as the cloud height is lowered as the relative separation of the tri-pole charges become significant in comparison with the distance to ground.

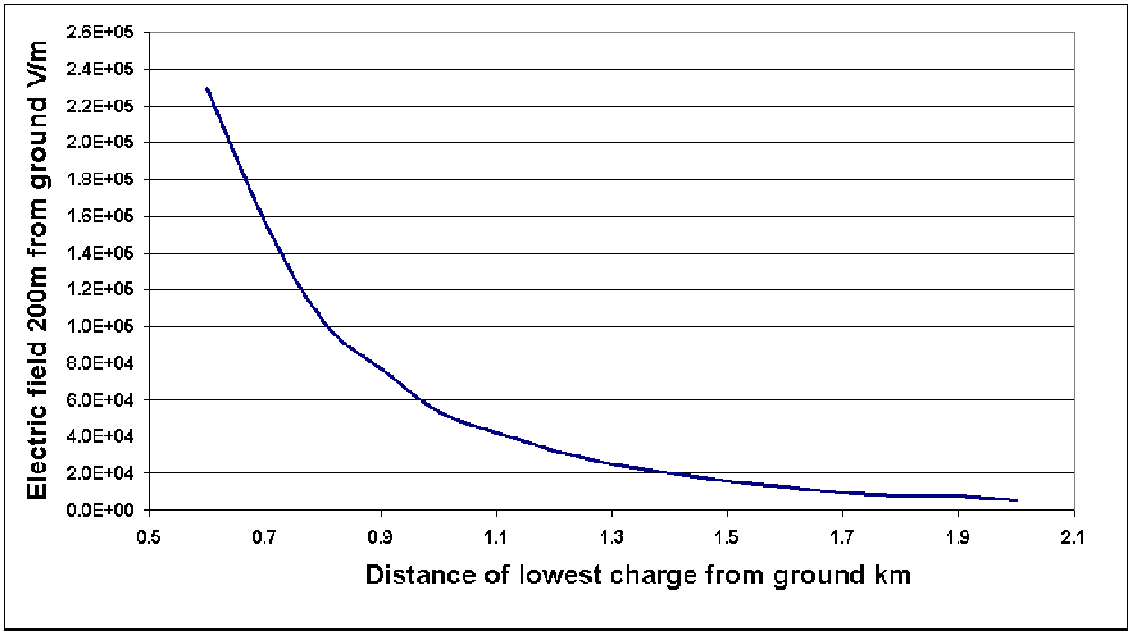

Figure 5-3 Changes in Ambient Field Due to Lowering of Charges

According to [55], the main electrification zone is lower in winter. The different vertical extension of the clouds and the different temperatures are also said to change the charge centers. A 1.5D model [55] showed there were strong positive fields for heights less than 1500m from the ground. For example, winter clouds over the North Sea have a stronger vertical field in the lower atmosphere [55]. The case of North Sea becomes particularly interesting as a lot of wind turbines are planned to be installed here. The ambient fields evaluated above will later be discussed in conjuncture with the stabilization field required for successful propagation of the lightning leader and also for streamer inception.

5.1.2 The Wind Turbine and Blade Model

The model used in the simulations is based on a 2MW present day wind turbine. The blade model used in the simulations presented is 40 meters long and is a simplification of a real blade in that it is taken to be made entirely of fibre glass. The chord length of the airfoil used for designing the blade is 2.75m, the chamber length (upper + lower) is 0.9m, and a thickness of 10cm is maintained throughout the blade. Due to the complicated shape and difficulty of meshing, these dimensions are maintained along most of the length of the model, though in real life blades, a single blade consists of several aerofoil profiles for different lengths of the blade. The chord length begins to decrease from 35 meters of the blade length onwards to end as the sharp blade tip with

a thickness less than 5mm. Integrated into the blade design is the lightning protection system. The tip receptor is placed 2.5 meters from the tip of the blade (37.5 meters from the root of the blade) and the remaining two receptors are placed evenly along the length of the blade. The tip receptor is usually a lot closer to the tip of the blade, but due to meshing difficulties in the FEA software, the position has been changed further down the blade. This should not affect the results, as still this is the main attachment point for the first 15m of the blade and there will be considerable amount of field enhancement. The receptors are 10mm in diameter and are connected to a down conductor that runs inside the hollow blade. The diameter of the down conductor is set to 10mm. The down conductor and the receptors are made of copper. The height from the bottom of the tower to the centre of the hub is 67.5m (Figure 5-4). The nacelle is 6m long, 4.5m wide and 6m high.

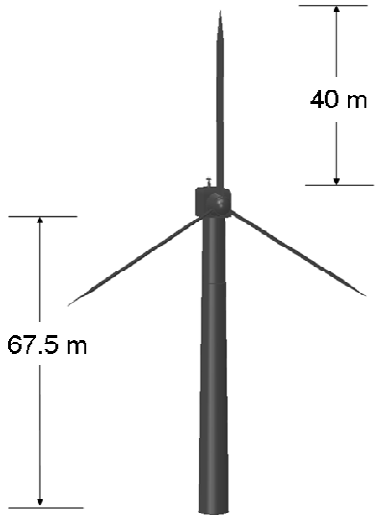

Figure 5-4 Wind Turbine Model

The wind instruments are placed at the rear of the nacelle. Wind instruments on the wind-vane are protected from lightning using lighting rods (Figure 5-5).

Figure 5-5 Wind Instruments Protected by Lightning Rods

The lightning rods protecting the wind instrument end in a hemispherical tip with a radius of curvature of 0.02m.

5.1.3 Analysis of Likely Locations For Formation Of Upward Initiated Lightning

The model of a wind turbine must be combined with information from the cloud model in the finite element analysis software to allow analysis of the likely points of upward lightning formation.

According to [56], the following set of events happen before a upward flash is initiated,

i. A thundercloud of relatively low height comes from a certain direction
ii. The electric field at the top of the grounded structure increases due to the charge in the thundercloud
iii. The electric field exceeds a critical value and an upward leader begins to develop from the top of the structure, or parts of the structure which are more prone to field enhancement, towards the charged cloud.
iv. When the upward leader reaches the charge center, lightning occurs.

The electric field applied in the model is a uniform electric field produced by a plane electrode located 200m above the ground. The magnitude of the applied electric field is based on the results found from Malan's charged cloud model in the FEA simulations already described. When the wind turbine is inserted into this electric field, field enhancement is seen at certain locations of the wind turbine.

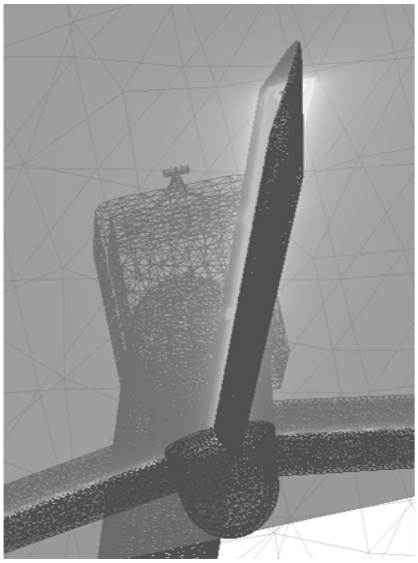

Figure 5-6 Field enhancement around the blade receptors (the locations of the receptors are circles). Light areas indicate high electric fields.

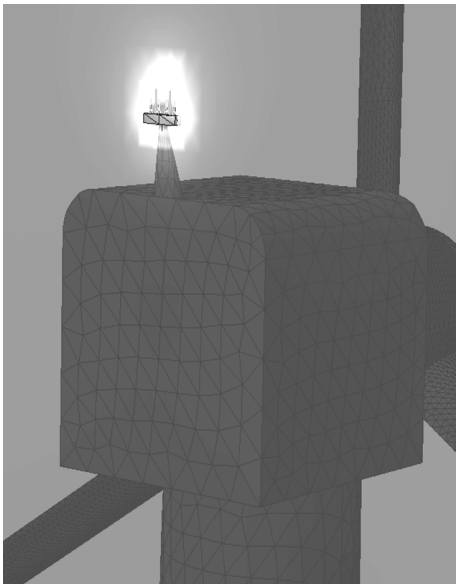

Figure 5-7 Field enhancement around the wind-vane

As is shown in
Figure 5-6 and Figure 5-7, the level of electric field intensification is particularly high around the wind instruments at the back of the nacelle and at the blade tip receptor.

The results from the FEA simulation show a high probability of upward streamer inception from the blades and the wind vane. The production of upward initiated lightning initially depends on a given level of electric field enhancement existing around a component such as the wind-vane / blade and also their position [14].

5.1.4 Streamer Inception

The present section will look at the electric field enhancement at different locations on the wind turbine, to try and find the component/points likely to incept streamers before others. Stable inception criterion is achieved, when the local field exceeds the corona inception field. The actual phenomenon behind the development of streamers is described in studies, such as [54, 57-59]. A brief description is presented below.

In non uniform fields visible and audible discharges are manifested before streamer inception. These are known as corona discharges. Corona discharges are localized hotspots of field enhancements and are usually visible before electrical breakdown. The field around the wind turbine blades will be non uniform due to the blades shape and rotation.

Peek's Law is commonly used for calculating the corona inception field in air for wires/coaxial cables [60, 61].

$$E_c = 3.15\times10^6\left(1+\frac{0.305}{\sqrt{\delta r}}\right)\ \text{V/m} \qquad \textbf{(5-1)}$$

Where, 'r' is the radius of the cable/wire and 'δ'' is the air density factor, and is calculated based on the pressure and temperature.

Though Equation (5-1) was derived for wires, a generalised model was derived by Hartmann [60, 61] which allows the use of Peek's law over a range of tip radii. Hartmann generalised equation is given by,

$$E_C = 2.594\times10^6\left(1+\frac{0.1269}{z^{0.435}}\right)\ \text{V/m} \qquad \textbf{(5-2)}$$

where '**z**' is radius of curvature of the rod tip [60, 61] .
Though Equation (5-2) can be used in determining E_c for the lightning rod protecting the wind instruments at the back of the nacelle, it is quite hard to relate the equation with the geometry of the receptors on the blade owing to their geometrical position and shape on the blade. Whilst the lightning rods protecting the wind instruments are

vertically positioned in the ambient field, the position of the receptors is changing constantly. In regards to the analysis performed in this chapter, the receptors are set in one position; however the receptors are placed positioned horizontally in the ambient field. Also the receptors are surrounded by a dielectric medium made of GFRP, this will change the inception criteria. Due to the lack of straightforward techniques for calculating the inception field over the receptors, the corona inception field is set to 3MV/m for both the lightning rod and the receptors on the blade.

The corona inception field E_c is reached in the vicinity of an electrode owing to the combination of the ambient field E_A and the field enhancement at the air terminations.

In the model used for this chapter, when the wind turbine is subjected to a uniform electric field, the lightning rods protecting the wind instruments show the highest field enhancement and begin to incept streamers at an ambient field of approximately 6kV/m. The lightning rods thus enhance the field 500 times. Similarly, the tip receptor on the vertically positioned blade begins streamer inception at 9.4kV/m. thus enhancing the field by over 320 times. When these values are compared to those created by a charged cloud (Figure 5-3), the receptors and wind-vane lightning protection should be able to emit upward leaders when the lowest positive charge is 2km and below. Such cloud heights can be found in all seasons meaning that upward lightning is likely to be a consistent threat should a thundercloud exist. The finding that the tip of the blade not being the most exposed part of the turbine is in contradiction with results from previous research [34, 35, 48].

While it is difficult to compare the field enhancement of the receptors on the blade with other results, due to the lack of any literature regarding the same, it is possible to comment on the field enhancement of the lightning rods protecting the wind instruments. According to [62], studies were performed on Franklin rods to analyse their efficiency. The results presented in [62] showed a field enhancement factor (tip intensified electric field/ambient electric field) for a 40mm tip diameter and 10m high rod (tip height-to-radius of curvature ratio of 500:1) is around 180.

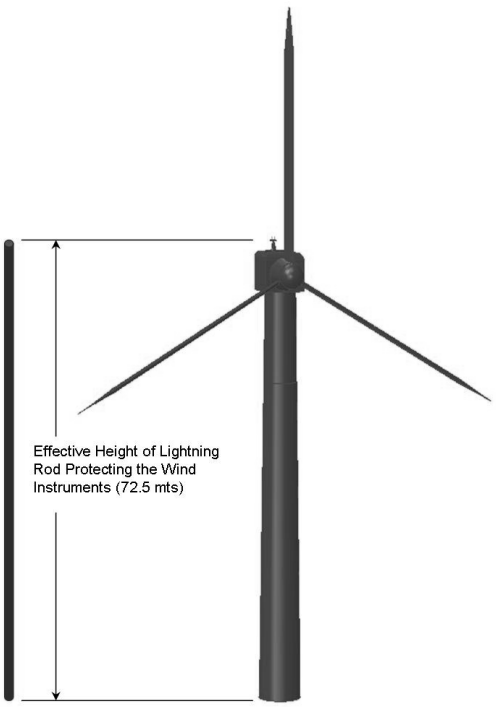

Figure 5-8 Effective height of the lightning rods that are protecting the wind instruments

The lightning rod presented in these simulations has a tip radius of 20mm but the tip is at a height of 72.5 meters from ground level. So, the lightning rod can be imagined to be effectively 72.5 meters long, (Figure 5-8) thus giving a height-to-radius of curvature ratio of around 3600:1. This shows that the inception criteria also depend on the tip radius. According to [18] the inception electric field does not depend on the gap length, the reason being that it is controlled more by the local electric field, created by the tip of the electrode which is not controlled by the gap length. In an attempt to increase the efficiency of the lightning rods at the back of the nacelle, the tip radius of rods was therefore decreased in the simulations, to see if this had any effect on the streamer inception. Figure 5-9 shows the different tip ends of the lightning rod. The two tip radii used were 0.02m and 0.002m.

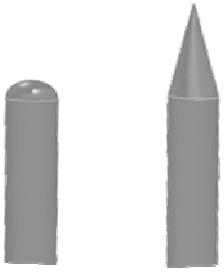

Figure 5-9 Tip radiuses for the lightning rod

The change in the tip dimensions increases the efficiency of the streamer inception. From the FEA results, the lightning rod with the lower tip radius enhances the field by a factor of 700, while its larger counter part enhances it by 500 times.

5.1.5 Leader Propagation

After successful initiation of a streamer, the background field/stabilisation field should be sufficient for the streamer to develop into a leader and also propagate towards the charged cloud

Unlike in downward propagating lightning where the stress at the positive leader tip from the grounded object is enhanced as it gets closer to the downward negative leader, in upward lightning, the positive leader tip potential gradually decreases (owing to voltage drop) as it progresses towards the charged cloud, whereas the potential of the charged cloud remains constant.

According to [63], for positive leader inception during upward initiated lightning

$$U_i \geq U_{lc} \qquad \textbf{(5-3)}$$

Where U_i, is the induced potential at the structure top and U_{lc}, is the critical inception voltage needed for streamer inception (this is set to 3MV/m in this section).

The critical inception voltage U_{lc} is given by the equation [63],

$$U_{lc} = 1556 / \left[1 + \frac{7.78}{\delta R} \right] \qquad \textbf{(5-4)}$$

Here δ is the effect of reduced air levels in mountainous regions and according to [63] this can be ignored for all tall structures with R >> 7.78 m, thus this is ignored in the case of this analysis as the wind turbine is over a 100 m tall. The function R is said to be almost equal to 2*h*(twice the height of the structure) for a big plateau and equal to *h* for flat ground. It has been selected as *h* in this analysis.

The Induced potential at the tip of the structure is a function of the ambient ground field E_g and the height of the structure

$$U_i = E_g h \ \text{kV} \qquad \textbf{(5-5)}$$

During the formation of upward leaders the stabilisation field needs to overcome the potential drop during its ascent to evolve into a successful lightning flash [63]. Rizk came up with the following criteria, which takes this potential drop into consideration for a moving upward leader,

$$U_i(z) \geq U_c(z) + \Delta U_l(z) \qquad \textbf{(5-6)}$$

Where: $U_i(z)$ Induced voltage at any point ***z,*** $U_c(z)$ is the critical inception voltage and $\Delta U_l(z)$ is the leader voltage drop at a length l_z

The leader voltage drop of the ascending leader from the top of the structure $\Delta U_l(z)$ at a length *lz* is given by

$$\Delta U_l(z) = l_z E_\infty + x_0 E_\infty \ln \frac{E_i}{E_\infty} \quad \textbf{(5-7)}$$

Where: x_0 = $v\theta$ (product of the ascending positive leader speed and the arc leader time constant)= ($2x10^4$) x ($50x10^{-6}$) m [49],

The leader is comparable to an arc-like discharge, with a mean voltage gradient that lies between a wide range. This gradient decreases with both leader current and time of existence of the leader [64]

E_∞ is the maximum or ultimate leader gradient =ranges from 3kV/m to 30kV/m [63], and E_i is the minimum leader gradient = 400kV/m [49].

Now adding all the information from Equations (5-4),(5-5),(5-6) and (5-7) the required stabilisation field is given by,

$$E_g \geq \frac{1556/\left[1+7.78/\delta h\right]+x_0 E_\infty \ln \frac{E_i}{E_\infty}}{h} \text{ kV/m} \quad \textbf{(5-8)}$$

Where *h* is the height of the structure. In addition, the final criterion that must be satisfied is:

$$E_g \geq E_\infty \quad \textbf{(5-9)}$$

Equation (5-8) and (5-9) are the necessary criterion an upward streamer needs to satisfy to evolve into an upward flash.

From Equation (5-9) it**Error! Reference source not found.** can be seen that the ambient field at ground level shall always have to be greater than the quasi stationary leader gradient, only in such cases shall the streamer develop into a leader. Thus the background field will always have to be greater than either 3kV/m or 30kV/m.

Also, according to [48], a simplified theory of Lalande's theory, for stable propagation of the leader the atmospheric electric field E_{atm} must be greater than the minimum value required for stable propagation of the leader E_{stab} which is given by the following:

$$E_{stab}(H) = \left[\frac{240}{1+\frac{H}{10}}+12\right].\delta, \quad \textbf{(5-10)}$$

In the above equation H, is the height (in meters) of the object on question, and δ, the air density is ≈1.

The leader stabilisation fields as a function of increasing height calculated for both Rizk inception criteria (both extremities of E_∞, 3kV/m and 30kV/m) and Lalande inception Criteria is shown below in Figure 5-10.

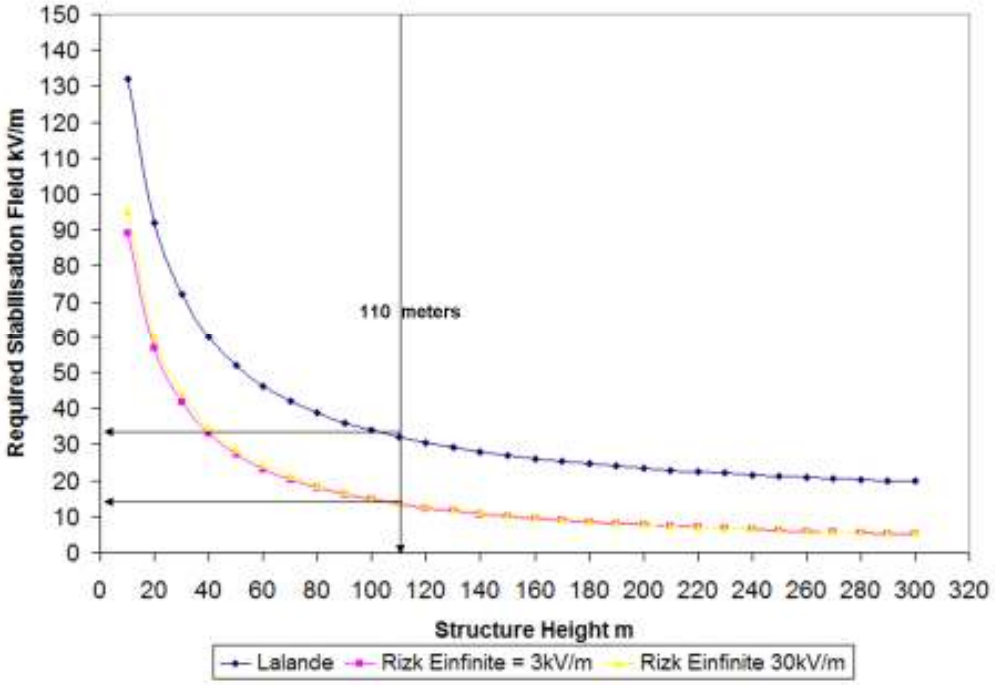

Figure 5-10 Relationship between structure height 'h' and required stabilisation field for occurrence of upward flash.

By dropping an imaginary line over the height of the structure on the x-axis and finding where this line intercepts the plotted lines, the required stabilisation field for that height on the y-axis, with respect to both Lalande and Rizk inception criteria, can be determined. The present wind turbine model is 110 meters high with one of its blade in the upright vertical position. Figure 5-10 indicates that according to Lalande's criteria the required stabilisation for a structure 110 meters high is higher than that compared to Rizk's. According to Rizk's second criteria in Equation (5-9) the stabilisation field should be greater than E_∞ (either 3kV/m or 30kV/m). From Figure 5-10 the required stabilisation field at E_∞ = 3kV/m and 30kV/m is around 15kV/m. From Lalande's criteria this is found to be around 35kV/m.

In the previous sections two vulnerable parts of the wind turbine have been identified, the tip receptor of the blade and the wind-vane at the back of the nacelle. With upward lightning leader inception being developed at both of these air terminals at moderate cloud levels, their progression into a successful strike completely depends on the background stabilisation field. According to Equation (5-10) the stabilisation field required for stable propagation of the lightning leader is indirectly proportional to the height of the structure.

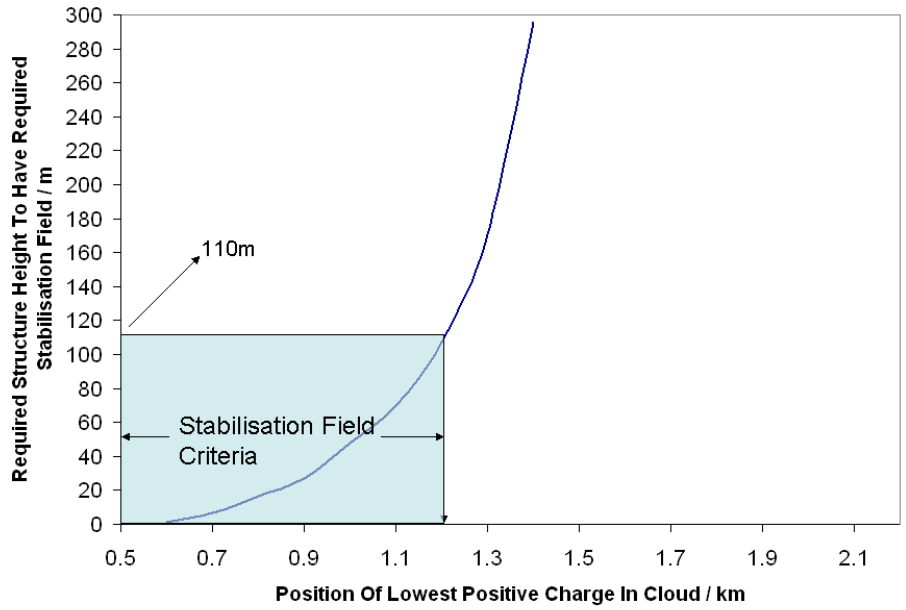

Figure 5-11 Height of lower charge center with respect to height for stabilisation field of blade tip receptor

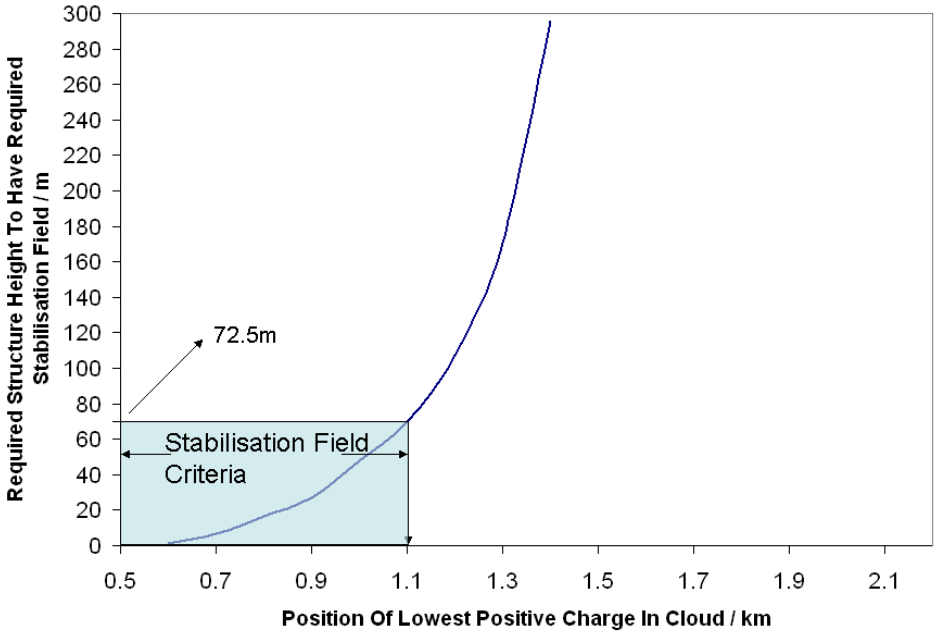

Figure 5-12 Height of lower charge center with respect to height for stabilisation field of wind-vane

Figure 5-11 and Figure 5-12 show the relationship between the height of the structure and the required height of the first charge centre to create a high enough stabilisation field for the incepted streamer to evolve into a lightning leader.

The tip of the wind turbine blade is at a height of approximately 110 meters. From Figure 5-11, the stabilisation field required for a for a streamer incepted from a structure of this height to evolve into a leader is equal to the field generated by the

cloud model whose lower charge begins at a height of 1200 meters. From Figure 5-3 this is approximately 30kV/m. The stabilisation field changes with the height, thus the position of the blade keeps changing this value. The calculation that has been done for the purpose if this analysis is when the blades are placed in an inverted 'Y' position. Secondly, the wind-vane at the back of the nacelle is 72.5 meters from the ground. The stabilisation field required for a steamer to evolve into a leader from a structure of this height is generated by a cloud whose lower positive charge is 1100 meters from the ground (Figure 5-12). From Figure 5-3 this is approximately 40kV/m. Unlike the blades, the fixed position of the wind-vane means this value remains constant. Both these values satisfy the criteria that is defined by Rizk in [63], i.e. Equation (5-9).

It has already been discussed in Section 5.1.4 that the inception criteria for streamers from the wind-vane is reached before the those from the blade tip receptor. It was also seen that the wind-vane and the blade tip receptor will be able to incept streamers when the lowest positive charge in the cloud is anything lower than 1.5 km. This could possible be explained due to the field enhancement at the tip of the lightning rods and their position in the ambient field. But once these streamers begin to develop, the background stabilisation field begins to determine if they would develop into upward leaders. Also from Figure 5-11 and Figure 5-12 the stabilisation field for a streamer emitted from the tip receptor on the blade can be generated from a cloud which is relatively higher than one which is required to create the necessary stabilisation field for a streamer emitted from the lightning rods at the back of the nacelle. Thus the streamers developed from the tip receptor will end up as upward leaders before those from the wind-vane. In such cases the streamers are incepted from the wind-vane again and again till the ambient field reaches the stabilisation field for this streamer to evolve into a leader.

As discussed in the previous section the field enhancement of the lightning rods, protecting the wind-vane can be manipulated by enhancing their tip radii. After the above discussion, the question arises as how necessary this is, as early streamer inception will not effect the overall process as the stable leader is only evolved when the ambient field reaches the minimum level and this does not depend on the geometrical shape of the air terminals, but rather depends on their position and height relative to the cloud height.

5.2 Conclusion

From the simulations based on the clouds models and that of the wind turbine the following can be deduced

1. Based on the results from the cloud models it can be said that the ambient electric fields increases with the decrease in cloud height. This proves that the winter clouds which develop at lower altitudes are capable of developing higher electric fields at ground than those compared to summer clouds.

2. When the results found from the cloud model are compared with the wind turbine model, the risk of lightning formation increases with low clouds. This directly when related to winter clouds, wind turbines are prone to a larger number of lightning strikes during winter compared to the rest of the year (as long as the charges are comparable).

3. Contrary to the general belief of the blades being the most vulnerable part of the blade, the wind-vane instruments pose a considerable risk for lightning attachment, especially under low cloud height and winter lightning. This is particularly relevant for offshore wind farms.

4. The lightning rods protecting the wind instruments of the wind turbine blades are the first to initiate lightning leaders, but with low cloud height, the blades become equally susceptible to lightning strikes. Low clouds develop enough electric field for the leader inception and propagation. Leader inception from the air terminals protecting the wind instruments can be controlled by varying the geometrical configuration of the tips of the lightning rods.

6 Interaction of Lightning Protection with Radar Cross Section Minimisation and Carbon Fibre Strengthening.

6.1 Introduction

Wind farm planning applications submitted to regional agencies for consideration in the UK often raise objections on the basis of the potential for radar interference due to their large radar cross section (RCS). This has stalled the development of large projects capable of supplying hundreds of megawatts of power to the nation. With the increase in U.K power needs and the governments target of reaching 10% of the countries electricity needs through renewable sources by 2010 [65, 66] there is a large increase in plans for installing larger offshore wind farms. Thus the challenge of tackling the problem of wind farm radar interference is now becoming essential.

Other areas of development have been in trying to make new multi MW blades stronger and light weight. This will become important as blade sizes increase for newer wind turbines of large power capacity. The weight will become an issue as most of the new wind turbines are being installed offshore and logistics of installing these mammoth components is a major cost factor in wind farm development. Present wind turbine designs are mainly manufactured using glass fibre reinforced plastic (GFRP) composites, but for increased sizes carbon fibre reinforced plastic (CFRP) composites are being introduced in addition to GFRP to reduce the weight. Though CFRP is ideally the suitable material for blade manufacture, GFRP has largely been the preferred option due to economical and cost effective reasons.

Measures of RCS reduction and blade strengthening involve the introduction of new layers, especially conductive, into the existing blade laminate. This will have an effect on the existing lightning protection systems installed in the blade. The present chapter will deal with the effect these layers will have on the efficiency of the lightning protection system.

6.2 Radar Interference and Mitigation

The actual process of how radar signals interact with a wind turbine or target is necessary to understand the impact of wind farms on radar. Radar provides its own energy in order to find a target. This energy is spread over a certain volume of space, depending on the returns, a target is located. The size of the object affects the energy

that has been reflected back/returned to the radar. Radar developers and operators devised a standard for target size to rate the performance of their systems [67]. This standard is called Radar Cross Section [67]. The RCS is determined by measuring, or calculating the energy that has been reflected by the target. Wind turbine towers, nacelles and blades reflect radar energy. The rotation of the blades causes Doppler reflections Figure 6-1.

Figure 6-1 Doppler interference

With blade tip speeds reaching 6 to 7 times the speed of wind and approximately reaching a velocity of 170 mph cause significant Doppler clutter [68]. Doppler is the change in frequency of a wave for an observing target relative to the actual source generating the wave. Many radars use this Doppler principle in recognizing targets. The large radar cross-section of wind turbines produces scatter and ghost targets on radars Figure 6-2.

Figure 6-2 Ghost target

The scatter is created due to the tower, blades and the nacelle. Investigating into the interference of wind farms on ships radar (which does not use Doppler) has confirmed that there is a significant impact as a wind farm will in general produce spurious returns on radar displays caused by multiple reflections from the static towers, as well as the rotating blades. Other effects such as beam spreading and side lobe detection due to the very high radar cross section of wind turbines [69] are also observed Figure 6-3.

Figure 6-3 Target Spreading and Side Lobe Detection [70]

When a target is hit by radar energy, part of this energy is reflected. This reflected energy in re-transmitted as side lobes. Though these side lobes are not as high in energy as compared to main beam, they still pose a significant distortion.

Wind turbines are large structures that are typically made of GRP and/or carbon fiber composite components mounted on steel towers. Full physical optics modeling of a typical 40 meter bladed turbine [69, 71, 72] at various rotation and yaw angles using the coordinate system shown in Figure 6-4, was undertaken by the Microwave and Communications Department at the University of Manchester, as part of the SUPERGEN Wind Program.

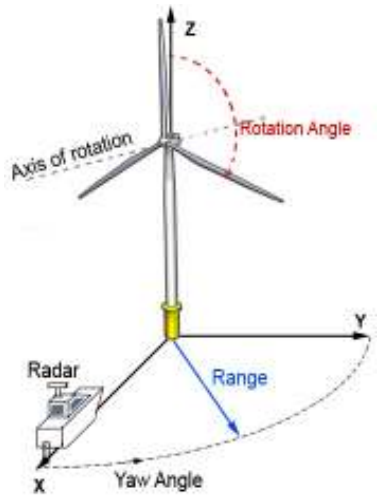

Figure 6-4 RCS Modeling Coordinate System

The results show that the RCS can be in the order of 60 dBms (10^6 m^2) at 9.4 GHz, which is of the same order as a large oil tanker broadside on [73]. It was found that the tower constitutes by far the largest source of scatter (approx. 80%) followed by the blades (5% each). The nacelle was only considered to be a significant source of scatter for 90° yaw case (i.e. broadside on) [73].

There have been several attempts to find a solution for this problem; these attempts can be widely classified into two groups,

1. Reduction of Radar Signature.
2. Radar System Modification.

While the latter deals with manipulating and modifying existing and new radar systems. Introducing filters into the radar signal processing in the affected radars reduces Doppler interference, but does not completely resolve the problem. The first method of reduction of radar signature is what this chapter will be dealing with. Most of the existing work in this section is in regards to Radar Cross Section minimization. The present section is aimed at examining the issues that result in the need to develop optimal solutions that can maintain lighting protection, minimize RCS and retain structural integrity – all within a neutral cost environment. Tests have been performed on hybrid material forms, suitable to be added to the blade laminate using existing manufacturing systems and which can be used as radar reflective surfaces. Work in this section has been carried out in conjuncture with the Microwave and Communications and The Northwest Composite groups at the University of Manchester.

6.3 Radar Cross Section Minimization of Wind Turbines

For an effective low radar cross section solution, shaping of the turbine is a potential option. RCS reduction of the tower and certain parts of the nacelle maybe achieved through shaping (a method in which the object is designed in such a manner that it does not return the radar signal). The design will involve in making sure that the high energy spikes reflected from the target do not point back to the radar. This method though does become quite complicated with the blades as their ability to generate maximum power from the wind is based on their aerodynamic profile, thus eliminating any sort of shaping or manipulating of it shape. Hence, the use of Radar Absorbing Materials (RAM) is essential, in order to reduce the radar echoes at the frequencies of interest. Radar absorber solutions soak the energy in the radar signal thus reflecting no returns to the radar. One possible absorber design is based on a resonant structure formed between an absorbing surface and a thin metallic layer buried within the composite structure of the blade laminate. This simplest radar absorber is commonly referred as the Salisbury Screen [68]. This kind of absorber consists of three layers, a ground layer (also known as a Perfect Electric Conductor, PEC), a dielectric layer which is placed a quarter of a wavelength from the PEC and a thin lossy screen. The principle behind the composite layer is that when the radar signal hits the initial

dielectric layer, it is split into two equal halves, One of these split waves is reflected back from the lossy screen while the other is reflected by the PEC. Whilst being reflected by the PEC, this wave has now shifted 180 degrees out of phase to the other wave. According to interference when two waves are 180 degrees out of phase they cancel each other, resulting in no output wave. Similarly if both the waves are in phase with each other, the output is twice the amplitude of each of the waves. This concept has been used in the composite RAM layer in this section, which has been intended to be used on wind turbine blades so as to reduce their RCS. Ideally RAM solutions would be light and thin to maintain the design profile of the turbine blade and avoid and significant weight increase. This structure offers compactness and low weight but the integral metallic layer may cause a considerable effect on

- Structural integrity of the blade.
- Complexity and cost of the manufacturing process.
- The lightning protection system.

To be practical, any radar absorber has to be thin, lightweight and low cost and importantly compatible to the manufacturing process. There are a number of possible absorber types but, to get compactness and low weight, these designs normally comprise a number of layers (at least two). The top layer(s) provide an absorbing material or structure; for example some designs use an absorbing printed circuit or carbon impregnated foams. All such designs need to be backed by a reflecting layer, which is in essence a metal sheet. An initial design is shown in Figure 6-5, where a lossy material is sandwiched between the top layer, which has a printed metallic pattern with a resistor and capacitors acting as resonance absorbers and the bottom layer, which is a reflecting ground plane made of a perfect electric conductor (PEC).

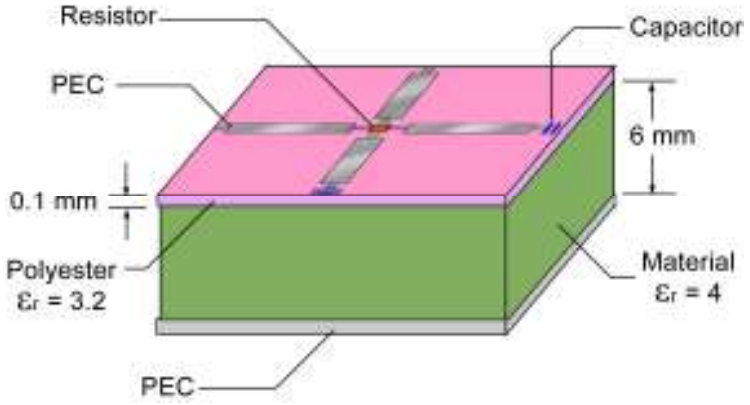

Figure 6-5 Initial Test Design for Stealth Solution at 3GHz

This metal sheet is part of the absorber and during the design process is used in conjunction with the top layer to ensures the incident microwave energy (or at least the major part of it) is "trapped" inside the absorber. Although the process is not perfect it avoids the need for very thick absorbers which are impractical for the blade RCS reduction.

6.4 Use of Carbon for Blade Structural Integrity Improvement.

As wind turbines continue to increase in size it is important to keep weight to a minimum to reduce self-weight fatigue and minimize loads on the tower, foundation and drive system whilst simultaneously maximizing stiffness of the structure to eliminate blade strike. The dynamic characteristics and the stresses of large turbine blade are mainly dependent on their masses. For this reason, materials of high fatigue strength, high stiffness and low density have to be selected. Fiber-reinforced composite is the best choice for the application at the moment, which has high specific stiffness and strength. The use of composite materials in wind turbine blades has resulted in large advances in blade size and resulting power output. Wind turbine blades tend to use mainly glass fiber composites with highly stressed regions being reinforced with carbon fiber composites. The good formability of the laminates allows building blade of high aerodynamic quality and very different profiles at the tip and root of the blade. Furthermore, it is possible to vary the stiffness of a cross section with a given contour. Since composite designs are mostly very safe in strength, one cannot only choose between different types of fiber, but it is also possible to vary the thickness of the laminates which are to be built up in layers. Finally, the composite materials have good corrosion resistance.

Wind turbines are fatigue-critical machines, namely the design of many of their components is dictated by fatigue considerations. The major materials used in the turbine are typically used in rotating machinery and towers [74]. Thus the turbine system is primarily composed of common structural materials with extensive engineering applications and databases. However, blades are unique structural components of each type of turbines. They are a minimum weight and expensive component that must serve a very large number of fatigue cycles during their service lifetime. Fatigue is the slow and progressive localized damage a component would experience due to the loading and stress cycles it undergoes during its operation. The fatigue cycle is usually represented by an S and N curve (Where ‘S’ is the magnitude of cyclic stress the component is subjected to, and ‘N’ is the number of cycles the component is subjected to before failure). Such a curve is shown in Figure 6-6.

Some of the components that undergo similar fatigue/stress cycles to wind turbine blades are shown in Figure 6-6. As shown in Figure 6-6, blades must ensure several orders of magnitude more cycles than an airplane.. Thus turbine blades are also fatigue critical structures. Moreover, the materials used in the turbine must be kept at a relative minimum to reduce the cost.

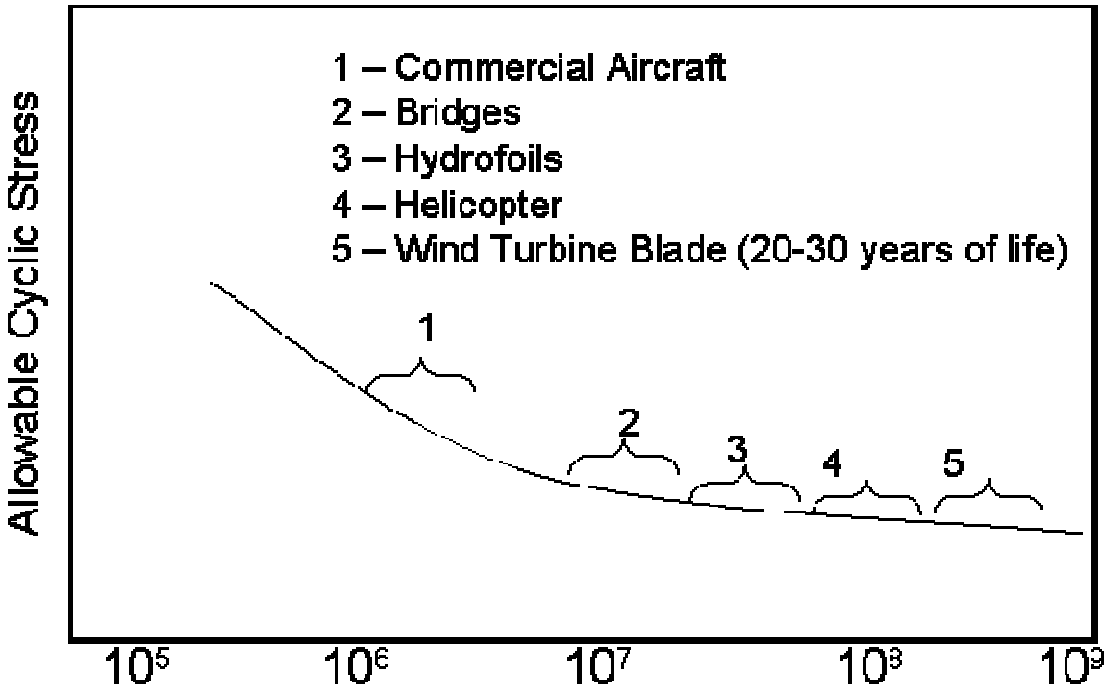

Figure 6-6 Schematic S–N curves for different industrial components [75]

Fiber composite materials are being used to provide the necessary structural performance but the introduction of an internal thin metallic layer could reduce the durability of the blade and promote failure. Furthermore the need to introduce a discreet metallic layer will introduce a further manufacturing step resulting in a cost penalty. As a solution to these problems Metal Plated Conductive Carbon fiber (MPCC) may be added as a layer on top of composite layers Metal Plated Conductive Carbon fibers (MPCC) combine the high electrical and thermal conductivity properties of metals with the high strength and low weight of carbon fiber materials. This material can range from 10%-65% metal by weight. Nickel and Copper/Nickel hybrids have been the primary metals of choice but the process can be adapted to plate other metals such as silver, gold, platinum and palladium. Comparative Scanning Electron Micrographs (SEM) & EDX has been used in to characterize these veils. Figure 6-7 shows the 100kg/m^2 MPCC under SEM microscopy.

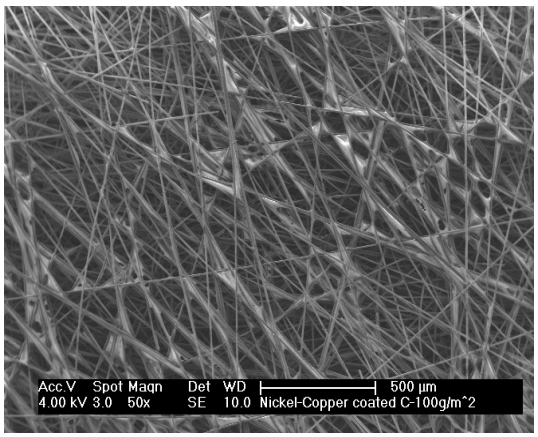

Figure 6-7 a micrograph of 100 Kg/m^2 MPCC under SEM

Qualitative characterization by EDX method shows that fibres in MPCC veils have been coated by Nickel and copper as described before (**Figure 6-8**).

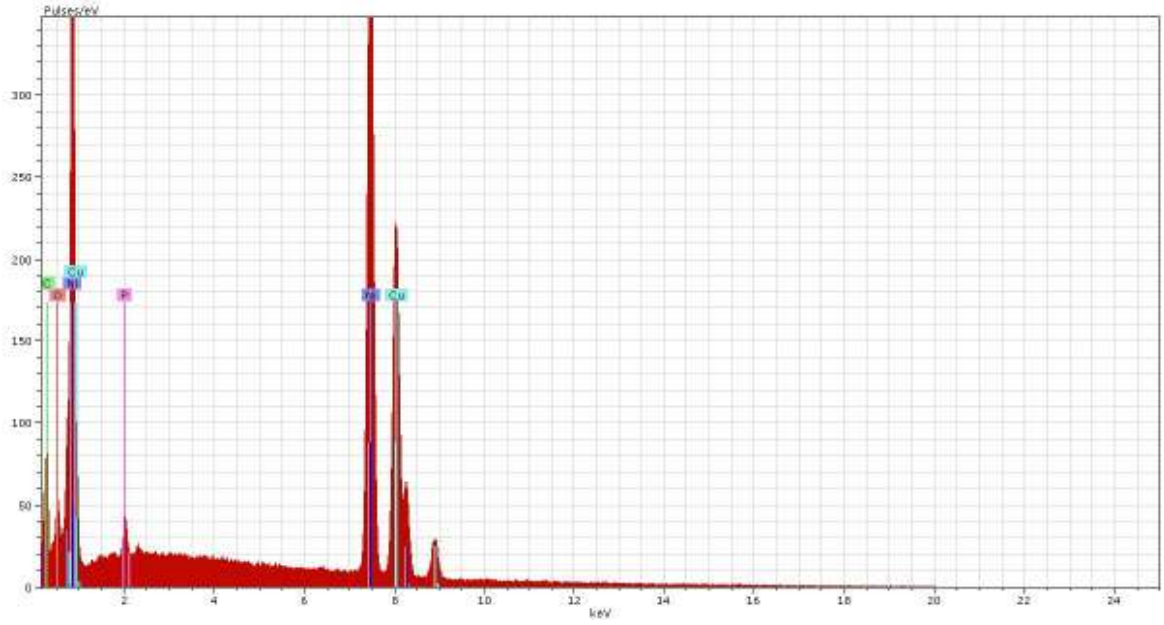

Figure 6-8 EDX characterization of MPCC veils

Quantitive characterization results in Figure 6-9 and Figure 6-10 shows that the fibers has been coated by Nickel and copper and then bonded by a bonding agent

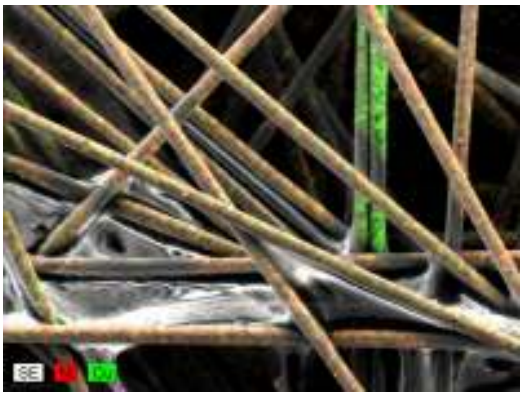

Figure 6-9 Mapping of Containing elements Copper and Nickel

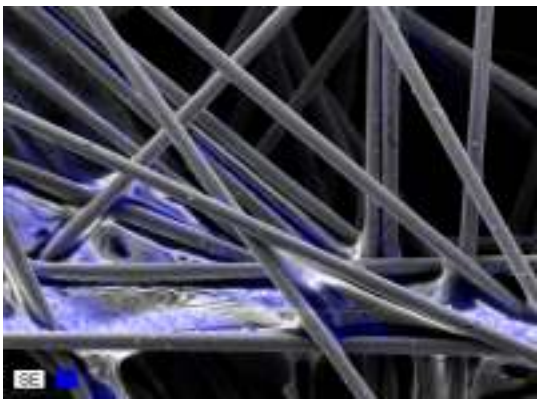

Figure 6-10 Mapping of Containing Elements Carbon

The above composite layer can be used for both increasing the strength of the laminate and also, due to the conductive elements on the carbon fibre, can be used as the reflective layer in the RCS solution.

6.5 Effect of RCS Solution on Lightning Protection System

The introduction of a thin conductive layer within the blade, that consists an internal lightning down conductor and receptors as a lightning protection system, could result in a change to the efficiency of the lightning protection system through a modification of the electric field around the receptor.

In addressing the effect of the RAM solution to Wind Turbine blades, two areas of the lightning protection system are considered; the impact of the RAM on lightning attachment points and the impact of the RAM on lightning current conduction.

6.5.1 Impact of RAM on Lightning Attachment Points

The efficiency of the lightning protection system is dependant on the effectiveness of the air termination points. In the case of the lightning protection system considered in this research, these are the receptors. Using FEA methods the electric field

enhancement at the receptor and the effect of integrating the conductive layer with the lightning protection system can be simulated.

Three models have been simulated using FEA methods. The models were later subjected to electro-static analysis in the pre-processor side of the software. All results are then analysed in the post-processor section of the software. In two of these models the conductive layer needed for the RAM solution has been integrated along with the existing lightning protection system. A cylinder ending whose tip ends in a cone was modeled and simulated. Though this is not an exact replica of the wind turbine blade, the results found from these are similar to those of a blade. This shape was chosen due to the simplicity in modeling an inner composite layer of small thickness, and meshing in the software. The cylinder is made of fiber glass and a relative permittivity of 6 was chosen. The conductive layer is 1mm thick which is comparable to the composite layer that has been tested.

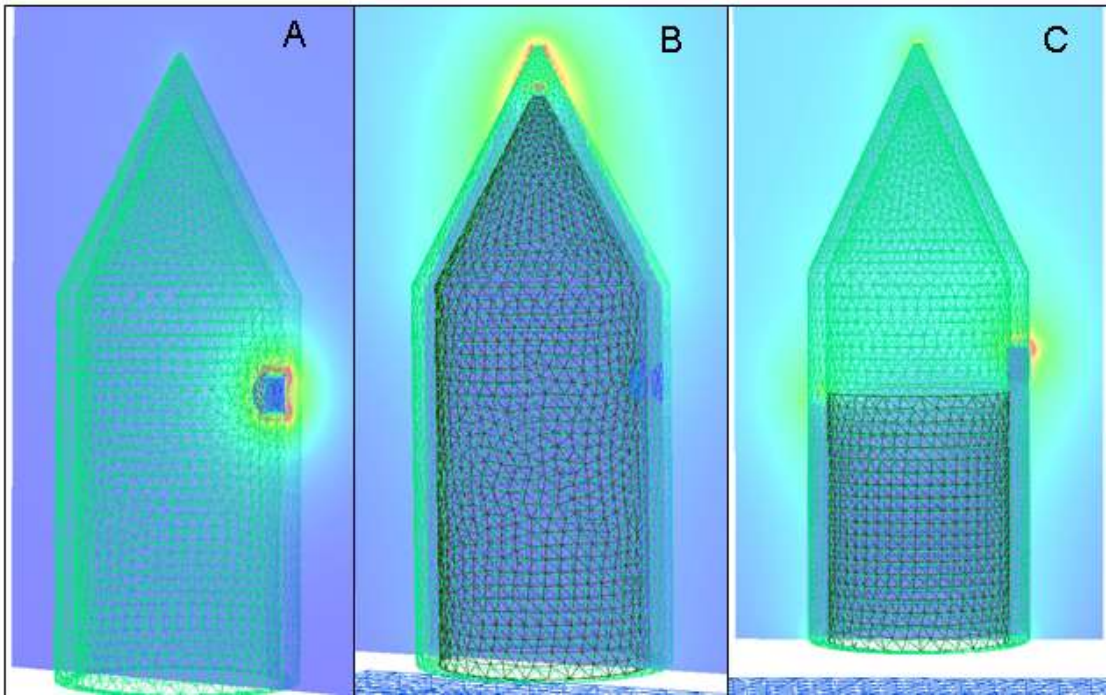

Figure 6-11 Effect of Conductive Layer on LPS (receptor penetrates blade laminate, but this is concealed due to field enhancement patch).

All the models are subjected to the same uniform electric field. The initial model (Figure 6-11A) is the case of a standard wind turbine blade with a receptor that is connected to a down conductor. In this simulation it can be observed that the point of highest electric field enhancement is the receptor made out of copper. Thus, theoretically this should be the first place for streamer inception. The next two simulations show the case where a conductive layer, which is could be used both for strengthening the existing laminate and also used for the RAM solution as a reflective service, is placed inside the blade

laminate. In the initial case this conductive layer is extended to the tip of the blade, and in the next the conductive layer stops right below the tip receptor. In Figure 6-11B, with the conductive layer placed under the blade laminate, it can be seen that the receptor is not the area of high field enhancement any more and instead there is a high electric field enhancement at the tip of the blade. This is undesirable, as this increases the risk of lightning attachment to areas of the blade away from the receptor and possible damage due to the same. In Figure 6-11C, where the layer stops below the receptor, the electric field enhancement is still the highest at the receptor. However, the ratio of the field enhancement at the receptor to that of the tip of the blade in Figure 6-11C is lower than the case where there is no internal reflective layer (Figure 6-11A), thus increasing the chances of a lighting attachment away from the receptor.

Similarly the model was subjected to a high electric field in the horizontal position (Figure 6-12).

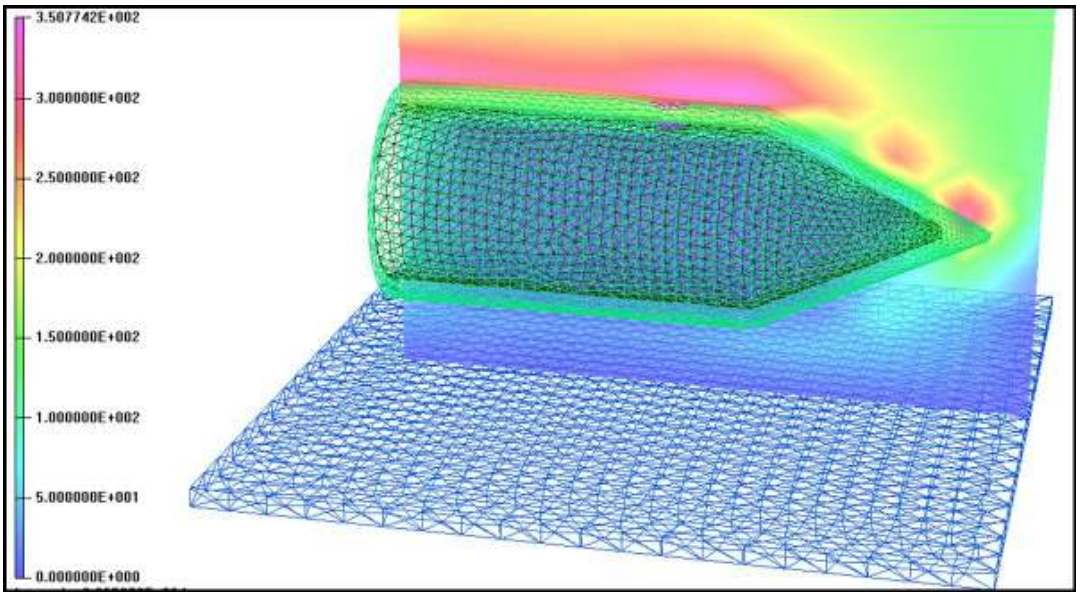

Figure 6-12 Effect of Conductive Layer on LPS (Horizontal Position)

The effect of the new composite conductive layer becomes much predominant in this orientation of the model. With most of the composite layer now under the uniform field, there is almost a constant field enhancement across the length of the cylinder. In the case of a blade this would translate into rick of lightning streamers emerging from across the length of the blade this increasing the risk of lightning attaching places other than the lightning attachment points. Table 6-1 shows the electric field enhancement at locations identified as possible attachment points from the simulations (Figure 6-11). The model itself is subjected to a uniform field of 12.5kV/m.

For the lightning protection system to perform efficiently, two key points must be fulfilled

- The field across the receptor must be higher than any other location on the blade, especially those locations which are not part of the lightning protection system (E_r).
- However the field at other locations of the blade, which are not part of the lightning protection system, should be as low as possible (e.g. E_b and E_t), thus avoiding the any risk of lightning attachment event at high ambient fields.

This can be verified by the performance ratio shown in Table 6-1. The variable, 'performance ratios' of the lightning protection system, is a comparison of the field enhancement across the receptor, to that seen across the tip of the blade and also through the bulk laminate. Ideally both these ratios have to be as high as possible, which would indicate a larger field enhancement across the receptor, in comparison to other areas. This in turn would confirm that in an event of lightning strikes, the receptor would be the first to initiate streamers, thus protecting other parts of the blade.

	Field enhancement around receptor (E_r)	*Field enhancement around tip (E_t)*	*Field enhancement bulk laminate (E_b)*	*Performance Ratios*	
				$\frac{E_r}{E_b}$	$\frac{E_r}{E_t}$
No Carbon	**240**	**18.7**	**28.3**	**8.4**	**12.8**
Full Carbon	**22**	**702**	**2.5**	**8.8**	**0.03**
Half Carbon	**57.8**	**29**	**4.6**	**12.5**	**2**

Table 6-1 Electric field measurement at key areas

From Table 6-1, the both the ratios are the highest when there is no composite layer in under the blade bulk laminate. Whilst the worst case scenario is when the composite layer covers the blade till the tip, where the tip is the point of high field enhancement and the receptor is significantly dulled. The receptor on the sample with no composite layer, effectively, will have the best lightning protection.

With lightning efficiencies expected to be at levels of 98%, with this sort of a lightning protection system, the new layer does decrease this efficiency. However, Table 6-1 is only a comparison between the electric field enhancements across the hotspots where possible lightning attachment could happen, these numbers cannot directly be related to the efficiency of the lightning protection system. The table only shows that the performance of the lightning protection system will be affected by the addition of the new layer. Further simulations followed by lab tests will help in creating a function

based on the field enhancements which should be able to calculate the efficiency of the lightning protection system.

Though the new layer is convenient to add to the existing blade laminate and process, it dulls the effect of the receptor and increases the lightning attachment on unwanted locations of the blade.

6.5.2 Impact of RAM on Lightning Current Conduction

Once lightning attachment is established the next purpose of the lightning protection system is to carry lightning current. Existing lightning protection systems are capable of carrying rated lightning current and are tested for upto 200 kA [1]. In order to add the new RAM solution the reflective surface will have to be bonded to the existing lightning protection system to avoid breakdown and flashovers between different conducting materials due to potential differences. However, once the conductive surface on the RAM solution is bonded it will have to be able to carry part of the lightning current. In order to test the behavior of the conductive surface when subjected to high currents, a hybrid composite veil was tested. There are many commercially available hybrid veils now. The present veil is a Nickel and Copper coated Carbon fiber veil. Ideally when this veil is put to the test, the sample should be able to distribute the strike test energy across its surface, thus eradicating any damage to layers underneath. Two types of veils were used a 50 g/m^2 and 100 $g/m^{2.}$ The resistivity of the samples was measured at around 7.7 Ωm in comparison to copper and stainless steel used on lightning protection systems of blades in service with resistivities of 17.8e-9 Ωm and 0.7e-6 Ωm.

Samples of different lengths and widths on this composite veil were tested. Help from the Northwest Composite Center at the University of Manchester was taken inorder to infuse resin into the composite veils, to see if this would change its electrical characteristics. This would also replicate the process that would go into actually fusing this layer into a normal blade laminate. The high current tests were performed at the high current facility based at Elemko SA, in Greece.

The test objects were tested for both lightning current conduction and attachment. Inorder to have a return path while testing these veils they were attached to copper electrodes. Figure 6-13 are those of the samples which are clamped to electrodes for uniform distribution of the current along the length of the sample. One end of the sample is connected to the source while the other is connected to the earth for the return path. Tests were designed to see the level of currents the samples could withstand before undergoing any damage. The first tests were started at the lowest

level possible at the facility, which was near to 15 kA. From Figure 6-13, it can be noted that the sample suffered severe physical damage at this level. This result was replicated on samples up to a width of 15, 10 and 5cms. Samples that were infused with a resin were difficult to handle as they were too brittle, but tests were also performed on strips of this material. It was observed that the samples were damaged at the same current level of around 15 kA. The one thing that did differ was the physical damage on the resin infused samples, as these tend to break apart rather than burn (Figure 6-14). This phenomenon can be explained to the addition of the resin to the veil itself.

.

Figure 6-13 Current Conduction Test (50g/m2 without resin, before and after test)

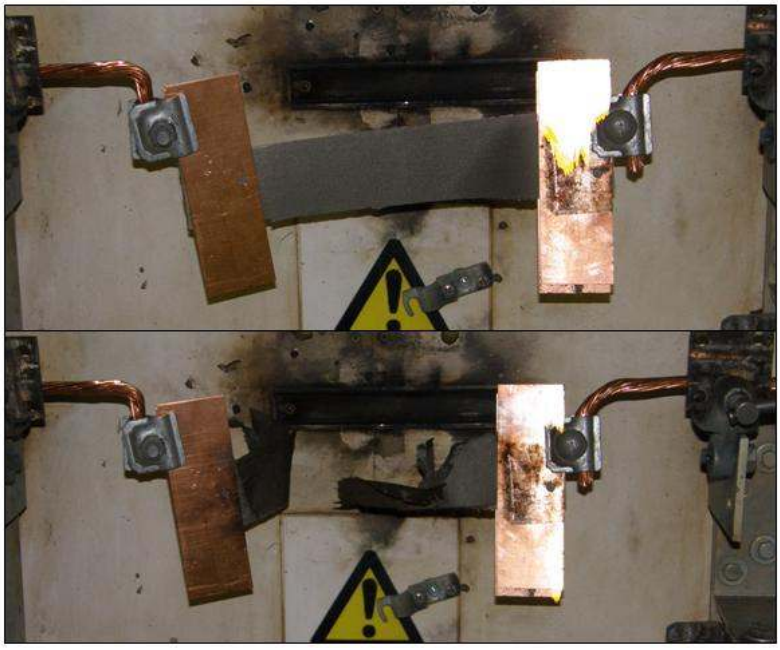

Figure 6-14 Current Conduction Test (50g/m2 with resin, before and after test)

All these tests were performed at a relative low level of peak current. Actual lightning standardization test levels for components which are connected to the air termination and down conductor lie between 100 – 200kA [1]. The new conductive layer failing at low peak currents will avoid manufacturers from using it in blade laminates as it would increase the risk of internal blade laminate damage. The failure of the layer could be avoided by using a thicker layer. But this inturn would cause a problem in integrating it into the blade laminate.

6.5.3 Selective Layering

From the above simulations it is seen that the conductive layer under the blade laminate effects the field enhancement around the receptor, and also causes field enhancement at unwanted regions. It is also seen that the layer is unable to carry low lightning currents. The results prompted into trying a new method, namely 'selective layering'. This is a process in which only parts under the blade laminate where treated with the new composite conductive layer. The idea is to leave areas around the receptor, in a bid to try and not disturb its enhancement efficiency. Though, this meant that the actual RCS solution would have to be selective as well. In this process a larger portion around the receptor was left untreated and so was the tip of the blade. The tip of the cylinder was untreated as previous simulations showed that this turned into an area of high field enhancement due to the addition of the composite layer (Figure 6-11B). Also in these simulations the new layer was not earthed. This would bring about a new challenge of trying to insulate this layer sufficiently such that no discharges would take place between the conductive elements. Assuming that there is sufficient insulation provided for this conductive layer between the blade laminate, a simulation was performed to analyse the results of selective layering with such a solution. Results of this are shown in Figure 6-15.

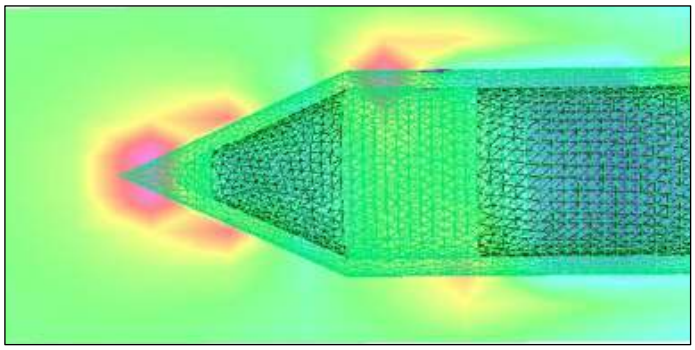

Figure 6-15 Selective Layering

Results from the selective layering show a large amount of field enhancement at the tip, and also, significant field enhancement at the edges where the selective layering starts. Though this still is considered as a possible option, much research is needed into the placement of this conductive layer and which parts will need to earthed and where not, suitably insulated from other conductive regions.
From the above tests it can be seen that integrating the additional conductive layer to the existing lightning protection system will be challenging and that the material initially selected is not robust enough. The conductive layer will have to be selected in such a way that it is electrically conductive enough to withstand part of the lightning current. Further research and testing is required into possible materials that can be used for both the RAM solution and the lightning protection system. Also future work could investigate the concept of having an exclusion zone around the receptor, in such a way that the receptor performance is not affected by the addition of these conductive layers into the blade laminate. The exclusion zone research would also have to highlight if the conductive layer than

6.5.4 Cost Effective Analysis of Lightning Protection Systems Equipped with RCS Solutions

The previous sections highlighted the risk, in regards to lightning attachment, of integrating an RCS solution into the existing blade laminate. Further research is being performed to find a possible solution to make the RCS solution work on new blade concepts. Though there is still a large way to go before these new systems can be integrated into the blade laminate, the present section looks into the effect the new layer would have on the overall costing of the blade systems with integrated lightning protection systems, assuming the efficiencies of the lightning protection system in not affected majorly.

It is hard to perform a cost effect analysis of the lightning protection of wind turbines installed with Radar Absorbent Material, as there is not much data available in regards to their costing and implementation. In this report an attempt is made to show the difference in the financial implications of a wind turbine rotor blade system with RAM and without. These financial implications might arise as it has been shown that the addition of the new layer decreases the efficiency of the lightning protection system, thus making the blades vulnerable to lightning strikes and prone to damage and subsequent repairs.

Wind turbine investment varies from location to location. While capital costs for offshore wind farms are quite huge, most of this is related to the cost of the wind

turbine itself. This excluding the work that has to be done to get it fully operational. A typical 2MW wind turbine installed in Europe cost an approximate 928,000€/MW. This is a figure that has been provided for wind turbines installed on land. For offshore wind turbines, this price will be higher. For offshore installations the investment would be high due to the involvement of special cranes, foundations and general logistics. According to [3] offshore wind turbines cost 20 percent more than their onshore counterparts. Taking this 20 percent into consideration, offshore wind turbines should cost an average 1.2M€/MW. According to [3]Rotor Blades on wind turbines amount from 16% to 34% of the total production cost. Blades for 3MW rated wind turbines are estimated to cost an approximate 200,000€ each. Thus, making the rotor blades the most expensive component of a wind turbine. It is thus essential to keep the costs of damage and repair to this component to minimum, if not none. Lightning is a concern for large wind turbine operators and manufacturers as it still is a major factor for causing damage to rotor blades. Hence most rotor blades are equipped with lightning protection systems. According to [46] the lightning protection systems amount to 2% of the total blade manufacturing costs for a blade made of GRP.

The addition of RAM to rotor blades affects the efficiency of the lightning protection system [76]. But initially it also increases additional weight to the blades. According to [77] applying a 5mm radar absorbent coat will add upto 1200kg to a large wind turbine blades. Now this is for a RAM solution that is a coating on rotor blades. In the research performed in this project, the RAM solution involved a couple (set of resisters and capacitors) of layers, which included passive and active elements [76], which means the weight would be even greater. One more main aspect, which is possibly the biggest constrain for any manufacturer, is the financial aspect of adding such a layer to the blades. Also, the layer would have to be easily included in the existing blade manufacturing process. Assuming that all these constraints are achievable and newer wind turbine blades are fitted with RAM solutions, there still would be an implication to the operation and management of the rotor blades.

To produce a cost effective analysis on the addition of the RAM to rotor blades and its implication on lightning protection systems, a wind farm consisting of 100 wind turbines offshore shall be assumed. Each of these wind turbines is rated at 3MW and has a rotor diameter of 90m. The height of the tower is 40m, thus the height of the wind turbine when the blade is in its vertical position is an approximate 130m. The wind turbines are arranged in 10 rows, and are assumed to be installed not far from the shore and on shallow waters. The analysed wind farm is assumed to be installed in the

North Sea, where the British government has actually planned to install 7000MW of offshore wind capacity [65].

6.5.5 Efficiency of the Lightning Protection System without RAM

The rotor blades are equipped with a receptor/down-conductor based lightning protection system. To perform a cost benefit analysis on the lightning protection, certain parameters regarding lightning statistics is necessary. To calculate the costs due to lightning damage, the statistical uncertainties of different variables such as lightning data itself needs to be dealt with. According to [23], the uncertainties in evaluating the cost of lightning damage are,

- Frequency of thunderstorms and lightning flashes
- The amount of damage resulting from a lighting strike/attachment
- Loss due to downtime in repairing damage.

Some of these uncertainties will be dealt with, such as assuming a constant lightning frequency for that area. This is not true in real case scenarios as the actual presence of large offshore wind farm does tend to effect the lightning frequency of that area [78].

For calculating the damage caused to a wind farm and the consequent downtime and repair, the number of strikes that the wind turbine will attract is necessary. For this Equation (4-1) (which has already been used in Section 4.1.3) will be used. This equation takes into consideration the number of lightning strikes that a wind turbine will attract based on its height and it collection area. According to [1] the number of lightning strikes that might endanger a wind turbine also include lightning within a collection area of 250m and lightning flashes on different service lines. These will be excluded in this analysis as it is assumed that the blades are only endangered by direct lightning strikes. This assumption might be true, as most of the damage that the blades do experience comes from direct lightning attachment. Nearby lightning poses a significant threat to the sensitive electrical and electronics systems in the wind turbine, but not necessarily to the wind turbine blades. It assumed that the wind turbines in the actual array are placed 250m apart from each other so us to eradicate the risk of lightning attachment from strokes attracted by other wind turbines in the farm. The ground flash density across the North Sea has been set to 0.6. This has been set after referring to different lightning maps over North Sea. Using Equation (4-1), the number of lightning strikes attaching to the wind turbine are an estimated 0.28 strikes per year per wind turbine. Over the entire wind farm of 100 turbines this relates to a total of 28 strikes per year. It must be noted that these are the number of strikes the entire wind

farm will experience, irrespective of where the lightning strike will actually attach on the wind turbine. From Figure 4-3 it is seen that a large number of strikes attach to other extremities of the wind turbine other than the blades. These could include the wind vane and lightning rods protecting the wind instruments. Taking this into consideration and assuming that only 50% (chosen for ease in calculation and also a rough estimate based on the distribution of lightning strikes between the blades and the wind instruments in Figure 4-3) of the actual lightning strikes that are attracted within the wind farm do attach to the rotor blades, a figure of 14 lightning attachments to the blades is reached.

The above calculation is based on the number of lightning strikes that would attach to the rotor blades over a period of one year. Most of the lightning strikes will be intercepted by the lightning protection system in the blades. The lightning protection system for rotor blades are said to be 98% efficient [1]. In other terms, 2 out of every 100 strikes, poses a significant threat to causing damage to the rotor blades. This does not signify a large number as it is very rare for a single wind turbine to experience this amount of lightning. But with plans to increase the number of offshore wind farms and the number of turbines in these farms [65], the probability of lightning attaching to the rotor blades and not being intercepted by the lightning protection system increases.

In case of the present offshore wind farm of 100 wind turbines, it was calculated that 14 strikes will attach to the rotor blades. Thus 0.14 flashes would attach to the rotor blades of each wind turbine. 98% percent of the above flashes are said to be intercepted by the lightning protection system, thus avoiding any damage to the blade. Thus only 0.000028 flashes would cause damage to wind turbines over a year. This does show that the new lightning protection systems have managed to reach a level where the actual damage on rotor blades is now very rare.

6.5.6 Efficiency of the Lightning Protection System with RAM

The introduction of the new RAM has shown it may decrease the efficiency of the lightning protection systems of the rotor blades. This increases the risk of lightning attaching to unprotected parts of the blade and causing subsequent damage. Blades with lightning protection are said to be 98% efficient, It is hard to predict the amount of damage a lightning strike could cause on a blade, thus making it difficult to estimate the cost of such a repair. But for all repairs there will be a certain amount of downtime, this downtime will vary according to the scale of damage. The downtime can be converted into amount of revenue lost. In this section the effect of not having a lightning protection

on the rotor blades and also the effect of decreasing the efficiency of the lightning protection system due to the RAM is analysed and plotted.

In the following analysis the following assumptions are made.

1. Every lightning strike that does not attach to the lightning protection system is said to cause complete damage to the blade, thus having to replace them.
2. Each flash causes damage on different wind turbines and two flashes will never strike the same turbine.
3. There is a minimum downtime of 4 weeks once there is a report of fault or damage on the wind turbine blades.
4. The present cost analysis only takes into consideration the revenue loss due to power, cost of blade and the cost of hiring a crane ship.

Previously it has been mentioned that the blades cost an approximate €200,000 each, also from [23] the cost of hiring a crane ship is around €45,000 to €90,000 Euros a day (this is a price that has been stated in 2002, and taking into consideration the yearly inflation, this price is definitely to have risen). In this calculation, the lowest approximation is taken into consideration for the crane ship and it is assumed that the crane is only needed for 2 days.
In the UK according to [3] the average price level for power is around 5.1 c€/kWh. Wind turbines do not generate power throughout the day. The capacity factor of wind farms in U.K is said to be around 30% [66], though this said to rise with lore and new wind turbines to be added to the grid. The revenue losses due to the lightning strike are calculated as follows;

Total Revenue Loss = *(Number of wind turbines offline* (=number of lightning strikes*lightning efficiency) * *Rated Capacity* (3MW) * *Capacity Factor* (0.3) * *Price of generated power* (5.1c€/kWh) * *Number of weeks of downtime* *7*24 hours)+(Number of wind turbines offline*€200,000)(= Blade Costs)+ €90,000 (crane ship hire * 2 days)

Using the above equation, a linear relationship occurs between the effectiveness of the lightning protection system and the loss of revenues. This is plotted in Figure 6-16.

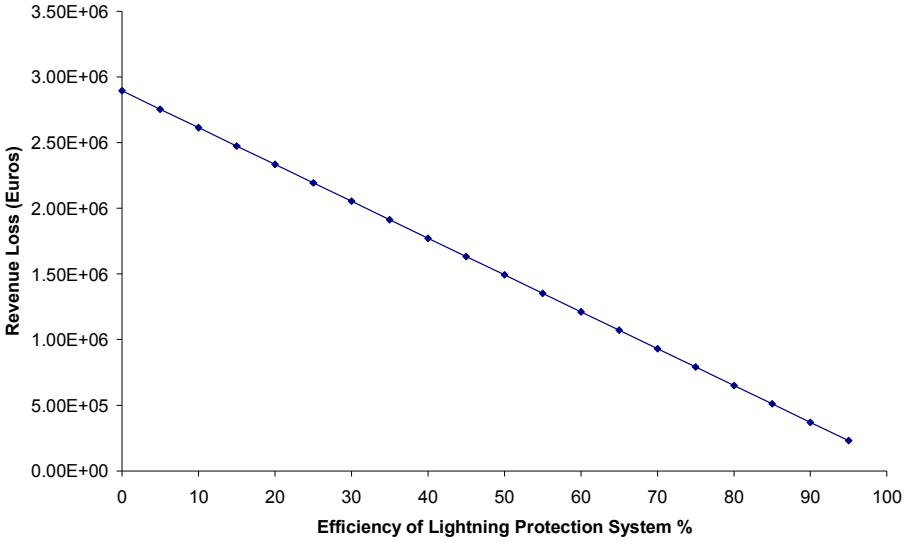

Figure 6-16 Revenue loss based on the Decrease in Efficiency

From Figure 6-16 it is clear that maximum revenue loss is experienced when there is no lightning protection present in the blades, as would be expected. But it must be noted that most of the loss is driven by the material cost of the new blade and also the crane ship.

In this context it must be remembered that there are other factors that would increase the revenue loss during downtime and repair. For an offshore wind farm these would include;

- Labour costs
- Other Logistics (other ships, equipment etc.)

Also for offshore wind farms weather conditions will play a major factor in the repairs. Repairs and service can only be performed in good weather conditions and there will be instances when the engineers will have to wait for favourable conditions to go offshore. These factors will also affect the relationship between total cost and lightning efficiency. Therefore Figure 6-16 is taken as a first order cost impact estimate.

The addition of the RAM the efficiency will drop as shown in Figure 6-16. Though it is not sure to what percentage level the efficiency would drop, the plot shows that even a lightning protection system working at 70% efficiency would cause considerable amount of revenue loss.

6.6 Conclusions

Finding from the above work can be summarised as,

1. Wind turbines do interfere with radar and one of the possible options to minimise this interference is RCS Reduction, by using Shaping and Radar Absorbing Materials.
2. Shaping possible for the Nacelles and Tower, but this is not possible for rotor blades, thus RAM are opted for this purpose.
3. The RCS solution for the blades includes conductive layers that will have to be included into the blade laminate and this will affect the performance of the lightning protection system.
4. An initial layer of the RCS solution was the conductive layer and it was concluded that it was possible to include this material into existing blade laminate processes.
5. The new layer affects the lightning protection system significantly. It reduces the lightning interception efficiency, thus increasing the risk of lightning attaching to unprotected sections of the blade. These were verified by 3D FEA simulation.
6. The new layer was tested for its performance in conducting high currents, according to the IEC 61400-24 standard. The material suffered severe damage at low peak currents, thus confirming that further studies were required on the material before it is introduced into the blade laminate.
7. The addition of the new layer fro both RAM purposes and also for strengthening the blade laminate has proved to effect the lightning protection system, this also translates into major losses in cost effective analysis, especially in areas of blade replacement costs and downtime.

7 High Voltage Testing of Blade Lightning Protection System

High voltage testing is performed to test the efficiency of lightning protection systems built in to the blades. This will help in the development of new blade models and the integration of new materials into the blade laminate. This becomes very important as manufacturers are pushing to find new composites and materials in developing much efficient and technologically advanced blade models. A test procedure will allow manufacturers to test new prototypes against standardised models. The new IEC 61400-24 'Lightning Protection of Wind Turbines' standard now includes a testing section especially for the rotor blades [79]. The testing section has been written to check the performance of new and existing lightning protection systems for rotor blades. The tests were formulated based on extensive knowledge of high current and high voltage tests on aircraft systems[80].

In this chapter the efficiency of a blades lightning protection system has been evaluated by testing it in accordance with the IEC 61400-24 'Lightning Protection of Wind Turbines' standard [1]. A new prototype blade loaded with carbon into its laminate is tested against a conventional blade model. The testing of both the conventional model and the new carbon loaded blade will help in determining the effect of the new carbon layer on the lightning protection system. Based on the results found from testing both blade types, the performance of the lightning protection on the new carbon loaded blade is analysed and commented on.

In addition to the tests specified in the standard, a new method for testing AC corona on blade tips has been formulated and performed to once again compare the performance of the lightning protection systems on both blade samples.

7.1 High Voltage Testing of Wind Turbine Blades

The outcomes of high voltage testing on rotor blades have been mentioned in the pervious chapter. These are [1],

- Location of possible leader attachment points and flashover or puncture paths on blades and non-conducting structures.
- Optimization of the location of protection devices (air terminals, receptors etc)
- Flashover or puncture paths, along or through dielectric surfaces.
- Performance of lightning protection devices.

The HV tests performed in this chapter are split into 2 different sections.

1. **Impulse Testing**
    - Streamer growth tests
    - Attachment point tests
2. **AC Testing**

Though AC tests are not generally used for evaluating the effect of lightning on electrical components, the ability to maintain a sustained corona using an AC test set enables to capture weak points across the sample much effectively on cameras. Whilst the first is performed using a high voltage impulse generator, the second has been performed using a cascaded AC transformer test set. Brief descriptions and working of these generators is also provided in this chapter.

7.2 Impulse Testing

Lightning leaders produce a rapidly changing electric field. The conditions required for rapidly changing electric fields can be replicated using an impulse wave, generated by a high voltage impulse generator. An impulse wave is one which reaches its peak value very rapidly and then decreases to zero in a time slower than the rise time.
It takes a double exponential waveform and is unidirectional. Figure 7-1 shows a typical impulse wave. An impulse wave is defined by its rise and tail times. The rise time is the time taken for the wave to reach 90% if its peak value (T_1). The tail time is on the decay side of the wave, and is the time taken for the wave to reach its 50% value (T_2).

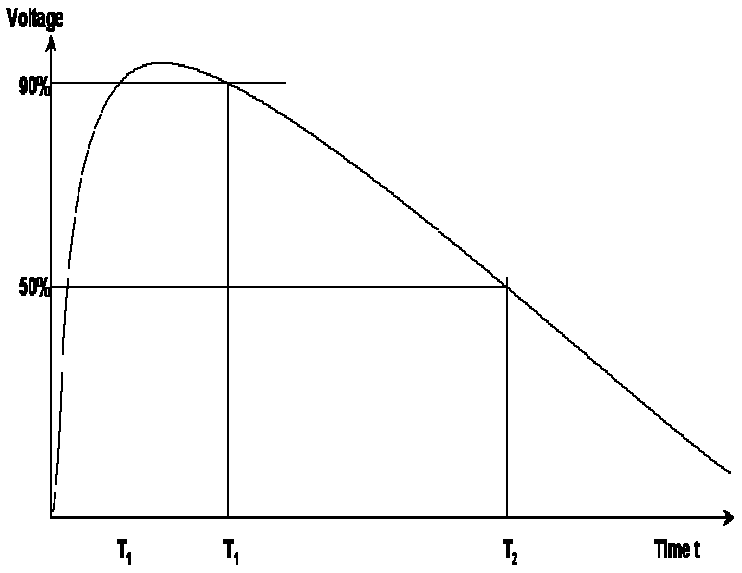

Figure 7-1 Impulse Wave

An Impulse generator has been used to generate the necessary impulses for the tests.

The basic circuit of an impulse generator is shown in Figure 7-2. It consists of a capacitor, which is charged to the required peak level and then discharged through a set of resistances. The value of these resistors determines the shape of the impulse.

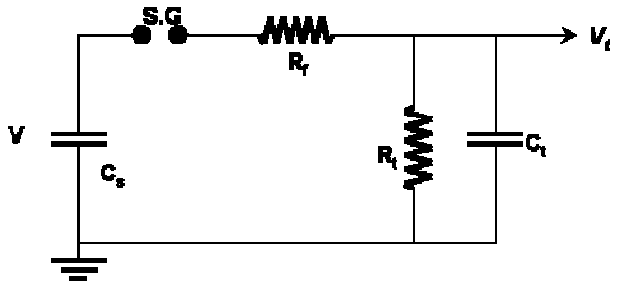

Figure 7-2 Circuit Diagram for a Single Stage Impulse Generator

The capacitor C_s is charged through a DC source till, the spark gap S.G, breaks down. At this moment, the voltage is impressed on the test object with a capacitance C_t. In the above circuit the two resistors R_f and R_t determine the shape of the impulse wave. The resister R_f determines the front/rise time of the impulse wave while R_t determines the tail/decay time. An analysis of the this circuit is presented in [81]. The output voltage of the above circuit diagram is given by,

$$v(t) = V\left[e^{\left(-\frac{t}{R_t C_s}\right)} - e^{\left(-\frac{t}{R_f C_t}\right)}\right] \quad \textbf{(7-1)}$$

From Equation (7-1) it is seen that the output voltage is mainly driven by the front and tail resistance.

The one stage impulse generator is not suitable for generating high voltage impulse waves. Marx suggested a way in which several large capacitors were charged in parallel and then discharged in series. A schematic 5 stage Marx impulse generator is shown in Figure 7-3.

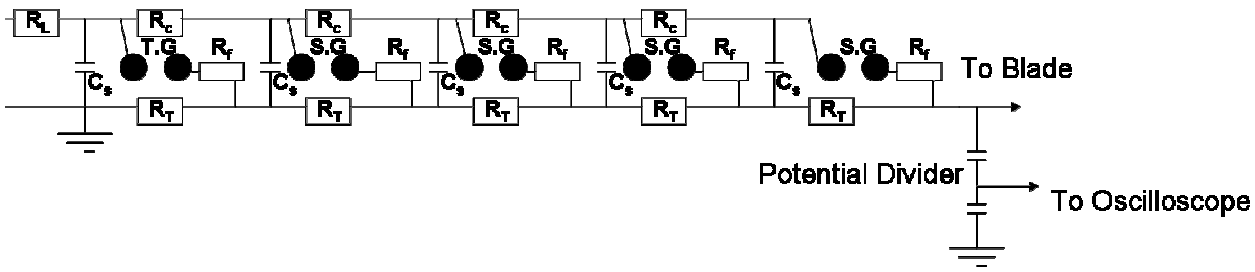

Figure 7-3 Schematic of a 5 stage Impulse Generator

Where,

R_L – Charging Resister, R_c – Series Resister, R_T – Tail Resister, R_F – Front Resister

C_s –Impulse Capacitor

The capacitors (C_s) are charged in parallel using the charging resisters (R_L, R_c). The initial sphere gap (T.G) is triggered using an external firing unit. Once there is breakdown across T.G, subsequent sphere gaps (S.G) breakdown, allowing the capacitors to discharge. The final voltage is a multiple of the number of stages and the voltage seen across each capacitor (C_s). Hence if a voltage V is seen across each of the capacitors C_s, a voltage of 5V is seen after the 5 stages.

The H.V impulse generator used in performing the tests on the blade samples is a 10 stage Marx generator, rated at 2MV. The impulse generated for the purpose of these tests has been proposed in [1]. The wave form is a switching type impulse with specifications as shown below,

Time to Peak T_1 or T_{peak} = 250 µs

Time to Half Value T_2 or T_{Decay} = 2500 µs

This waveform is also selected as the rise time allows the development of streamers from the blade sample. The tolerance levels for the switching impulse are given in the IEC 60060 -1 'High Voltage Testing Techniques – 1' [82], and are shown below

Time to Peak T_1 or T_{peak} = ± 20%

Time to Half Value T_2 = ± 60%

A positive impulse within the stipulated tolerance levels and with the rise and decay times as stated in the standard is shown in Figure 7-4.

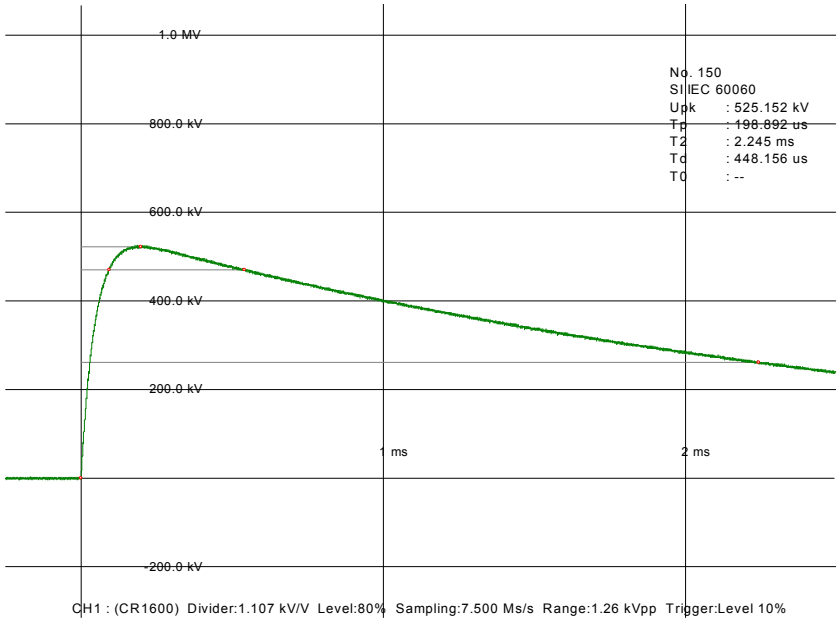

Figure 7-4 Positive Switching Impulse of 525kV

7.3 Streamer Growth Tests

During a thunderstorm the electric field around the blade increases, thus giving rise to streamers and lightning leaders from the blade tips or points of high field enhancement. This could also be the case if a downward lightning leader approaches the blade, also giving rise to streamers and answering leaders. The location of the streamers, lightning and answering leaders is crucial in determining the efficiency of the lightning protection system. Points of high field enhancement are those prone to develop streamers, and are potential attachment points during a lightning strike. These points should be rated to withstand the lightning current and also ensure the safe conduction of the lightning current without damaging other parts of the blade. In these tests, these points of high field enhancement are identified. Using both positive and negative impulses, streamer growth on the blade tip is captured and the location is identified to determine the efficiency of the lightning protection system.

7.3.1 Test Specimen

Tests were performed on Wind turbine blade tips, 3.5 metres long. Two kinds of samples were used for these tests,

- ***Conventional Blade Samples.***

  The samples are made of GFRP, and have an integrated receptor based lightning protection system.

- ***Carbon Based Blade Samples***

  Unlike the conventional blade samples made out of GFRP, these blade tips have a layer of carbon part of the blade laminate. These blades were manufactured as prototypes for reduction of RCS, and prior to these tests had not been subjected to any lightning tests. The results of these tests were thus vital in determining whether they were capable of handling actual lightning attachment and the energy transfer because of the same.

All the tips are manufactured in the same way as conventional blades, and defects are avoided in order to make the tests as realistic as possible. A tip of this size means it can be tested in the available lab space, and also the tip blade section is the most vulnerable part during lightning attachment.

7.3.2 Test Set Up and Method

The experimental set up of the tests is shown in Figure 7-5 and Figure 7-6.

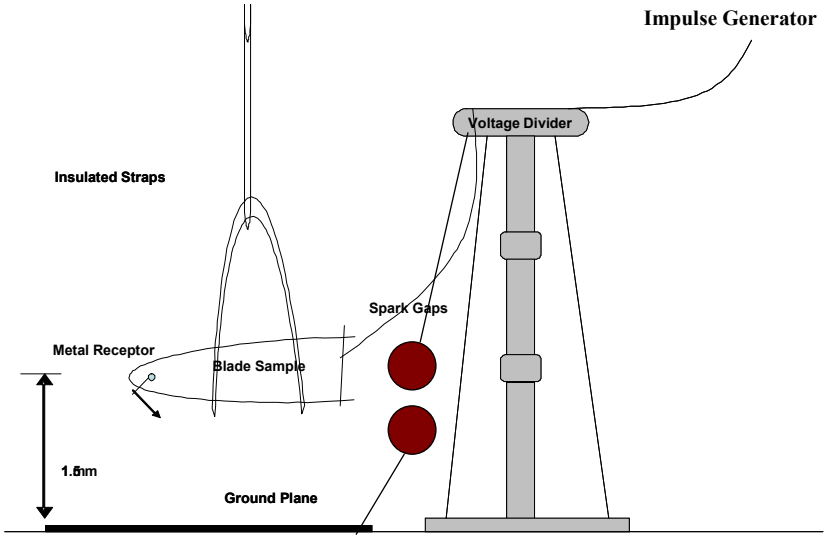

Figure 7-5 Schematic of Test Set Up for Streamer Test.

1. The blade was held by insulated straps on the crane and was positioned horizontal to the ground plane. This can be seen in Figure 7-5.
2. The ground plane below the test object was made of several metal sheets, all joined together using conductive tape inorder to avoid any joints and make sure edges are kept far away from the specimen. The dimension of the entire ground plane was 5m x 6.25m. This is shown from the aerial view of the experimental set up in Figure 7-6.
3. The height of the blade from the ground plane was adjusted in such a manner that, the receptor is set at 1.5m from the ground plane.
4. The down conductor of the blade lightning protection system is connected to the impulse generator. It was ensured that the connection is made in such a manner that the leads and the down conductor are always at a higher distance from the ground plane as compared to the receptor/ground plane.
5. To make sure that there was no risk of flashover between the receptor and the ground plane (as the basic aim of these tests is only to initiate streamers from the blade surface), the generator settings were calibrated to find the voltage, at which the blade initiates visible streamer activity, but not enough to cause a flashover.

Figure 7-6 Aerial View of Test Set Up in the H.V Lab

6. The calibration of the generator was performed by draping the entire blade with aluminium foil (Figure 7-7), making sure that the receptor was in contact with the foil. It is also connected to the down conductor via leads.

Figure 7-7 Blade wrapped in Aluminum Foil

7. A switching impulse was applied through the impulse generator on the covered blade. The amplitude of the impulse is increased till there is a flashover between the aluminium foil and the ground plane.
8. In the above tests, the flashover occurred at 635kV. The point of flashover was from the tip of blade (covered in aluminium foil). This voltage was noted down.

9. The aim of the tests is to try and develop streamers, ideally from the receptors, and at the same time try and avoid flashover between the receptor and the ground plane. The sphere gaps are used to ensure there is no risk of flashover.
10. Once the flashover voltage was determined with the aluminium foil, the distance between the sphere gaps was set, such that there is definite breakdown between spheres at 635kV. This minimises the chances of flashover between the receptor and the ground plane once the aluminium foil is removed. Figure 7-8 shows the initiation of streamers from the tip of the aluminium covered blade. Here the flashover has been avoided, by setting the sphere gaps to the appropriate distance.

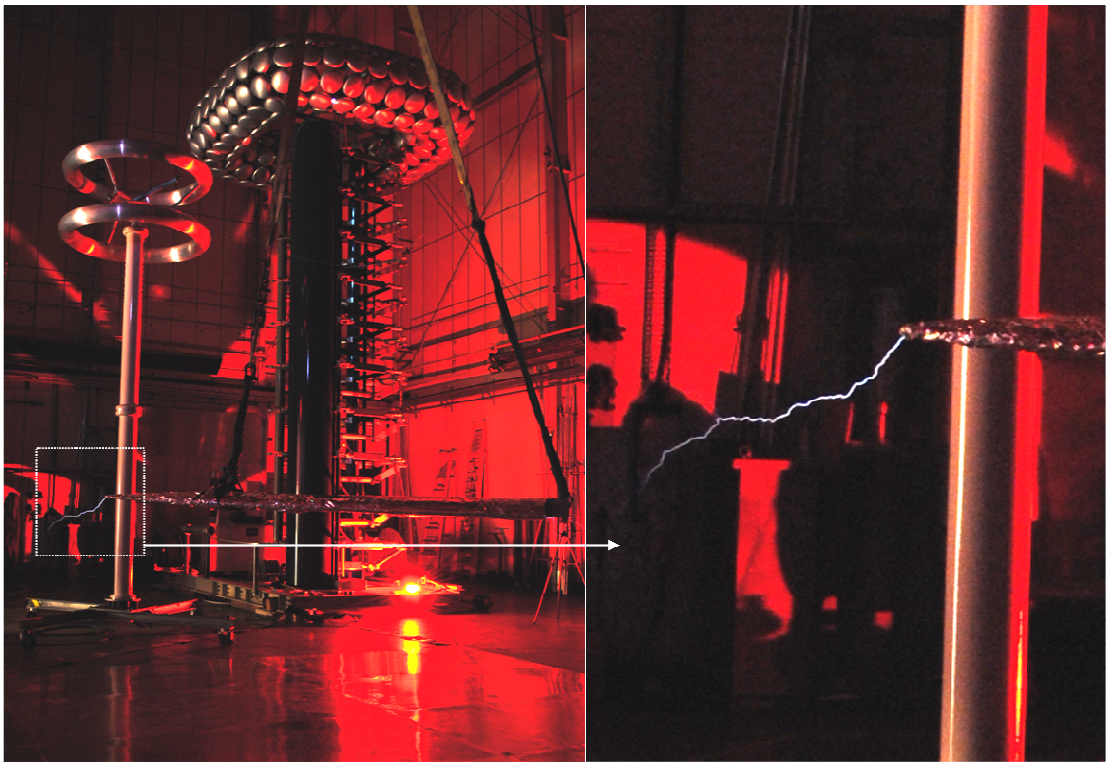

Figure 7-8 Streamer Initiation in presence of Sphere Gap

11. With the sphere gaps set at the required distance, the aluminium foil was removed from the blade.
12. The blade was subjected to switching impulses, starting from 400kV and in incremental steps of 50kV each time (the limit was set to 600kV, to minimise the chances of flashover between the receptor and the ground plane). For each of these pulses UV pictures are captured.

After each pulse the blade was inspected to make sure no damage was caused from the streamer initiation points. These tests were performed by placing the blade in different orientations, these are shown in Figure 7-9.

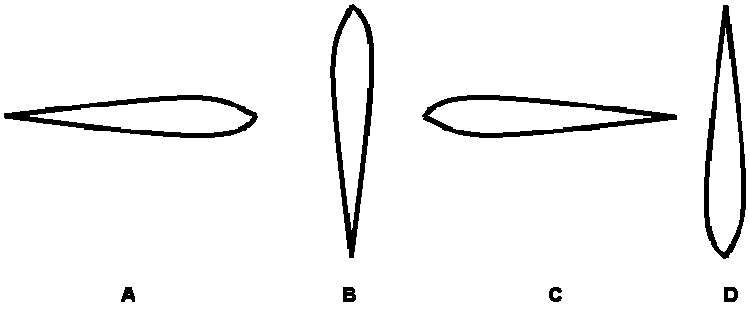

Figure 7-9 Blade Orientations

The blades were tested against positive and negative switching pulses in all orientations. The streamer propagation is caught on UV camera and the location from which it is initiated is analysed.

7.3.3 UV Camera Specifications

Most of the emitted light during streamer propagation is at a wavelength which is not possible to be detected by the naked eye or conventional cameras. In reality regular cameras restrict the passage of ultra violet light. Thus for the purpose of capturing UV light during the streamer initiation a UV sensitive camera and lenses were used. A Hamamatsu C8484-16C camera was used for these tests. The UV camera has a spectral response as shown in Figure 7-10.

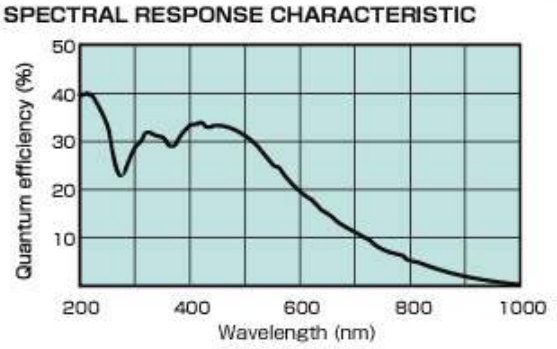

Figure 7-10 Spectral Response of UV Camera

Lightning streamers and discharges were found out to be within this range, and initial trials on the camera showed that it was capable of capturing the phenomenon.

Unlike conventional cameras, the UV camera is directly connected to a computer using a IEE 1394 firewire cable. The cable itself is connected to PCI frame grabber card that is provided along with the camera and can be installed on any conventional desktop. The imaging software provided with the camera allows the recording of single images or recording of several single images from a fixed time sequence. By using the feature where a sequence of images can be captured, the camera is triggered a few seconds before the lightning impulse, thus making sure that the camera definitely captures the streamer activity. Even with this feature, it is possible to miss the streamer initiation as

there is a risk of the streamer initiation to happen in-between the single images the camera captures. The UV camera does not come with an inbuilt lens. Thus it is essential to have UV sensitive lenses. A UV-Nikkor 105mm f/4.5s was used for this purpose. This lens is used for photography that demands capturing the invisible spectrum of at ultraviolet wavelength.

7.3.4 Results of Conventional Blades

As mentioned before, these tests have been performed in addition to the attachment tests, which shall be explained later in this chapter. The major difference is that these tests tend to be non-destructive. The results of these tests will throw light on the behaviour of the blade when a negative downward leader (replicated by positive impulse test) and positive downward leader (replicated by negative impulse test) approach a blade. The streamers tend to begin at voltages of around 500kV. But the phenomenon becomes much visible at 600kV and easier to capture on the UV camera. A similar result was found in the remaining orientations under positive streamers. Figure 7-11 and Figure 7-12 show positive streamers being emitted from the receptor on the conventional blade sample in two different orientations at 600kV .

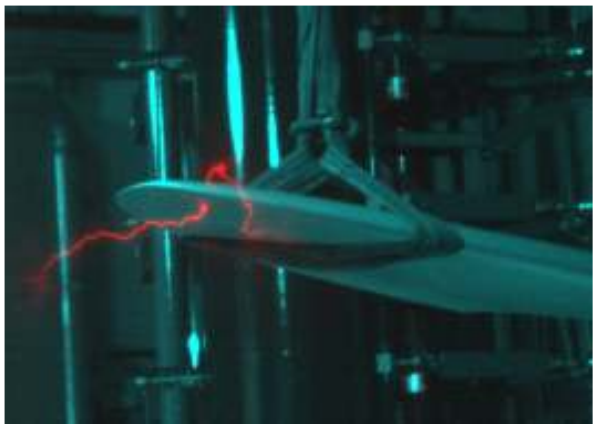

Figure 7-11 Positive Streamers from Receptor on Convention Blade Sample at 600kV (Position A)

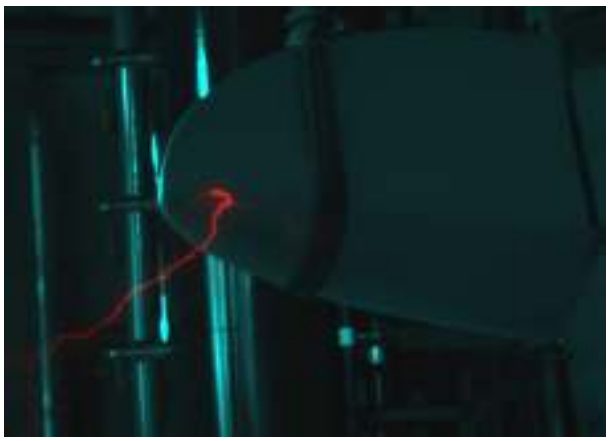

Figure 7-12 Positive Streamers from Receptors on Convention Blade Sample at 600kV (Position D)

The voltage required for negative streamers is almost twice as much as that required for positive streamers. Even at twice as much of the voltage the streamers are not well defined on the UV camera, compared to those of positive. Also it can be observed that whilst the positive streamers tend to move away from the receptor, the negative streamers move along the surface of the blade. Figure 7-13 and Figure 7-14 show the streamer initiation and propagation under negative impulse voltages.

Figure 7-13 Negative Streamers from Receptors on Convention Blade Sample at 950kV (Position B)

Figure 7-14 Negative Streamers from Receptors on Convention Blade Sample at 950kV (Position C)

This can be explained due to the accumulation of surface charge over the blade surface during the negative impulses. This phenomenon is explained in [24].

The conventional idea is that when a high voltage of a certain polarity is applied across an electrode, space charges of the same polarity build up near the electrode and the surface next to it. As the field is increased, the surface charge increases, thus repelling ions of the same polarity away from the surface and the electrode. This second set of

surface charge (also known as second corona) attracts ions of the opposite polarity, eventually causing a flashover. But this is not usually the case, as the surface charge tends to affect the breakdown voltage. Photo-ionisation on the surface of the blade gives rise to positive surface charge. The polarity of this charge is positive irrespective of the applied voltage [24].

The presence of this positive surface charge could explain the reason to why the streamer propagates across the blade surface and also could explain the reason to why the voltage is twice as high for visible negative streamer, as compared to their positive counterparts. When the receptor is acting as a positive electrode, positive ions build up near the receptor. These ions are repelled from the blade, due to the positive surface charge, thus shortening the gap for the breakdown. At the same time electrons from the ground are attracted, once this channel is complete flashover or breakdown occurs, this is shown in Figure 7-15.

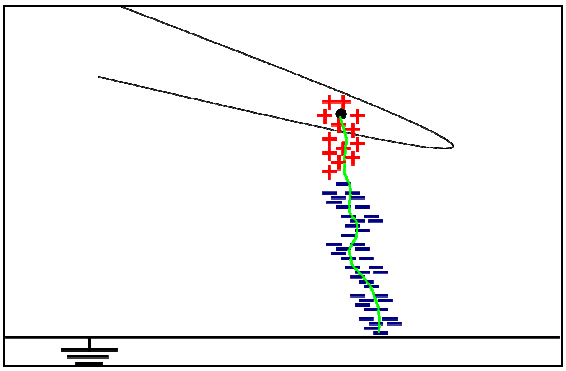

Figure 7-15 Positive Flashover Over Blade Surface

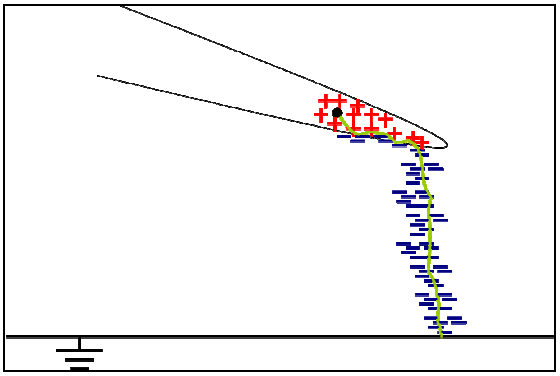

Figure 7-16 Negative Flashover Over Blade Surface

However when the receptor acts as a negative electrode, as the voltage is increased, electrons due to the ionisation of the air around the receptor are attracted to the positive surface charge. These would then ionise gas molecules around the blade surface, giving rise to more electrons and positive ions, and at the same time reducing the gap between the ground electrode and receptor (Figure 7-16). Further photo-ionisation give rise to more electrons, and eventually complete the channel between the receptor and the ground plane causing flashover.

7.3.5 Results of Carbon Loaded Blade Samples

Once the conventional blade samples were tested for streamer growth, the carbon loaded blade samples were tested. This would highlight any difference in the performance of the lightning protection system due to newly added carbon layer into the usual non-conducting laminate. Due to constraint on time and lab availability, the carbon loaded blade had not been tested in all the different orientations for the streamer tests.

Streamer initiation on the carbon loaded blades begins at around 400kV, this is lower in comparison to that of the conventional blades devoid of the carbon layer. Figure 7-17 shows the streamer development on the carbon loaded blade at 600kV in orientation A. Contrary to the response of the receptor on the conventional blade, those on the stealth blade failed to initiate streamers. Instead of the receptors, the tip begins to initiate streamers. This is undesirable as it puts unprotected parts of the blade at risk due to lightning attachment.

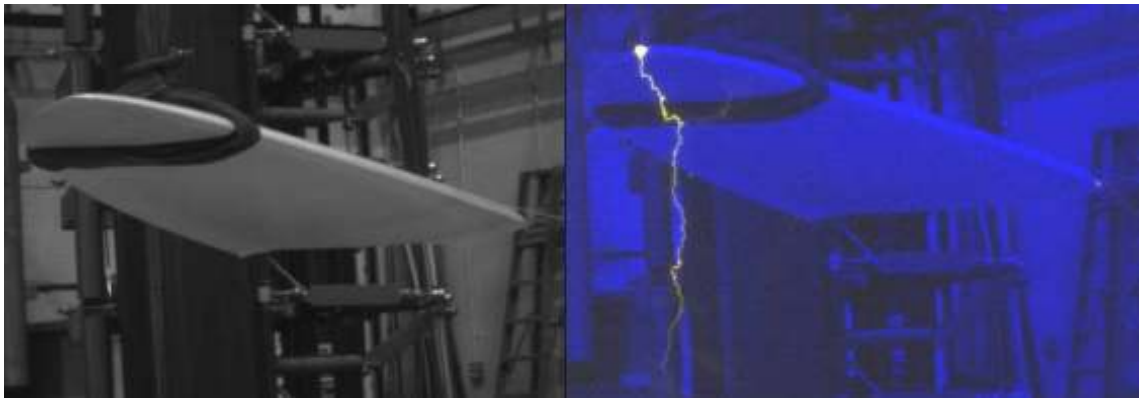

Figure 7-17 Positive Streamers from Tip on RCS Blade at 600kV in Position A (left figure to show blade in day light for comparison)

The addition of the carbon layer invariably dulls the field enhancement across the receptor, thus putting the rest of the blade at risk due to lightning attachment. This effect has already been highlighted previously in the FEA simulation performed in Section 6.5.1.

Figure 7-18 Negative Streamers from Tip on RCS Blade at 1050kV Position A (left figure to show blade in day light for comparison)

In Section 6.5.1, a cylinder shaped model, replicating the tip of the blade was modelled with an inner carbon layer. The results showed considerable field enhancement at the tip of the blade and at the same time a dulled receptor. The results for the carbon based sample shown in Figure 6-11, predicted a high field enhancement at the tip indicating a possible hotspot for lightning attachment and streamer propagation under high ambient fields. Figure 7-17 confirms that the tip will be at high risk due to the addition of the inner carbon layer.

A similar response is seen when the blade is subjected to a negative impulse. Figure 7-18 shows the development of the streamer from the tip. The location of the streamers does not appear to start from the tip, this can be explained to the fact that all UV pictures have been taken in no light and then have been merged with the actual blade pictures taken in light using in-house imaging software. The mismatch of the streamer with the tip can be explained to the fact that the position of the blade had moved prior to taking the UV picture. Figure 7-19 shows the streamer growth on a conventional camera and confirms the streamer initiation form the tip of the blade and not the receptor.

Figure 7-19 Negative Streamers from Tip on RCS Blade at 1050kV (Position A) from conventional camera

The introduction of the carbon layer in the blade laminate changes the field distribution around the blade. In a conventional blade, the gap between the receptor and the ground plane can be compared to a point - plane gap. Here the point being the receptor and connected to the high voltage end. Thus the point of high field enhancement is the receptor, even though it is surrounded by an insulating medium, GFRP, the blade laminate.

In the Carbon loaded blade the carbon layer is connected to the receptor and now the gap can be compared to a plane - plane gap, or to a certain extent a uniform field. The receptor now does not enhance the field, thus allowing any area on the blade to start streamers and possible lightning attachment.

The following are summarised from the streamer growth tests,

- Streamer activity is seen from the receptor of the conventional blade sample, however, carbon loaded blades initiate streamer from the tip of the blade, indicating possible weak points.
- It was found easier to capture positive streamers, and also the voltage required for positive streamer initiation is low in comparison to negative.
- Negative streamer is not as defined as the positive streamer, and the propagation has been seen to follow the surface of the blade, whilst the positive moves away from the blade surface.
- The results from the streamer tests show that there is a significant effect of the carbon layer on the performance of the receptor. This dulling effect has already been confirmed in the FEA testing performed in Section 6.5.1.

7.4 Attachment Point Tests

During a thunderstorm the background field across the wind turbine increases, either due to an approaching downward leader, or the high ambient field caused due to low level clouds (upward initiated). There will be considerable amount of field enhancement around the receptors on the wind turbine blades. If this electric field reaches a certain value (theoretically 3MV/m) they begin to emit answering leaders (in the case where a downward initiated lightning leader approaches) or upward leaders (in the case of upward initiated lightning). These tests have been formulated to try and replicate the phenomenon of answering or upward leader attachment by inducing a high voltage across the lightning protection system, and verify its efficiency. These tests are specifically designed for the tip section of the blade, as this is the part of the blade which is at higher risk of lightning attachment.

The samples used for these are the same samples used for the streamer tests. The blade samples are manufactured with an inbuilt receptor/down conductor based lightning protection system. The receptor is the preferred attachment point during a lightning strike. If the lightning strike attaches to any other location on the blade, there could be a possibility of significant damage to the blade. These tests are particularly interesting in the case of the carbon loaded blade as it has been found from the previous streamer tests that the receptor has significantly lost its efficiency to enhance the electric field, thus affecting its primary purpose of preferred lightning attachment.

7.4.1 Test Set Up and Method

The test set up and methodology for the attachment tests is similar to that followed for the streamer growth tests.
The test set up differs in a few areas and these are mentioned below.

1. The main aim of these tests is to analyse the attachment points during lightning attachment, thus flashover between the air termination and the ground plane is necessary. Unlike the streamer growth tests, the spark gaps are removed so as to create successful flashover between the blade and the ground plane (Figure 7-20).

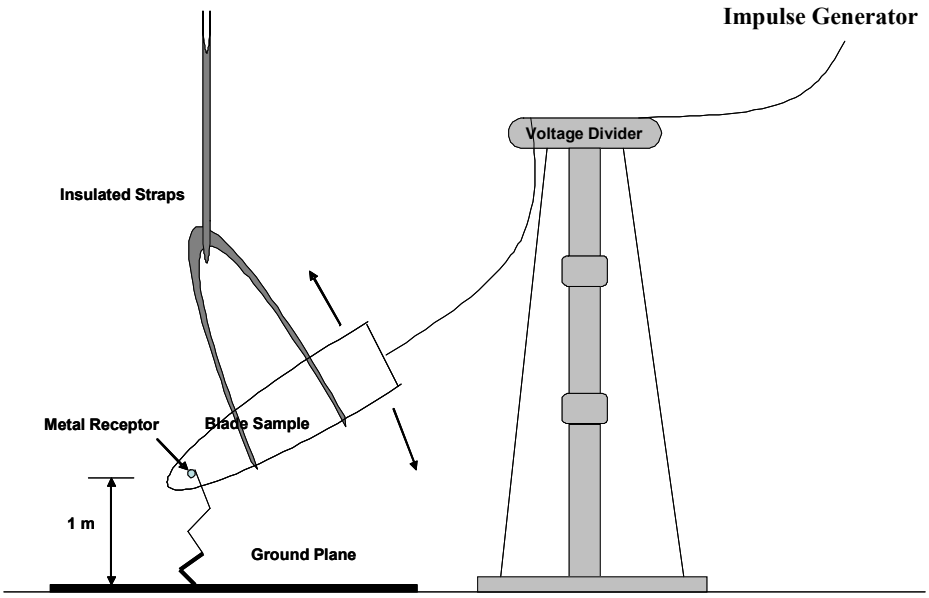

Figure 7-20 Schematic of Test Set up for Attachment Tests

2. In addition to the different orientations, the blades are tested at different angles with respect to the ground plane. These are shown in Figure 7-21. The idea of this is to replicate the blades rotation and its impact on the lightning protection system during the lightning attachment process.

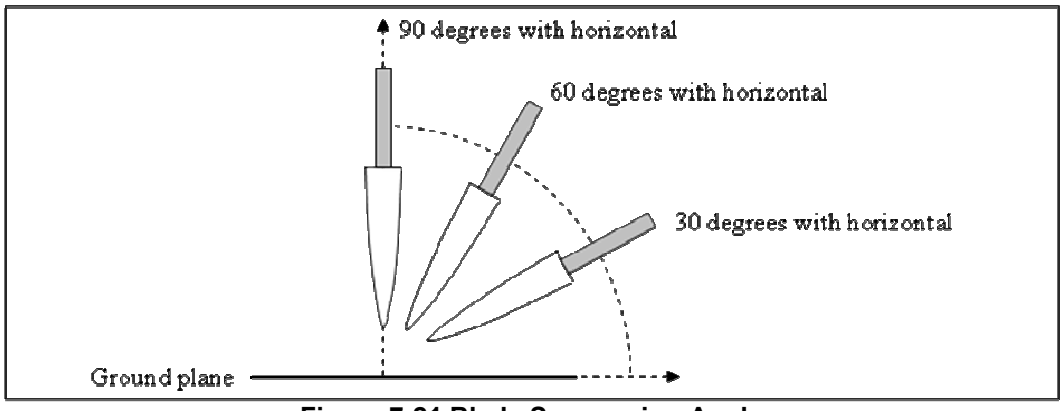

Figure 7-21 Blade Suspension Angle

3. The distance between the air termination point and the ground plane is set to 1m, in contrast to the 1.5m of the streamer growth tests.
4. The calibration of the generator is performed in a similar fashion to the streamer growth tests. However, once the breakdown voltage with the aluminum foil is determined, the foil is removed and the blade is subjected to approximately the same voltage that is believed to cause flashover between the blade and the ground plane.
5. Two digital cameras have been used to capture the lightning attachment process. The cameras have been set on a low shutter speed, and are triggered remotely using an infra red remote a few seconds before the flashover.

7.4.2 Results

Once the breakdown voltage for a blade covered in aluminum is determined, the aluminum foil is removed and the impulse voltage is set to a level close to that where breakdown is believed to occur in absence of the foil. Usually the blade samples are tested in all 3 angles, with all four orientations (A,B,C and D). These tests are performed using switching impulses of both positive and negative polarity. The switching impulse with rise, decay times and tolerance levels similar to that shown in Figure 7-1 are used in these tests.

Due to limited availability of the high voltage lab, it was decided that the blades be tested in Orientation A (Figure 7-9) for all three angles (Figure 7-21) for positive switching impulse. The positive switching was chosen as a flashover in the 1m gap can be successfully satisfied in this polarity. The results are interpreted as follows.

- If the flashover occurs between the receptor and ground plane the blade is deemed to have passed the attachment tests.
- If the flashover attaches to anywhere else on the blade, other than the receptor, the blade is deemed to have failed the lightning attachment tests.

Table 7-1 shows the results of the attachment tests.

Blade Type	Orientation	Angle of Blade	Polarity of Impulse	Peak Voltage kV	Pass/Fail	Figure
Conventional	N/A	90	Positive	500	Pass	Figure 7-22A
Conventional	A	60	Positive	450	Pass	Figure 7-22B
Conventional	A	30	Positive	500	Pass	Figure 7-22C
Carbon Loaded	N/A	90	Positive	400	Fail	Figure 7-23

Table 7-1 Test Results of Attachment Tests

From the results it is seen that the conventional blade sample passes the test in all angles. Figure 7-22 shows the flashover between the receptor and the ground plane. Also magnified next to each of the discharges is the actual connection point, between the leader that initiates from the ground plane and the one that initiates from the tip receptor. The connection point between the leaders is mostly away from the receptor, especially in the case where the blade is 30 and 60 degrees inclined to the ground plane. These results can be compared to those found in [83]. The tests performed in

[83], also state that the connection point in the case of negative polarity switching impulses is much nearer to the receptor. This could be to the fact that the voltage required for successful breakdown in negative polarity is twice as much as that compared to it positive counterpart. The increased time in producing the negative impulse, allows the streamer from the ground plane approach closer the receptor, thus allowing a connection nearer to the blade [24].

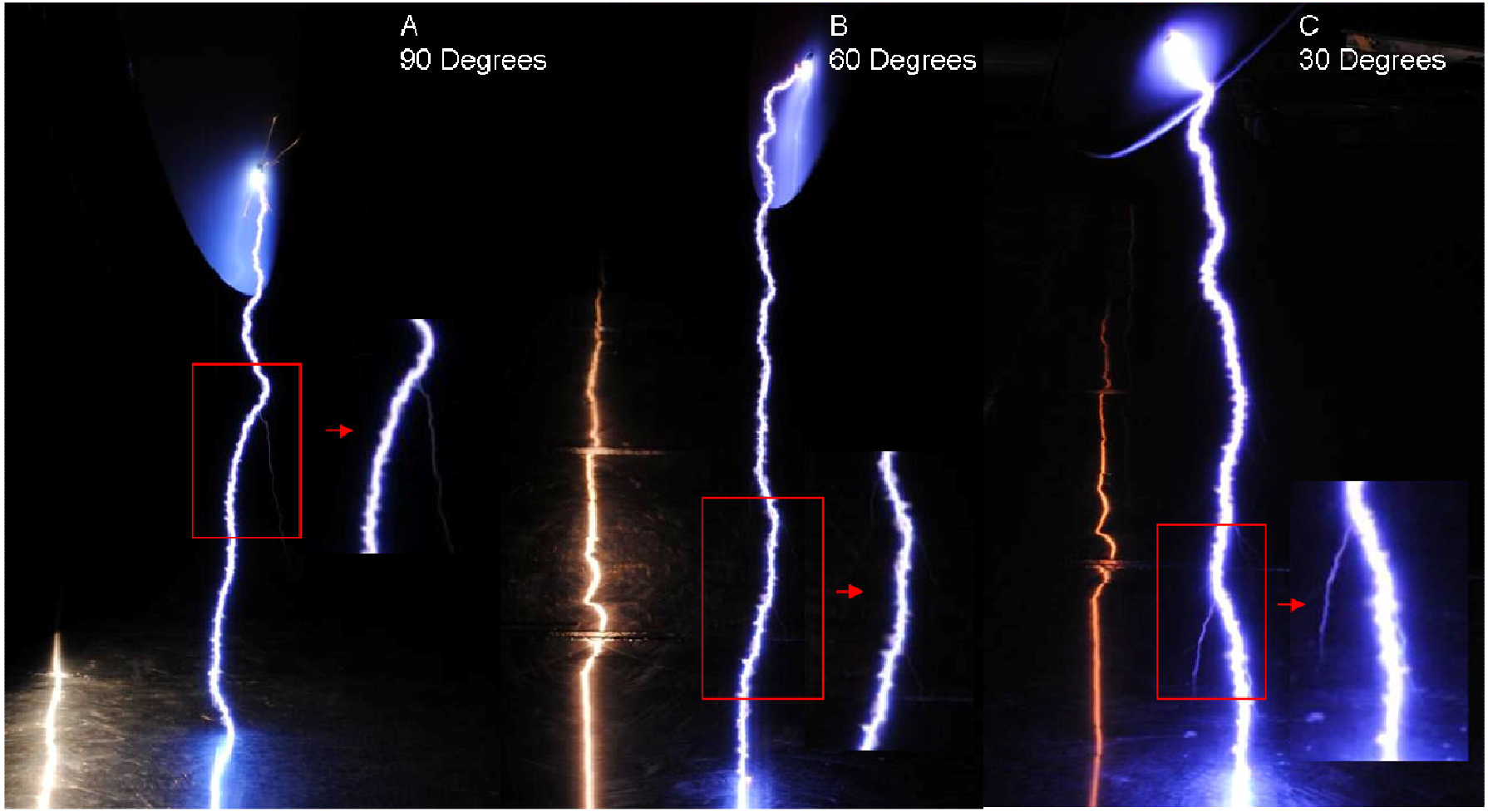

Figure 7-22 Attachment Tests in all Three Angles with respect to Ground Plane

In contrast to the conventional blade, the carbon loaded blade failed the test in the first orientation. The flashover happens between the tip of the blade and the ground plane. This can be seen in Figure 7-23.

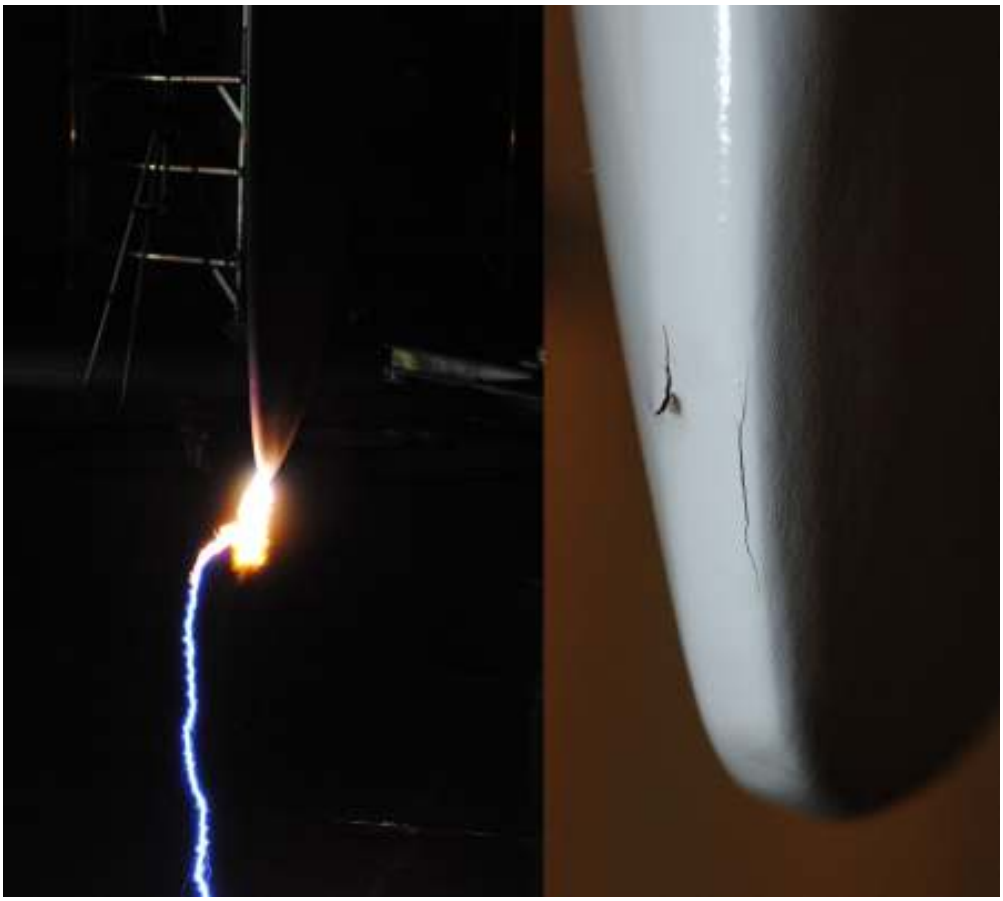

Figure 7-23 Tip Breakdown of Carbon Loaded Blade and Resultant Damage

Figure 7-23 shows the failure of the blade and the damage that it sustained during this breakdown. The damage appears as a puncture at the tip of the blade sample. This is inline with the streamer tests, as they have shown high field enhancement at the tip of the blade, indicating a possible risk of lightning attachment at this point (Figure 7-18 and Figure 7-17. Though it is hard to confirm that the streamer growth and puncture occur at the same location on the blade tip, it can be confirmed that the addition of the carbon layer to the existing laminate overrides the field enhancement at the receptor. The carbon layer also enhances the field at the tip of the receptor, thus invariably making this a point of likely attachment during a lightning strike. The results of these tests also coincide with the FEA analysis performed in section 6.5.1.

7.5 AC Corona Testing

AC voltages are usually not used for lightning tests. But with the help of the AC test set available at the National Grid Power Systems Lab, it was decided to test the blade samples for electric field enhancement and corona using high AC voltages. These tests are intended to capture corona hotspots and locations of high electric fields on the UV camera.

These tests are the first of their kind. The advantage of testing the blades under the AC stresses is that there is sustained growth of corona while the voltage across the down conductor is kept high enough. This corona is constant till the volts across the test set are totally dropped. This gives a better control of capturing potential weak points/hotspots on the blade tip. The idea still remains similar to the initial leader tests. During the AC stresses, the only hot spots, technically, should be the receptor. Thus indicating that under a high electric field, the receptor would be the first to initiate streamers. On the contrary if there are other locations of corona growth and hotspots, this would indicate a potential weak location that might fail during a lightning attachment, especially in the case of the carbon loaded blades.

These tests are presently research oriented and the results will help in determining if the test is capable of being introduced as a standardized test. The biggest advantage of these tests is the ability of being able to correlate tests obtained in the lab with those performed using FEA methods. However, inorder to have a benchmark for the already standardized tests and not to affect the blade samples in anyway, these tests have had to be performed after concluding the streamer and attachment tests.

7.5.1 AC Cascaded Test Set

Single test transformers for high voltages are both heavy and logistically difficult to install. To overcome this problem, transformers are connected in cascade to reach higher voltages.

The basic description of a cascaded transformer is given in several parts of the literature [84-86]. A brief description of the same is given below.

Figure 7-24 shows a two cascaded transformer. The key points of the transformer are,

- The primary winding of the first transformer (A'A) is connected to the supply voltage V_1.The first transformer and the tanks are both kept at ground

potential.

- The primary winding of the second transformer (A2'A2) is connected to the high voltage side of the first transformer. This connection is made through the tapping (C'B'). This tapping is selected in such a way that the voltage across (C'B') is equal to the supply voltage, V_1.

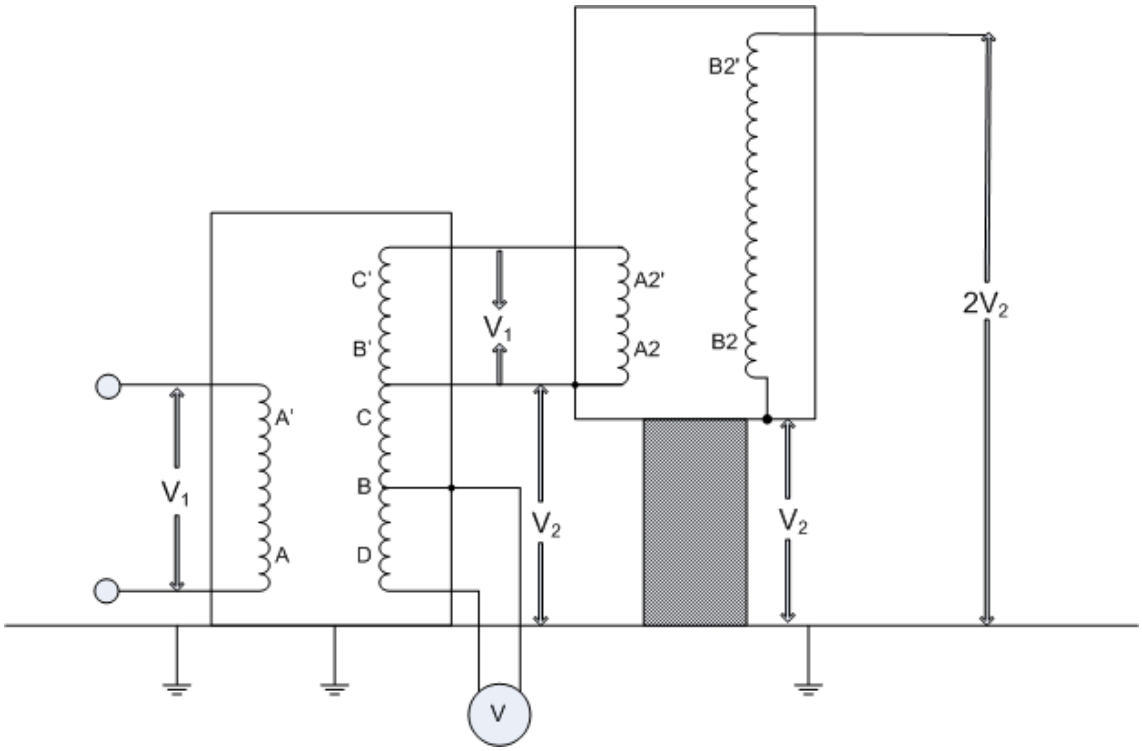

Figure 7-24 Schematic of Two Cascaded Transformers

- The second transformer and its tank are kept insulated and above the ground, and B2 of the secondary winding of the second transformer is connected to the tank for the full secondary voltage of the first transformer.
- The voltage across B2' and the ground is now twice the output V2, of the first transformer.
- An 800kV test set was used for the purpose of the tests in this section.

7.5.2 Test Set Up and Method

The test set up of these tests is similar impulse testing. In these tests the down conductor of the blade samples was connected to the AC test set as shown in the Figure 7-25. The receptor is maintained 1m above the ground plane, to avoid flashover at high voltages. The voltage on the transformer is increased till there is visible corona on the blade tip. This is observed on the live view of the UV camera. The UV camera is set to capture the first 40cm of the blade, as the receptor is covered into this length. The voltage at which the UV camera captures corona is noted down.

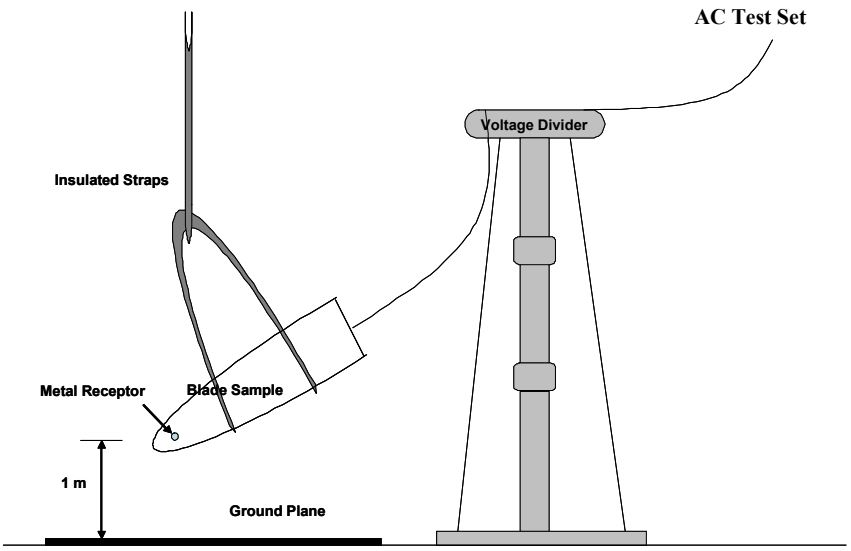

Figure 7-25 AC Corona Test Set Up

The tests were performed with the blade horizontal to the ground plane and in orientations, A and D (Figure 7-9).

7.5.3 Results and discussion

The conventional blade begins corona initiation at 100kV AC. Figure 7-26 shows the corona at 133kV AC in Position A.

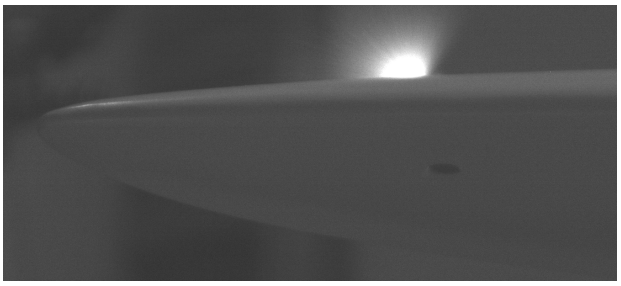

Figure 7-26 Corona Inception at the Receptor (Position A) at 133kV AC

A similar result is seen when the blade is placed in a 'D' Orientation. This can be seen from the Figure 7-27. The corona initiation in this orientation begins at about 95kV AC.

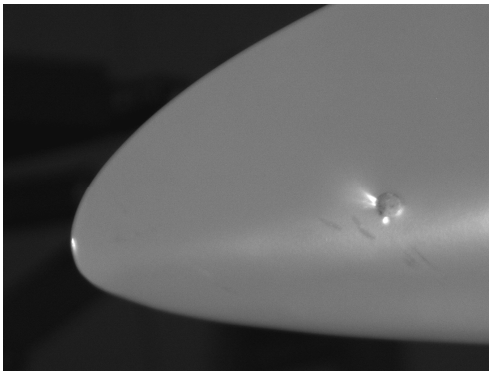

Figure 7-27 Corona Inception at the Receptor (Position D) at 100kV

From the above figures, the point of highest field enhancement is the receptor. This is a positive result and coincides with that of the streamer initiation, indicating that the receptors on the blades are more susceptible to lightning attachment than any other part at the tip. However, Figure 7-27 also shows that the tip of the blade begins to initiate corona too. Though the corona is not as significant as that seen on the receptor, it highlights the risk of lightning attachment on unprotected parts, even on conventional blades. This field enhancement can be due to minor damage caused because of the previous streamer and attachment tests, or even a minor manufacturing defect, such as bumps on the layer which eventually are hotspots for corona and streamer initiation.

Interesting results are seen when the carbon loaded blades are put through AC stresses. Corona inception of the carbon loaded blades begins at approximately 100kV AC. The carbon loaded blades, in contrary to the normal blades, showed areas of high field enhancement and corona from areas other than the receptor. These can be seen from Figure 7-28.

Figure 7-28 is the UV capture of the receptor on both sides of the carbon loaded blade when subjected to 133kV AC. Whilst, some of the corona is seen in areas where the blade has been damaged due to the attachment tests, there are areas where corona is initiated which was not involved to the damage caused in attachment tests. These could be possible attachment points for further damage. The intensity of corona at the location damaged due to previous attachment is high compared to any of the other hotspots. This could be explained due to deposition of carbon at this location, created due to the puncture from the attachment tests. This deposition of carbon enhances the already high electric field distribution, due to its conductive nature.

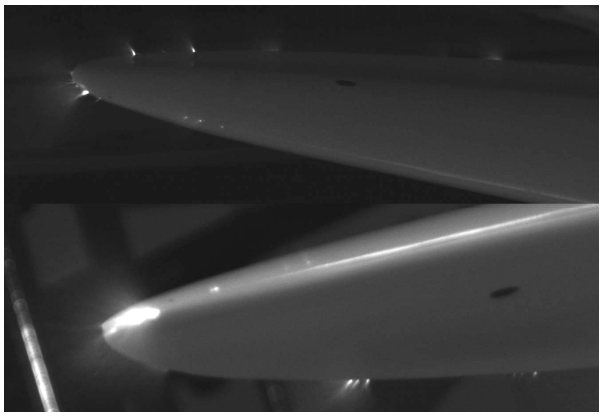

Figure 7-28 Corona Inception from Blade Tip on Carbon Loaded Blade (Position A) at 135kV

Also, comparing these images with those of the conventional blade, the receptor

seems to show no field enhancement.

The voltage was increased to over 250kV and even at these high levels, the receptor still showed no significant field enhancement. Figure 7-29 shows a completely dulled receptor, showing no signs of corona initiation, whilst there are other localized hot spots mainly near the tip showing high corona.

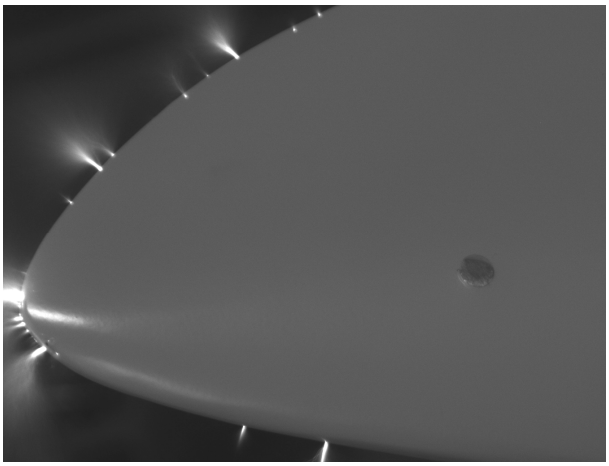

Figure 7-29 Corona Inception from Blade Tip on Carbon loaded blade (Position D) at 250kV

From Figure 7-29, the localized hotspots become more noticeable. But instead of a steady increase of corona inception all around the edges, there are only a few localized areas where the corona dwells and increases with the increase in voltage. There could be different reasons for this. The carbon layer, which is part of the blade laminate, ends a certain distance before the tip. During the HV tests, internal discharges travelling towards the edge of the blade internally. These could possibly create localized damage and create hotspots for high corona activity during the AC tests.

Also, from previous streamer tests, it is seen that there was a lot of streamer activity from the tip of the blade. Each time such a streamer is initiated from the tip, it leaves a weak spot. This might not be visible to the naked eye, but at high fields this will become a likely attachment point and also likely point for corona activity. There is a possibility that these hotspots could also be manufacturing defects. This is unlikely, as it is very rare to such an abundance of defects in one blade, but there is a possibility that these defects added to the above causes, create a large number of hotspots for corona formation.

The results of the above AC tests were verified using FEA methods. Inorder to correlate the results found from the high voltage AC testing, flat samples of the blade laminate were simulated and subjected to electrical stresses. An example of such a flat panel model is shown below in Figure 7-30.

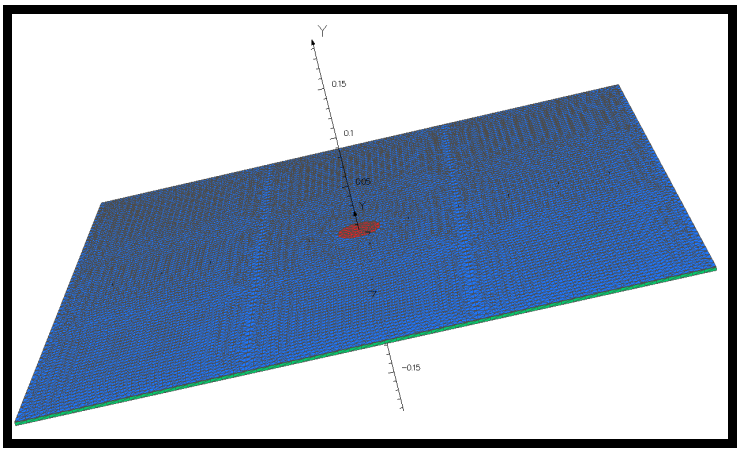

Figure 7-30 Flat plate Model with Receptor

The flat plate model is not an exact replica of the blade section which consists the receptor, but for simplicity in modelling and meshing this was chosen. The flat plate consists of the different layers that were involved in manufacturing the blade itself. The main layers in the blade are glass fibre (approximately 3mm thick) and gel coat (less than 1mm) in the case of the conventional blade and an additional carbon layer (1mm thick) in the case of the carbon loaded samples. The actual sample is 60 x 60 cm wide. The receptor is 2cms in diameter and the shape of the receptor is the same to what has been installed on the blade itself. The flat plate section is modelled in a bid to replicate the section of the blade that houses the receptor. The distance between the receptor and the ground plane is set at 1m, similar to that maintained in the AC corona lab tests. In the simulations, the receptor of both samples (carbon loaded and conventional) is connected to the HV source. They are subjected to a constant voltage of 95kV. The results of the analysis are shown in Figure 7-31.

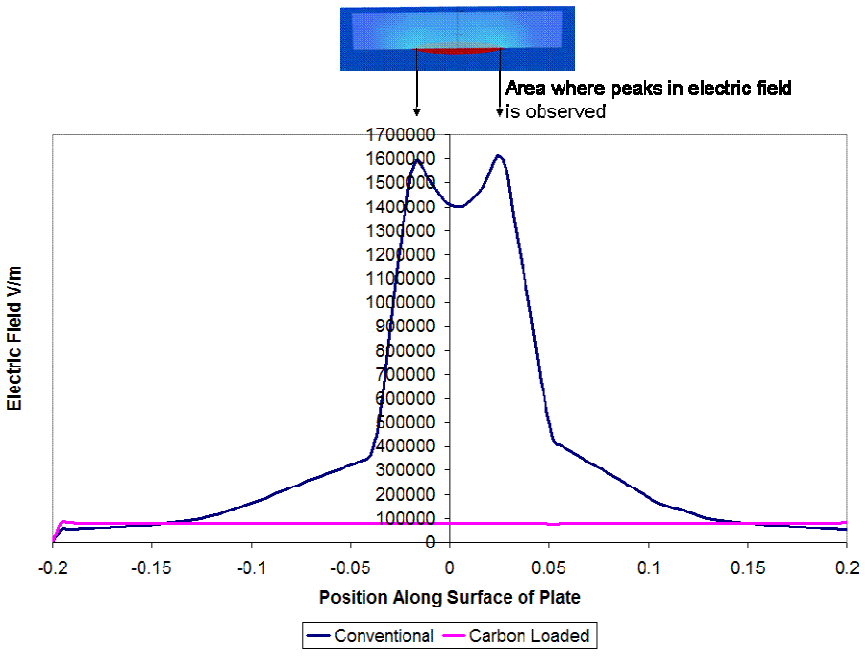

Figure 7-31 Field Plot across the Receptor on the Flat Plate Model

The results show the field enhancement across the receptor. The field line plotted above, runs just above the receptor and shows a high field enhancement at the edges of the air termination for the case of the sample based on the conventional blade laminate. However for the carbon based sample, the field across the receptor is completely nullified. This obviously is due to the introduction of a conductive layer (carbon) amidst the existing GFRP. These results coincide with the lab tests, indicating the risk of lightning attachment to other places on the blade when a carbon layer is introduced into the blade laminate.

The results of the flat plate sample based on the conventional blade from the simulation are numerically compared with those obtained in the lab. The lab tests showed corona inception at 100kV AC on the conventional blade and for the case of the carbon loaded blade the corona inception begins at 103 kV AC, but this corona is visible on the tip of the blade (Figure 7-29), and not on the receptor.

For consistency the corona inception is assumed to begin at electric fields of 3MV/m. Thus it can be said that the electric field across the receptor of the conventional blades reach 3MV/m at 100kV AC and initiate corona. The simulations on the other hand, show that at a voltage of 100kV (RMS), the field at the edges of the receptor is the highest and reaches to a maximum of 1.7MV/m.

This variation in results could be explained to the following:

- The difference in the shape of the model.
- The meshing of the model will make a significant change to the results, the smaller the mesh, the accurate the results. But this takes a lot of computational resources and time, thus a coarser mesh had to be used.
- The atmospheric conditions in the lab will effect the results. However the FEA software does not have the capability of introducing parameters such as temperature and pressure into the simulations.
- The physical condition of the blade itself could make a difference in the results. While the plate that has been simulated and tested using FEA methods, is assumed to be new, the actual blade sample had been subjected to impulse testing and this could possible have a determinant effect on the receptor and the lightning protection system.

With respect to the samples based on the carbon loaded blade, it can be

confirmed that there is significant effect on the receptor due to the carbon layer. The electric field across the receptor reaches a maximum of 81kV/m, a significant 21 times less than the samples with no carbon layer. The receptor is dulled and does not reach the corona inception field, thus allowing unprotected parts of the blade, to reach this field and initiate corona. This can be confirmed from Figure 7-29, where the tip begins corona before the receptor.

7.6 Conclusions

From the lab tests and the FEA computational tests on both the conventional blade and the normal blade the following conclusion have been made.

1. Streamer initiation tests show positive results on the conventional blade, where the receptor begins streamer propagation before other parts of the blade.
2. Streamer initiation on the carbon loaded blades begins from the tip of the blade instead of the receptor, indicating the carbon layer reducing the efficiency of the receptor in initiating streamers.
3. The attachment tests show that conventional blades pass the tests according to the IEC 61400-24 standard, whilst the carbon loaded blades fail the same.
4. The carbon loaded blades are damaged due to the attachment tests. The failure happens at the tip of the blade, appears in the form of a puncture. The location of the puncture is seen close to that where the streamers developed during the streamer initiation tests.
5. AC corona tests have been performed on both the conventional blade sample and the carbon loaded blade. Results indicate a significant deterioration in the receptor efficiency of the carbon loaded blade, and also show many corona hotspots around the tip of the blade, which could be possible attachment points during lightning.
6. Results if the AC corona tests were confirmed with FEA results of flat plate models of the blade laminate section which houses the receptor.

8 Material Enhancement for Improved Lightning Protection

In many high voltage applications surface discharges, streamers and corona cause component damage. Outdoor high voltage insulators are a very good example for this. Due to accumulation of dust and moisture, surface currents prevail on the material. These surface currents evaporate accumulated moisture causing non-uniform drying, thus giving rise to Dry-Bands. Dry-Bands are localised evaporated film of electrolytes with a high resistivity. The formation of dry-bands increases the risk of flashover in high voltage insulators. Thus the ability of insulating materials of not allowing the dissipation of accumulated charge causes damage over elongated periods of time. This phenomena of surface discharges is quite common in wind turbine rotor blades. Localised heating and discharges result in tracking and erosion on the surface of wind turbine blades, which is usually seen around the air terminations or receptors of rotor blades. Formation of local weak points could result in streamer growth, thus resulting in lightning attachment to unprotected parts of the blade. This risk of such damage will increase in the case of offshore wind turbines due to the surrounding environment, where moisture and salt accumulation is inevitable. To overcome such damage and improve material performance, industries and researchers have been looking onto fillers and additives. For example, the addition of fillers is not a new concept in increasing the electrical breakdown strength in dielectric materials.

In this section new ideas and concepts have been discussed, to use the principle of fillers and additives on rotor blades in an attempt to improve their lightning efficiency and better electrical stress performance. This section will mainly look at two areas of the lightning protection system, the air-terminations (receptors) and the down conductor.

8.1 Material Enhancement around the air terminations (receptors)

The main air-terminations of the blade are the receptors in a down conductor and receptor based lightning protection system. It has been discussed in the previous chapters how important it is to ensure that these are the points of highest field enhancement. It is not only necessary to ensure that the field enhancement is high in this region, but for successful lightning attachment, the ratio between the field enhancement at the receptor and the rest of the surface should be as high as

possible. This allows the streamers to develop from the receptor earlier in comparison to other unprotected parts of the blade. A brief description of this is given below.

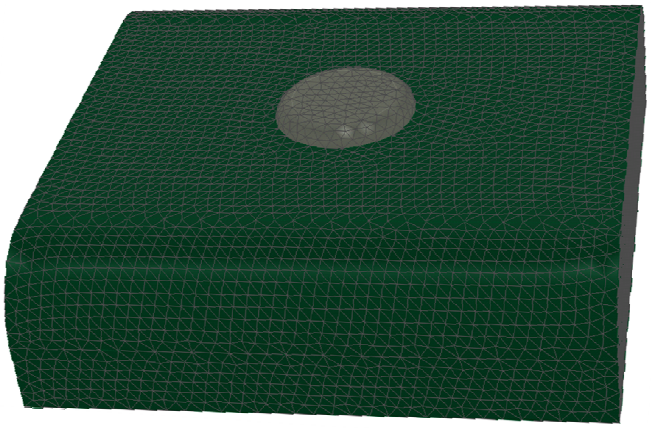

Figure 8-1 Receptor in Glass Fiber Composite Laminate

Figure 8-1 shows how the receptor is surrounded by glass fiber. Assuming the field is enhanced around the receptor by a factor of K_r and the field on top of the glass fiber laminate is enhanced by a factor of K_g. It becomes vital that K_r /K_g is as high as possible. The idea is to ensure that even at high ambient fields, this ratio remains large. If not, at high ambient fields, the glass fiber will begin to emit answering leader or upward leaders alongside the receptor thus increasing the risk of lightning damage to the blade. One other factor of the material that needs to be considered, whilst manipulating the material characteristics, is the actual electric field in the bulk laminate itself. The improvement to the field enhancement on the surface of the receptor must not increase the field inside the bulk laminate itself. If the electric field enhancement in the bulk is enhanced by a factor of K_b, the ratio K_r/ K_b should be as high as possible. Failure in maintaining a high ratio, will risk in the breakdown in the bulk laminate causing weak points and possible attachment points.

One idea of improving this ratio was to increase or manipulate the dielectric permittivity of the material around the receptor. This was done in order to make the receptor look “attractive” during a thunder storm. This is a novel approach and not much research has been done in relation to its use on wind turbine blades.

Many researchers have used fillers to increase the dielectric permittivity of materials. These fillers increase the relative permittivity and improve stress relief performance in insulation systems. The minimization of electric stress reduces the effects of arcing on the surface of insulating materials [87]. This property would help surfaces near the wind turbine from tracking and erosion. Many have investigated the functions of different fillers and the effect of the concentration level of the filler in the base material [88,

89].Fillers that have been used to improve the dielectric permittivity of material are Silicone Carbide (SiC), Barium Titanate ($BaTiO_3$), and a composite of Barium Titanate and Alumina. By controlling the volume of the added filler the dielectric permittivity can be increased in the base material. But there is a limit to the amount of filler that can be added to the base material, as after a certain percentage the filler does not tend to mix and air entrapment in the material will cause problems in making void free and homogenous composites [87]. In this section the addition of barium Titanate to areas around the receptor is investigated.

Barium Titanate is known for its property of increasing the dielectric permittivity of materials. It also exhibits a non-linear dielectric property, thus becoming really useful in stress relieving of materials that are exposed to non-uniform fields. The non linear behaviour or barium Titanate has been studied in many parts of the literature, an example of such a study is [88]. According to [87] the introduction of fillers to 230kV bushings increased the relative permittivity from 2.7 to 15 and also reduced the maximum electric stress by a factor of 2.

The present idea is to treat the area around the receptor with this material and see if this reduces the electrical stress around the receptor but keeping the field enhancement at the receptor the same or improve it.

8.2 Variable Permittivities for better breakdown performance

For successful lightning attachment at the receptor, the ratio between the field enhancement at the receptor and the rest of the surface of the blade should be as high as possible. This allows streamers to develop from the receptors earlier in comparison to other unprotected parts of the blade. As this ratio decreases, the chances of lightning attaching to unprotected parts of the blade increases, thus increasing the risk of physical damage to the blade.

The composite blade is usually made of several layers of fiber of different thickness and is finished with a gel coat on the top. These layers vary according to manufacturer. Different layers could be added to this composite for strengthening purposes, Figure 8-2, is just an example of what the cross-section of the blade laminate would look like, and shows the different layers, all combined, to form the glass fiber composite.

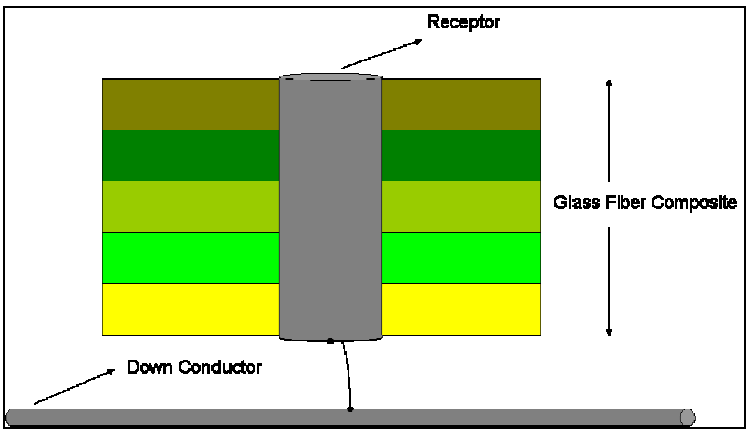

Figure 8-2 Receptor and Blade Cross Section

Initial FEA models were modelled to see if varying permittivity around the receptor would make a difference to the electric field around it. Cylinder models of 20cm long were built, which consisted of a metal rod, surrounded by layers of insulating material, of different permittivities. The metal rod is 4cm wide, and is surrounded by insulating layers each 1cm thick. This is not an exact replication of the receptor construction on a blade, but the initial results from these simulations will answer if the electric field distribution around the metal rod does change due to the change in the material characteristics.

Different variations were performed to analyse their effect on the field enhancement around the metal rod. For the first set of simulations the area around the receptor is changed in such a way that the dielectric permittivities of the different insulating layers are descending moving away from the metallic rod. This is denoted at 'Descending' in the analysis (Figure 8-3).

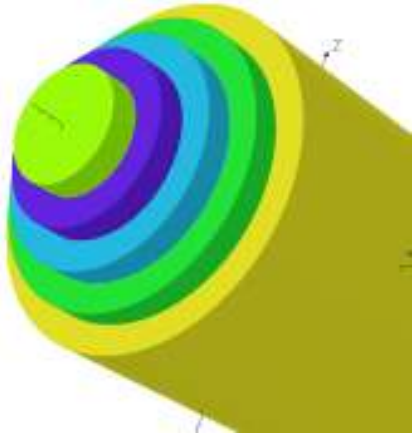

Figure 8-3 Variable Permittivity (unidirectional)

The next simulation involved in changing the permittivities in the ascending order moving away from the metallic rod. Other combinations of changing the permittivities were thought in the form of changing the material characteristics in cross layers,

i.e multi-directional.

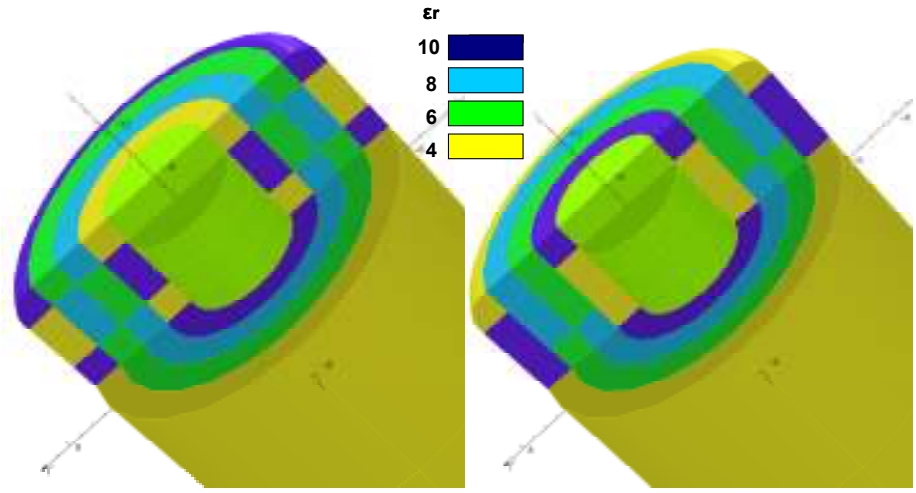

Figure 8-4 Variable Permittivity (multi-direction)

As shown in Figure 8-4, the permittivities of the dielectric material surrounding the receptors were manipulated both in the lateral and radial direction. No particular order has been maintained in applying this cross-ply material around the receptor. The first 4cm of the model is subjected to this cross-ply method and the distribution of the various permittivities can be seen from Figure 8-4. The different permittivities of each layer can be distinguished by the colour of the layer, and is highlighted in Figure 8-4. All the above models are subjected to an electric field inorder to find areas of high field enhancement. Theoretically the areas with the highest electric field enhancement would be the first to incept streamers.

Results of these tests are shown in the table below.

	Field Enhancement Receptor (K_r)	Field Enhancement Glass Fibre (K_g)	Field Enhancement Bulk (K_b)	Ratio 1 (K_r)/ (K_g)	Ratio 2 (K_r)/ (K_g)	Ratio 1 + Ratio 2
Descending	1.89	3.00	1.16	0.63	1.64	2.27
Ascending	2.10	3.35	0.24	0.63	0.62	1.50
Radial 1	1.98	2.94	1.33	0.67	1.49	2.16
Radial 2	1.95	3.08	1.85	0.63	1.06	1.69
No Material Manipulation	2.28	3.69	0.66	0.62	3.45	4.07

Table 8-1 Results of variable permittivities

From the results, it is seen that the receptor surrounded by a material with homogeneous permittivity yields the highest ratio, followed by the case where the permittivity of the dielectric is descending moving away from the receptor. But the interesting result is the decrease in the field across the actual glass fibre in all the simulations, suggesting that the material enhancement can effect the field distribution and improve performance. However, the decrease in the field enhancement across the glass fibre surface comes with the decrease of field enhancement across the

receptor and also field enhancement in the bulk laminate. The increase in the bulk laminate, could lead to possible breakdown through the solid, leading to possible hot spots for lightning attachment and further damage.

These simulations show a possibility for material enhancement and its applications in improving the overall electrical performance. However further research is necessary in finding a neutral ground where the performance across all areas, i.e, receptor, glass fibre surface and bulk laminate, is achievable.

8.2.1 Lab Test to Verify Material Enhancement

The above concept of variable permittivity was tested in the lab with samples prepared using epoxy and barium titanate. The flat plate samples prepared were 35cm x 35cm wide and 2.5cm thick. Two samples were manufactured one made out of only epoxy and the other where the epoxy was added with the filler material barium titanate. To mimic the receptor a metal cylinder 2.5cm in diameter and 2.5cm long was set in the middle of the samples. This cylinder in the sample is connected to a metal rod that runs right through the epoxy sample. Figure 8-5 shows the finished sample. This metallic cylinder will replicate the receptor of a blade.

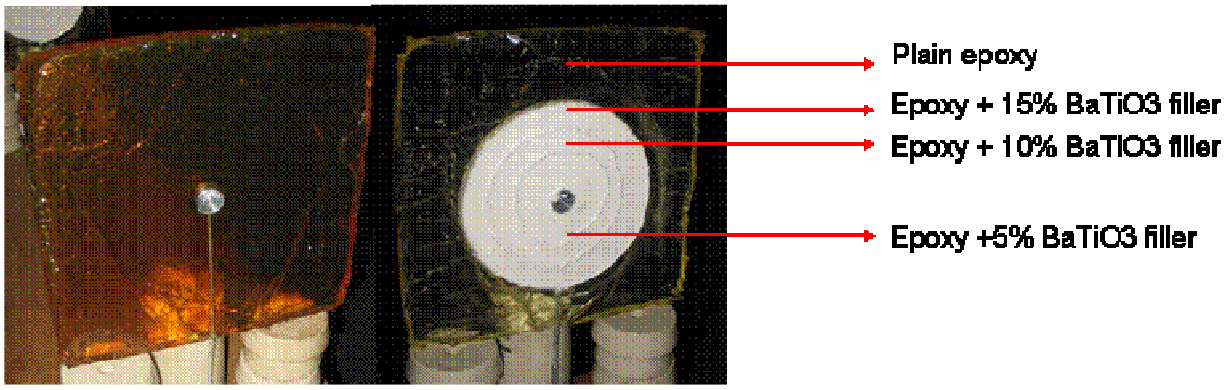

Figure 8-5 Sample with epoxy and barium titanate mixture

As previously mentioned, barium titanate is known for its field dependant permittivity. Taking this into consideration the second sample was prepared in such a way the concentration of the barium titanate was increased moving away from the receptor, in the simulations this has been named as ascending. This sample was selected from the results of Table 8-1 as this model showed a considerable decrease in the field enhancement in the bulk laminate and also a high field enhancement across the receptor. Three different filler concentrations of barium titanate were used in making this sample, 15%, 10% and 5% by weight. This is shown in Figure 8-5. The

samples were subjected to high voltage A/C fields to observe corona initiation at the metal electrode in the middle of the samples.

Figure 8-6 Testing of epoxy samples for Corona

The samples were placed underneath a HV electrode which was energized by the AC test set (Figure 8-6). The voltage on the AC test set was increased till there was visible corona on the samples (these experiments had been performed before the acquisition of the UV camera, thus the actual corona phenomenon has not been captured). It is assumed that the field at which visible corona is noticed is 3MV/m. The results obtained for the lab tests (shown in Table 8-2) are later compared with the same tests replicated in the FEA package (Figure 8-7).

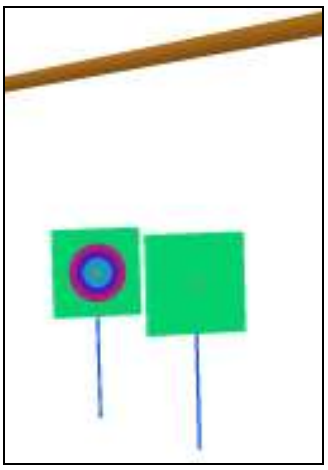

Figure 8-7 FEA simulation of epoxy sample testing

The relative permittivity of the epoxy was chosen as 3 in these simulations, and as for the epoxy filled with Barium Titanate, a field dependent permittivity based on Equation (8-1), is chosen.

$$\varepsilon_r = 6.4 + 1.2E \qquad \textbf{(8-1)}$$

This equation is an extract from [90]. The equation is only valid for silicon gel samples filled with barium titanate and for 15% concentration by volume. The present

samples have been mixed based on their volumes, but in epoxy and not silicon. And the above equation has been set for all the concentration levels in the simulations, as at the time of this research; this information was the only literature available in regards to this parameter. The voltage applied across the H.V electrode is the RMS value of the voltage at which corona inception was noticed in the laboratory experiments.

The results are calculated by finding the electric field distribution across the H.V electrode and the ground at points of interest, with and without the samples. Thus, to find the field without the samples, a H.V electrode and ground plane are simulated as shown Figure 8-8.

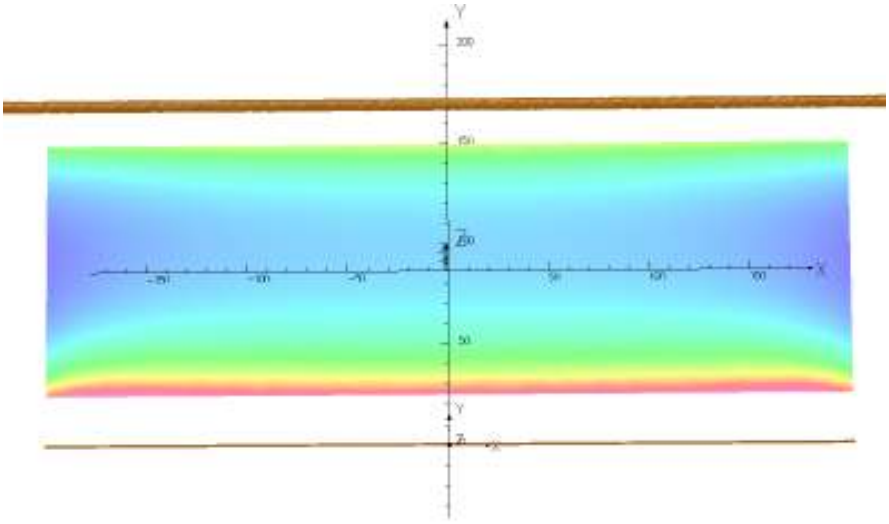

Figure 8-8 Field distribution calculation between HV electrode and ground

Then the samples are placed in the same environment and subjected to the same voltage parameters and the field at points of interest is noted down.
The results obtained from the simulations and lab tests are as follows

- **Corona inception voltage in lab (V_i) Volts** – Voltage at which corona was visibly detected on the samples in the lab tests.
- **Electric field at receptor E_{rl} at (V_i) Volts (lab tests) -** Electric field at the receptor in lab tests at corona inception voltage (V_i) Volts. This has been assumed as 3MV/m, a value that has been adapted in many areas in the previous chapters.
- **Electric field at receptor E_{rs} at (V_i) Volts (simulation)** – Electric field at the receptor in simulations at (V_i) Volts.
- **Ambient Field in Absence of sample E_a at (V_i) Volts (simulation) –** Electric field distribution between the high voltage electrode and the ground plane in absence of the samples itself.

Using these values a field enhancement factor for the samples in the lab tests and the simulations are calculated and are shown in Table 8-2

	Corona inception voltage in lab ($\mathbf{V}_i$) Volts	Electric field at receptor $\mathbf{E}_{rs}$ at (V_i) Volts (simulation)	Electric field at receptor $\mathbf{E}_{rl}$ at (V_i) Volts (lab tests)	Ambient Field in Absence of sample **Ea** at (V_i) Volts (simulation)	**Field Enhancement Factor at receptor**	
					Simulation $K_s = E_{rs}/E_a$	**Lab tests** $K_l = E_{rl}/E_a$
Epoxy Sample	1.58E+05	2.08E+06	3.00E+06	4.55E+04	45.7	65.9
Epoxy + Filler Sample	1.67E+05	5.38E+05	3.00E+06	4.80E+04	11.2	62.5

Table 8-2 Results of varying permittivity experiments (lab tests)

The results show that the electric field around the sample surrounded by one material shows the maximum field enhancement both in the simulations and the lab tests. One noticeable result is the difference in the field enhancement factor of the epoxy + filler sample in the lab tests and the simulations. This can be explained to the input parameter i.e. dielectric permittivity in the simulations and the related assumptions made for barium titanate. Equation (8-1) has been used in the simulations, which have been tried to replicate the lab experiments. This permittivity is based for 15% concentration of barium titanate filler based in silicon, thus, there is a risk in assuming these results are applicable for barium titanate filler based in epoxy let alone for all three concentration, 5, 10 and 15%. The difference in the results can also be explained to the non – linearity of the samples that have actually been prepared for the lab tests and those modelled for FEA simulation. Whilst the former have manufacturing defects, such as sharp edges and uneven surfaces due to hard nature of actually preparing the samples, the models built for simulations are close to ideal, where there is usually no manufacturing defect.

The above tests were performed in an attempt to try and increase the efficiency of the receptor. From the above results it is clear that maintaining a homogenous material around the receptor yields best field enhancement and performance across the receptor. But the change in the field around the receptor due to material enhancement and manipulation shows that there is still a possibility of being able to increase performance of the receptor if the right materials are chosen. Also the decrease in the electrical stresses across the surface of the blade laminate due to material enhancement remains an area of key interest. Further research is needed to

investigate this possibility, and into different field dependant fillers.

8.3 FEA testing of down conductor field distribution

During a thunder storm the blade is subjected to high fields. Certification of the blades is usually performed based on the performance of air terminations. Not much information is available to the effect of the high electric fields on the internal down conductor system. When the electric field around the blade is high enough for the air terminations to emit streamers, the down conductor inside the blade will be under high electrical stresses as well. Thus it would be appropriate to analyse the electric field distribution on top of the down conductor.

The large sizes of these blades make it hard to test in reality. The lack of large facilities to house these blades means that only a part of the blade can be tested. The FEA model overcomes this drawback as the whole blade can be tested, size not being a constraint. The blade that was used in Section 5.1.2 whilst modelling the wind turbine in previous sections was used for the IEC tests as well. The present tests, that are simulated in the FEA Software, were done similar to the initial leader attachment test [1] (Figure 7-20). However there is a difference in how the sample is connected to the HV source. In the lab tests the down conductor is connected to the HV source, but in the simulations the high voltage source is connected to a flat electrode on top of the blade and the lightning protections system is set at 0V or earth. This enables to calculate the field enhancement fairly without complications as the flat electrode will in general create a uniform field. Results from the simulations are shown in Figure 8-9 and Figure 8-10. Areas of field enhancement can be seen by the high concentration vectors around them.

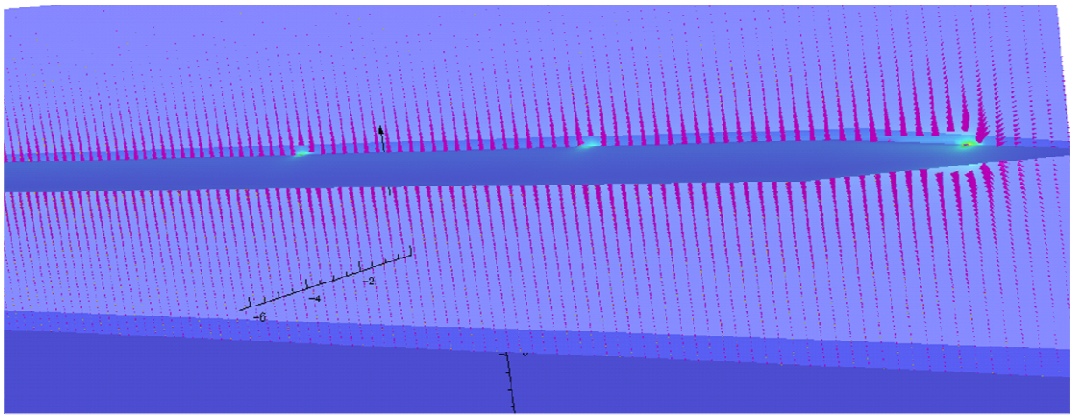

Figure 8-9 Field Enhancement of Blade

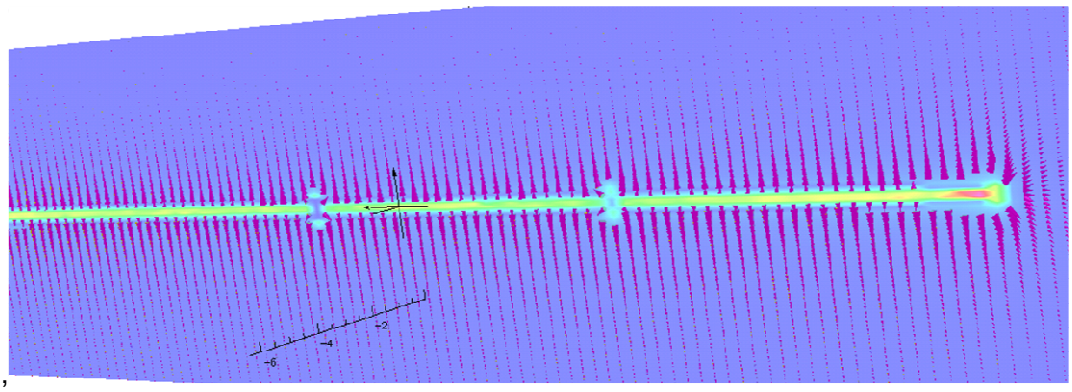

Figure 8-10 Field Enhancement on Down Conductor

From Figure 8-9 it is seen that the receptors are the points of high field enhancement, this correlates to the results found in the lab tests performed on the conventional blade sample in (Section **Error! Reference source not found.**). But the field enhancement does not stop on the receptors. Figure 8-10 shows the field enhancement on the down conductor. At the applied voltage of at 600 kV across the flat electrode, the inception field criteria is not met on the receptor or the down conductor, at higher fields there is a possibility of streamer development and due to this, discharges inside the blade. Internal discharges in the blade are not good for the integrity of the glass fiber composite. Prolonged discharges on the inner surface might lead to the weakening of the blade material causing dielectric breakdown. Streamer inception and propagation inside the blade, due to the down conductor, can cause punctures and burns. This is a phenomenon that is quite often seen in aircraft radomes Figure 8-11

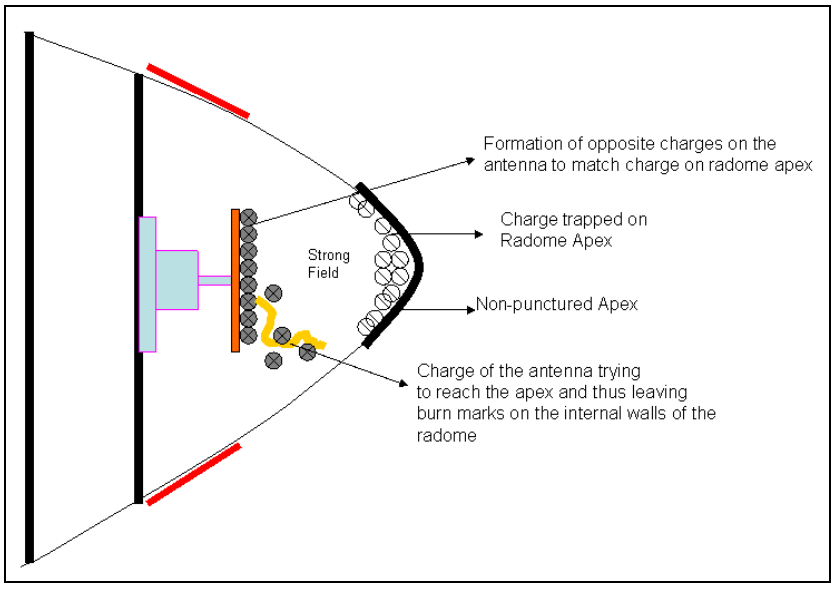

Figure 8-11 Formation of internal discharges in aircraft radomes [91]

To minimize the possibility of any internal discharges, the IEC 61400-24 standard

[1] states that the down conductor needs to be insulated. However, there are no guide lines to how thick this insulation coat needs to be in the standard. In an attempt to test the effect of an insulating layer on the down conductor, tests are performed on the down conductor coated with an epoxy of different thickness varying from 0 to 10mm. The results of the IEC initial leader attachment tests on the blade are shown in Figure 8-12 for the down conductor with and without an insulating layer.

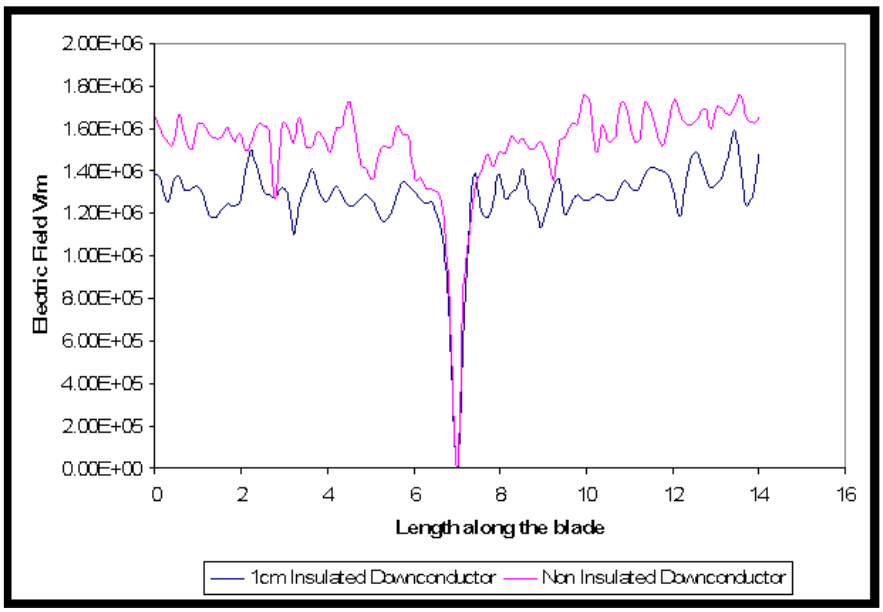

Figure 8-12 Electric field distribution over down conductor

Figure 8-12 shows the electric field distribution 1 cm above the down conductor (the field line runs along the down conductor inside hollow blade). The sudden drop in the field is when the plot goes through the receptor, thus showing no field enhancement. From it is seen that the field on top of the down conductor in the absence on an insulating layer is around 1.6MV/m (The noise in the plot can be explained to the mesh sizing). When this is compared to the electric field distribution of the down conductor that is covered with an insulating layer of 1cm thickness, the electric field distribution 1cms above the down conductor is around 1.4 MV/m, thus showing a large decrease in the field enhancement. The increase in the thickness of the insulating layer decreases the field enhancement, this can be seen from the results shown in Table 8-3.

Insulation Thickness	Electrical Field (Receptor) E_R	Electrical Field (Down conductor) E_{DC}	Ambient Field E_A	Field Enhancement Factor	
				Receptor $K_R = E_R / E_A$	Down conductor $K_{DC} = E_{DC} / E_A$
No Insulation	2.00E+06	1.90E+06	600000	50	47.5
5mm	2.06E+06	1.74E+06	600000	51.5	43.5
7mm	1.81E+06	1.65E+06	600000	45.25	41.25
1cm	1.91E+06	1.38E+06	600000	47.75	34.5

Table 8-3 Results of down conductor insulation.

As mentioned before the insulation on the down conductor is required to minimise the development and growth of internal streamers. From Table 8-3 it can be argued that the highest field observed on top of the down conductor in absence of any insulation is less than the streamer inception field, 3MV/m. Thus, contradicting the actual need for any kind of insulation at all. However, there are a couple of reasons insulation is essential eventhough the streamer inception field is not reached in these simulation. Firstly, the present tests have been simulated at a voltage of 600kV. But, in reality, the actual field required for inception of streamers under the cloud is quite low as seen from FEA experiments in previous sections. Cloud height affects the ambient field in which the blades rotate, if the cloud height is lower, the field would be higher thus allowing the surface of the down conductor to emit streamers/answering leaders. Secondly, the blades are revolving constantly in the field created by the thunderstorm cloud. Thus the position of the blade also effects the electric field distribution. In theory the worst position should be the vertical position, where the field enhancement would be the highest. In such a case the field required for the receptors and the down conductor to emit streamers would be much lower, increasing the risk of internal discharges.

8.4 Conclusions

The present chapter was a look in areas that have not been tried in the wind turbine industry prior to this attempt. The results have been summarized below;

1. Barium titanate filler based samples were tested for their non-linear dielectric permittivities, and their application in wind turbine blades. Initial samples were modelled in the FEA package, and tested to see if the field dependant permittivity had an effect on the field enhancement around the receptor.
2. Results showed that the electric field enhancement around the receptor was influenced on the orientation of the filler material and its concentration levels. However, the field enhancement around the receptor decreased in all cases.
3. Based on the results of the FEA simulation, flat plate samples were prepared using barium titanate and epoxy mixtures. These samples were tested in the HV laboratory for corona inception. Results showed a good correlation with the FEA simulations.
4. The importance of an insulated down conductor was discussed in relation to the new IEC 61400 – 24 standard. Using FEA methods a full scale blade model with an inbuilt lighting protection system, was tested to evaluate the electric field distribution on the down conductor system.
5. Results showed a significant decrease in the field enhancement for a down conductor covered in 1cm insulations as compared to one which is not. This is an important factor for minimizing internal discharges, inside the blade spar, as this might cause burns and punctures over the life span of the blade.

9 Conclusions

9.1 Lightning Data Analysis

The lightning data analysis shows that the wind instruments at the back of the nacelle are at risk to lightning attachment, as much as the blades. It was found for the offshore wind farm, 55% of the strikes were registered on the wind instruments, whilst the remaining was registered on the rotor blades. This is in contrast to finding of previous researchers. The PCS cards used for registering the lightning strikes have been tested to answer the discrepancies they showed whilst analysing the lightning data analysis. These discrepancies have been identified and the interpreted such that the results can be modified accordingly. High current tests on the PCS cards showed that the cards were unable to register lightning strikes of peak currents less than 5kA, which is 2kA more than stated by the manufacturer. The cards have a tendency to record 41kA, for all peak currents between 30 – 60kA.

Existing wind turbine blades are now required to withstand lightning currents of upto 200kA. With only a few lightning strikes assumed to be exceeding 200kA in the lightning data analysis, the question arises to how economical it is to be designing lightning protection system to withstand this current level. However, at the moment it is hard to change this level, as the data analysed in this thesis, comes from controlled set of one offshore wind farm, and other controlled sets from different regions would be required to come to a proper consensus.

Using the probability distribution of the IEC 61400-24, Lightning Protection of Wind Turbines standard, different scenarios were built, using the peak current data from the lightning analysis. It was found that the inclusion of 80% of upward initiated lightning into the actual probability distribution made a perfect fit to the real data, indicating a large proportion of lightning strikes to wind turbines being upward initiated.

9.2 Modelling of Upward Lightning Attachment to Wind Turbines

With limited facilities available for testing these large structures, it is important to find alternate methods for lightning analysis of wind turbines. A full wind turbine model was built, including the wind vane and the wind instruments. The rotor blades of the model were modelled with a built in receptor and down conductor based lightning protection system. At the time of writing this thesis, this was the only known FEA model which has been able to include the material characteristics of different components on the wind turbine, instead of assuming it as a completely conductive structure. The wind turbine model was subjected to electric fields that would be experienced by a wind turbine during a thunderstorm. These electric fields have been calculated by modelling different cloud models using finite element methods. It was seen that the wind vane at the back of the nacelle was at high risk to lightning attachment along with the blades. The importance of geometrical shape and position in regards to field enhancement was highlighted when the tip receptor enhanced the ambient electric field created by the thundercloud by a factor of 320, whilst the lightning rods protecting the wind instruments enhanced the field by a factor of 500. These results coincide with those found in section 4.1.1.

Electric field analysis based on previous knowledge of streamer inception and leader propagation, indicated that the tip receptor on the blades and the lightning rods protecting the wind instruments begin streamer initiation at approximately the same time. However, the stabilisation for stable leader propagation was fulfilled by the tip receptor before the lightning rods. FEA results indicated that at low cloud heights, inception criteria and stabilisation fields are fulfilled by both the wind vane and the tip receptor. This basically indicated that the risk of lightning attaching other areas increases with low cloud height, particularly seen during winter.

9.3 Interaction of Lightning Protection with Radar Cross Section Minimisation and Carbon Fibre Strengthening.

Carbon fibre for radar cross section minimisation and strengthening of the blade was found to affect the efficiency of the lightning protection system. FEA analysis and lab tests were performed to find the detrimental effect, of adding a carbon layer into the existing glass fibre laminate, on the lightning protection system. A new composite layer capable to be used for strengthening purposes and as part of the RCS minimisation solution was tested. FEA models were analysed for lightning attachment, and initial results indicated a complete dulled receptor due to the addition of the new composite layer. Results indicated that the electric field at the tip of the receptor was reduced by almost 90% when the carbon layer was added to the existing, non conductive glass fibre laminate. Results also showed a large increase in the electric field around the tip of the blade after the addition of the composite layer. The field enhancement increased 55 times in comparison to when there was no composite layer present in the glass fire laminate. This increases the risk of lightning attachment to the tip of the blade.

Any part of the lightning protection system must be capable of carrying full or part of the lightning current. The new composite layer was tested for high current conduction, and results indicated that the layer was unable to withstand full lightning current of 200kA, and started to show considerable damage at low currents of 5kA. A statistical analysis on how the carbon layer would relate to revenue loss due to increase in lightning strike related damage was performed.

9.4 High Voltage Testing of Blade Lightning Protection System

High voltage lab tests were performed on a conventional blade sample and a prototype sample, which included a conductive layer between the glass fibre laminate. Tests were done to see the effect of the new layer on the performance on the existing lightning protection system. Tests were conducted in accordance with the IEC 61400-24 'Lightning Protection of Wind Turbines' standard.

Streamer tests were conducted using the impulse generator and using a high specification UV camera the phenomenon was captured for both blade samples. Results indicated that for the conventional blade streamers begin from the receptor indicating the lightning protection system working. However, the prototype carbon samples showed streamer inception from the tip of the blade instead of the receptor. This indicates possible hotspots for lightning attachment and damage. The receptor in the carbon loaded blades was completely dulled thus confirming to simulations performed in the previous chapters. Results indicated that the streamer initiation begins at approximately 500 kV for both blade samples in positive impulse. The streamer is well defined and moves away from the blade. However, it is hard to capture negative streamers, and inception begins at almost 950kV for the conventional sample and 1050 kV for the carbon loaded sample. The negative streamer also tends to propagate along the surface of the blade.

The conventional blade passed the attachment tests, however the carbon loaded blade failed these tests. Attachment point on the carbon loaded blade happened at the tip instead of the receptor. This resulted in a puncture at the tip of the blade section. This once again confirms the risk of lightning attaching to unprotected parts of the blade due to the inclusion of a conductive layer into the glass fibre laminate, proved by FEA results in section 6.5.1.

AC corona tests were performed the blade samples. This is the first attempt to use HV AC voltages for testing blade samples. Results indicated that corona inception began at almost 100kV for both blade samples; however the location of corona inception was different in both cases. Whilst the conventional blade shows visible corona at the receptor, the carbon loaded blade shows no corona at the receptor and instead shows localised hotspots of corona inception all over the blade tip, indicating possible attachment points.

9.5 Material Enhancment for Improved Lightning Protection

In an effort to increase the efficiency of the lightning protection system, a new idea of improving the material performance around the receptor has been thought of using electric field dependant filler, Barium Titanate. FEA simulations were performed to see the effect of the filler in different orientations to the receptor. Results showed that the addition of the filler based material around the receptor changed the electric field distribution. However, the best results were still observed when the receptor was surrounded by one homogeneous material. The receptor on the sample with one homogenous material showed a field enhancement of 65.9 times, whilst the filler based material showed a field enhancement of 45.7. These results were confirmed by performing AC corona tests on samples, where a receptor was surrounded by the filler and epoxy.

Insulated down conductor systems were compared to non-insulated counterparts using FEA methods. Results showed a 1cm insulation around the down conductor reduced the field enhancement by a factor of 12 in comparison to a non insulated down conductor. Such insulation will reduce the risk of internal discharges, which over time could develop in burns and punctures resulting to weak spots for lightning attachment.

10 Future Work

A relatively new field, there is still a considerable amount to be learnt from the lightning phenomenon on wind turbines blades. The present thesis has been able to highlight some of these areas. From the findings of this research, a set of ideas which hold scope for future research have been highlighted below.

10.1 Data Analysis

- Lightning data analysis of the Nysted offshore wind farm has shed light on how different components of the wind turbine are at equal risk to lightning attachment as the blades. This analysis has only been possible due to the availability of a controlled set of measurements taken by the operator and the wind turbine manufacturer. The major drawback still remains that there is not enough data over the wind turbine life span. With wind turbines expected to last atleast 20 years, it will be very useful to perform a data analysis for a longer periods in comparison to a few years as this would help in comparing parameters stated in the new IEC 61400-24 standard.
- The results from the data analysis showed that there are a large number of strikes on the blades and the wind vane. However, it must be noted that most of the peak current registrations systems are only connected to these components, thus making it impossible to have a record of lightning strikes attaching at other areas of the wind turbine. Encouraging wind turbine manufacturers to include these in their existing wind turbines will help in identifying other areas prone to lightning attachment and help in detailed analysis.
- Data analysis on a controlled set of measurements from an onshore wind farm will help in understanding the lightning phenomenon on land based wind turbines. This will also be helpful in identifying if the moving wind farms offshore have increased the lightning strike frequency.

10.2 3D Electrostatic Modelling

- 3D electrostatic analysis of a wind turbine model for upward initiated lightning has been performed in this thesis. This is relatively simple to analyse in comparison to downward initiated lightning, as this would involve in

actually modelling the downward stepped leader in real time. This would need a lot of computational power. But it will be a challenge to model such a leader and compare the lightning attachment process on a wind turbine with that of an upward initiated lightning attachment.

- The performance of the lightning protection system is rated on its efficiency. But there are no particular guidelines to how this can be calculated. It will be very useful to be able to calculate the efficiency based on the field enhancement. As this would allow 3D models to be verified for their efficiencies without undertaking expensive lab tests. However, it must be noted that lab tests will have to be involved in actually finding out a relationship between electric field enhancement and efficiencies.

10.3 Material Enhancement and Carbon Fibre based Laminates

- All the 3D electrostatic models that have been performed, in this thesis and by other researchers, relate to a wind turbine rotor being static. Those who have verified lightning attachment in different orientations of the rotor, still perform the analysis with the rotor not moving. It has been confirmed that the lightning phenomenon is affected by movement of the attaching surface, especially in aircraft. Future work could involve trying to simulate electrostatic analysis on moving rotors as this will be key in understanding the importance of receptors further down the blade.
- The move to introduce carbon into the existing blade laminate, both for RCS reduction and strengthening, brings new challenges to the lightning protection system. Selective layering is still a plausible option, but this has to be done very carefully and different models will have to be analysed before finding a blade model that is capable of maintaining a high lightning protection efficiency and being able to provide good RCS reduction and strength.
- There is still scope of material enhancement around the receptor to make it attractive to lightning attachment. Materials with field dependant conductivities could be used to make sure that lightning attaches to the receptor and also to reduce tracking and surface erosion. Further lab tests on flat plate samples could show positive results.

11 Reference

1. 61400-24, I., *Wind turbine generator systems – Part 24: Lightning protection for wind turbines"* June 2000.
2. EWEA, *Wind Status Report January 2007.* 2007.
3. EWEA., *Wind Energy - The Facts: A guide to the technology, economics and future of wind power.* 2009: earthscan.
4. Group, C.-K.W.A., in *http://www.ckwag.org/issues.html*. 2008.
5. Guard, U.S.C. *SUSTAINABLE ENERGY - WIND POWER - WIND 101*. 2009 [cited 2009 21 september]; Wind Turbine Components]. Available from: http://www.uscg.mil/d1/SFOSouthwestHarbor/innovation/wind/wind_101.asp.
6. Jenkins, N. and J. Walker, *Wind Energy.*
7. Cotton, I., *Lightning Protection of Wind Turbines.* 1999.
8. Rakov, V.A. and M.A. Uman, *Lightning - Physics and Effects.* 2000.
9. Uman, A.M., *Natural Lightning.* IEEE Transactions On Industrial Applications, 1994. **30**(3).
10. Uman, *The Lightning Discharge*. 2001: Dover Publications, INC.
11. Berger, K., *Novel Observations on Lightning Discharges: Results of Research on Mount San Salvatore.* Journal of the Franklin Institute, 1967. **283**(6): p. 478-525.
12. Berger, K. Anderson, and R.B.a. Kröninger, *Parameters of Lightning Flashes.* Cigré, 1975. **3**(41): p. 23-37.
13. Garbagnati, E., Marinoni, F., and Lo Piparo, *Parameters of lightning currents. Interpretation of the results obtained in Italy.* In Proceedings. 16th international Conference on Lightning Protection, Szeged, Hungary., 1974.
14. Golde, R.H., *Lightning Volume 1 : Physics of Lightning.* 1977.
15. Popolansky, F., *Frequency distribution of amplitudes of lightning currents.* Electra, 1972(22): p. 139-47.
16. Franz Fuchs, Ernst Ulrich Landers, Rudolf Schmid and J. Wiesinger, *Lightning Current and Magnetic Field Parameters Caused by Lightning Strikes to Tall Structures Relating to Interference of Electronic Systems.* IEEE Transactions On Electromagnetic Compatibility, 1998. **40**(4): p. 444 - 451.
17. Diendorfer, G., et al., *Lightning Current Measurements in Austria - Experimental Setup and First Results.* 25th International Conference on Lightning Protection, Rhodes, Greece, 2000.
18. Cooray, V., *The Lightning Flash.* 2003.
19. Sorenson, T., *Lightning Registration Systems - Analysis, Optimization and Utilization*, in *Electrical Power Engineering Department*. 1995, Technical

University if Denmark: Copenhagen. p. February 1995.

20. *Project FINO 3 http://www.fino3.de/Joomla/index.php.*
21. Eriksson, A.J., *The incidence of lightning strikes to power lines* IEEE Transactions on Power Delivery, 1987. **v PWRD-2**(3): p. 859-70.
22. McNiff, B., *Wind Turbine Lightning Protection Project NREL Subcontractor Report, SR-500-31115.* 2002.
23. Rademakers, L., et al., *Lightning Damage of OWECS.* 2002(Part 1: "Parameters Relevant for Cost Modelling").
24. Madsen, S.F., *Interaction between electrical discharges and materials for wind turbine blades – particularly related to lightning protection*, in *Ørsted•DTU, Electric Power Engineering* 2006, The Technical University of Denmark.
25. Ian Cotton, Nikos Hatziargyriou, Maria Lorentzou, Nick Jenkins, S. Haigh, and M. Hancock, *Lightning Protection Of Wind Turbines - A Designers Guide To Best Practice*. 1999, University Of Manchester: Manchester.
26. Cotton, I., *Lightning Protection of Wind Turbines.* 1998.
27. Madsen, S.F., *Interaction between electrical discharges and materials for wind turbine blades – particularly related to lightning protection.* 2006.
28. 62305, I., *Protection against lightning — Part 1: General principles.* BS EN, 2006.
29. Szedenik, N., *Rolling sphere – method or theory?* Journal of Electrostatics, 2001. **51-52**: p. 345-350.
30. DEFU, *Lightning Protection of Wind Turbines - Edition 1.* 1999.
31. Naka, T, Vasa, J N, Yokoyama, S, et al., *Study on Lightning Protection Methods for Wind Turbine Blades.* IEEJ Transactions, 2005. **125**(10).
32. Glasfiber, L. *LM Lightning Protection*. [Web Article] 2006 [cited 2007; Available from: http://www.lmwindpower.com/Blades/Products/Lightning.aspx.
33. Troels S. Sorenson, J.A.P., Blas Hermoso, Joan Montanya, et al., *The update of IEC 61400-24 Lightning Protection of Wind Turbines.* 29th International Conference on Lightning Protection of Wind Turbines, 2008.
34. K Bertelsen, H.V. Erichsen, M.V.R. Skov Jenson and S.F. Madsen, *Application of numerical models to determine lightning attachment points on wind turbines*, in *International Conference on Lightning Protection*. 2007: Uppsala.
35. Alonso, M.A. and I.A. Larrion. *Calculation of electric fields in a wind mill due to a lightning discharge using finite elements method*. in *International Conference on Lightning Protection*. 2004. Avignon, France.
36. Bruce, G., *Effective Lightning Protection For Wind Turbine Generators.* Energy conversion, ieee transactions on, 2007. **22**(1): p. 214-222.
37. Sorenson, F.M.L.a.T., *New Lightning Qualification test Procedure For*

Large Wind Turbine Blades.

38. Madsen, S.F., et al., *Experimental Investigation of the Relationship between Breakdown Strength and Tracking Characteristics of Composites.* Nordic Insulation Symposium, 2005.
39. Larsson, A., et al., *The lightning swept stroke along an aircraft in flight. Part I thermodynamic and electric properties of lightning arc channels.* J. Phys. D: Appl. Phys., 2000(33): p. 1866–1875.
40. Larsson, A., P. Lalande, and A. Bondiou-Clergerie, *The lightning swept stroke along an aircraft in flight. Part II: numerical simulations of the complete process.* J. Phys. D: Appl. Phys., 2000. **33 3**: p. 1876–188.
41. OH, L.L. and S.D. SCHNEIDER, *Lightning strike performance of thin metal skin.* Conference on Lightning and Static Electricity, 1975.
42. http://www.jomitek.dk/, accessed January 2008.
43. T. Sørensen, P Johansen, Hans Ove Nielsen, M. L. Olsen, et al., *Lightning Strike Sensor for Power Producing Wind Turbines.* European Wind Energy Conference and Exhibition, Nice, France, 1999.
44. J. Schoene, M. A. Uman, M. Aurele, K. J. Rambo, J.E. Jerauld, and G. Schnetzer, *Testing of the OBO Bettermann Peak Current Sensor System for Lawrence Livermore National Laboratory.* Lawrence Livermore National Laboratory, 2005.
45. OBO, Bettermann. *http://www.obo-bettermann.com/en/pdf_kataloge.shtml*. [cited 2007 August 2007].
46. Rademakers, L., et al., *Lightning Damage of OWECS "Part 3 - Case Studies".* ECN publication, 2002.
47. Durstewitz, M., *"Wind Energy Report Germany 2001; Annual Evaluation of WMEP"; ISET, Germany.* 2001.
48. Alonso, M.A. and D.C. Irastorza, *Dynamic Wind Turbine Lightning Protection Behaviour Under Strom Conditions.* 29th International Conference on Lightning Protection, 2008.
49. Rizk, A.M., *A model for switching impulse leader inception and breakdown of long air-gaps.* IEEE Transactions on Power Delivery, 1989. **4**(1): p. 596 - 606.
50. Miyake, K., Suzuki, T. Takashima, M. , M. Takuma, and T. Tada, *Winter lightning on Japan Sea coast-lightning striking frequency totall structures* IEEE Transactions on Power Delivery, 1990. **Volume: 5**(Issue: 3): p. 1370-1376.
51. Aguado, M., ,B, Hermoso, P, Martinez Cid, *Risks Assessment For Lightnings Strokes in Wind Farm Installations.* High Voltage Engineering Symposium, 1999.
52. Anderson R.B and E. A.J, *Lightning Parameters for Engineering*

Application. Cigré Electra, 1980. **69**: p. 65-102.

53. Montanya, J.R., F. ; Rubinstein, M. ; Bermudez, J.L. ; Sola, G. ; Hermoso, B., *Protection of Large Wind Turbine Blades against Lightning.* 29th International Conference on Lightning Protection (ICLP), Uppsala, Sweden, 2008.
54. Akyuz, M. and V. Cooray, *The Franklin lightning conductor: conditions necessary for the initiation of a connecting leader.* Journal of Electrostatics, 2001. **51**: p. 319-325.
55. Broc, A., et al., *Lightning strike to helicopters during winter thinderstorms over North Sea.* Aerospace Science and Technology, 2005. **9**: p. 686-691.
56. Shindo, T. and Y. Aihara, *A shielding theory for upward lightning.* Power Delivery, IEEE Transactions on, 1993. **8**(1): p. 318-324.
57. Allen, N.L. and P.N. Mikropoulos, *Streamer Propagation along Insulating Surfaces.* IEEE Transactions o,n Dielectrics and Electrical Insulation, June 1999. **Vol. 6 No. 3,**: p. 357-362.
58. Goeliany, N., et al., *A simplified model for the simulation of positive-spark development in long air gaps.* J. Phys. D: Appl. Phys, 1997. **30**.
59. Becerra, M. and V. Cooray, *A self-consistent upward leader propagation model.* J. Phys. D: Appl. Phys, 2006. **39**: p. 3708 - 3715.
60. Hartmann, G., *Theoretical Evaluation of Peek's Law.* Industry Applications, IEEE Transactions on, 1984. **IA-20**(6): p. 1647-1651.
61. D'Alessandro, F., *The use of [`]Field Intensification Factors' in calculations for lightning protection of structures.* Journal of Electrostatics, 2003. **58**(1-2): p. 17-43.
62. Moore, C.B., et al., *Lightning Rod Improvement Studies.* Journal of Applied Meteorology, 2000. **39**(5): p. 593-609.
63. Rizk, F., *Modelling of Lightning Incidence to Tall Structures Part I: Theory.* IEEE Transactions on Power Delivery, 1994. **Vol. 9**(No. 1): p. 162-171.
64. Rizk, F., *Modeling of Proximity Effect on Positive Leader Inception and Breakdown of Long Air Gaps.* Power Delivery, IEEE Transactions on, 2009. **24**(4): p. 2311-2318.
65. BWEA. *BWEA Offshore Wind, Round 2 Map (http://www.bwea.com/offshore/round-2map.html)*. 2009 [cited 29 January 2010].
66. BWEA. *BWEA Briefing on UK Wind Capacity Factors (http://www.bwea.com/ref/capacityfactors.html)*. 2009 [cited 29 January 2009].
67. Sweetman, B., *Stealth aircraft*. 1986: Airlife Publishing Ltd.
68. Knott, E.F., *Radar Cross Section*, in *Radar Handbook*, M.I. Skolnik, Editor. 1991.

69. Dabis, H.S. and R.J. Chignell, *Wind turbine electromagnetic scatter modelling using physical optics techniques.* Renewable Energy, 1999. **16**: p. 882-887.
70. BWEA, *Investigation of Technical and Operational Effects on Marine Radar Close to Kentish Flats Offshore Wind Farm*. 2007.
71. Pinto, J., *Stealth Technology for Wind Turbines - Addressing the Aviation and Marine Radar Issues*. 2006.
72. Rashid, L.S. and A.K. Brown. *RCS and radar propagation near offshore wind farms*. in *Antennas and Propagation Society International Symposium, 2007 IEEE*. 2007.
73. Danoon, R.L., *Impact Modelling of Offshore Windfarms on Marine Radars*, in *Microwave and Communication*. 2010, University Of Manchester: Manchester.
74. Shokrieh, M.M. and R. Rafiee, *Simulation of fatigue failure in a full composite wind turbine blade.* Composite Structures, 2006. **74**(3): p. 332-342.
75. Herbert, J.S., *A summary of the fatigue properties of wind turbine materials.* Wind Energy, 2000. **3**(1): p. 1-34.
76. Peesapati, V., et al., *Resolving Performance Conflicts In New Wind Turbine Blade Designs.* European Wind Energy Conference and Exhibition EWEC, Marseille, France, 2009.
77. Nusca, A. *'Stealth' wind turbines avoid aviation radar interference*. 2009 [cited; Available from: http://www.smartplanet.com/business/blog/smart-takes/stealth-wind-turbines-avoid-aviation-radar-interference/1853/.
78. Peesapati, V. and I. Cotton, *Lightning Protection of Wind Turbines – A Comparison between Real Lightning Strike Data and 3D – Finite Element Lightning Attachment Analysis.* The 1st International Conference on SUPERGEN, 2009.
79. Troels S. Sorenson, J.A.P., Blas Hermoso, et al., *The Update of IEC 61400-24 Lightning Protection of Wind Turbines.* Proceedings of the 29th International Conference on Lightning Protection, 23rd - 26th June 2008.
80. ED-81, S.A.A.E., *Aircraft Lightning Environment and Related Test Waveforms.* 2001.
81. Kuffeland, E. and M. Abdullah, *Generation of High Voltages*, in *High voltage engineering*. 1978, Pergamon Presss.
82. IEC, *60060 - 1 High Voltage Test Techniques Part 1: General Definition and Test Requirements.* 1989.
83. Madsen, S.F., et al., *New test method for evaluating the lightning protection system on wind turbine blades.* 2009.
84. Kuffel, E. and M. Abdullah, *High voltage engineering*. 1970, Oxford, UK: Pergamon. x+337.

85. Allen, N.L., *High Voltage Engineering and Testing, Edited by H M Ryan.* 1994.
86. Naidu, M.S. and V. Kamaraju, *High-voltage engineering*. Second ed. 1982, Delhi: McGraw-Hill.
87. Cherney, E.A., *Silicone rubber dielectrics modified by inorganic fillers for outdoor high voltage insulation applications.* Dielectrics and Electrical Insulation, IEEE Transactions on, 2005. **12**(6): p. 1108-1115.
88. Robertson, A.J. and A.D.A. Hall, *Nonlinear dielectric properties of particulate barium titanate-polymer composites.* J Journal of Physics D: Applied Physics, 2008. **11**.
89. Auckland, D.W., W. Su, and B.R. Varlow, *Nonlinear fillers in electrical insulation.* Science, Measurement and Technology, IEE Proceedings -, 1997. **144**(3): p. 127-133.
90. Wang, N., et al., *partial discharge control in a power electronic module using high permitivity non -linear dielectrics.* Accepted for IEEE Dielectrics and Insulators, To be Published, 2010.
91. Hall, A., *Thunderstorm Protection of Aircraft Radomes.* 2005.

12 Appendix

Publications (Conference and Journals)

Paper 1: Lightning Protection of Wind Turbines – A Comparison of Lightning Data and IEC 61400 -24. Presented at the International Conference on Sustainable Power Generation and Supply, 2009, held in Nanjing, China.

Paper 2: Lightning Protection of Wind Turbines - A Comparison of Real Lightning Strike Data and Finite Element Lightning Attachment Analysis. Presented at the International Conference on Sustainable Power Generation and Supply, 2009, held in Nanjing China.

Paper 3: Resolving Performance Conflicts in New Wind Turbine Blade Designs. Presented at EWEC 2009, held in Marseille, France.

Paper 4: Lightning Protection of Wind Turbines – A Comparison Of Measured Data With Required Protection Levels. Accepted for publication in the IET Renewable Energy Journal. Awaiting publication.